AFRL-RX-WP-TM-2010-4084

COLLABORATIVE RESEARCH AND DEVELOPMENT CONTRACT

Delivery Order 0037: Mechanisms Causing Fatigue Variability in Turbine Engine Materials

Sushant Jha

Universal Technology Corporation

MAY 2008
Final Report

AIR FORCE RESEARCH LABORATORY
MATERIALS AND MANUFACTURING DIRECTORATE
WRIGHT-PATTERSON AIR FORCE BASE, OH 45433-7750
AIR FORCE MATERIEL COMMAND
UNITED STATES AIR FORCE

NOTICE AND SIGNATURE PAGE

Using Government drawings, specifications, or other data included in this document for any purpose other than Government procurement does not in any way obligate the U.S. Government. The fact that the Government formulated or supplied the drawings, specifications, or other data does not license the holder or any other person or corporation; or convey any rights or permission to manufacture, use, or sell any patented invention that may relate to them.

This report was cleared for public release by the Wright-Patterson Public Affairs Office and is available to the general public, including foreign nationals. Copies may be obtained from the Defense Technical Information Center (DTIC) (http://www.dtic.mil).

AFRL-RX-WP-TM-2010-4084 HAS BEEN REVIEWED AND IS APPROVED FOR PUBLICATION IN ACCORDANCE WITH ASSIGNED DISTRIBUTION STATEMENT.

*//Signature//	//Signature//
RITA SCHOLES Program Manager Business Operations Branch Integration and Operations Division	ROBERT ENGHAUSER Acting Chief Business Operations Branch Integration and Operations Division

This report is published in the interest of scientific and technical information exchange, and its publication does not constitute the Government's approval or disapproval of its ideas or findings.

*Disseminated copies will show "//Signature//" stamped or typed above the signature blocks.

REPORT DOCUMENTATION PAGE

Form Approved
OMB No. 0704-0188

1. REPORT DATE *(DD-MM-YY)*	2. REPORT TYPE	3. DATES COVERED *(From - To)*
May 2008	Final	02 June 2005 – 01 February 2008

4. TITLE AND SUBTITLE
COLLABORATIVE RESEARCH AND DEVELOPMENT CONTRACT
Delivery Order 0037: Mechanisms Causing Fatigue Variability in Turbine Engine Materials

5a. CONTRACT NUMBER
F33615-03-D-5801-0037

5b. GRANT NUMBER

5c. PROGRAM ELEMENT NUMBER
62102F

6. AUTHOR(S)
Sushant Jha

5d. PROJECT NUMBER
4349

5e. TASK NUMBER
L0

5f. WORK UNIT NUMBER
4349L0VT

7. PERFORMING ORGANIZATION NAME(S) AND ADDRESS(ES)

Universal Technology Corporation
1270 North Fairfield Road
Dayton, OH 45432-2600

8. PERFORMING ORGANIZATION REPORT NUMBER
S-531-037

9. SPONSORING/MONITORING AGENCY NAME(S) AND ADDRESS(ES)

Air Force Research Laboratory
Materials and Manufacturing Directorate
Wright-Patterson Air Force Base, OH 45433-7750
Air Force Materiel Command
United States Air Force

10. SPONSORING/MONITORING AGENCY ACRONYM(S)
AFRL/RXOB

11. SPONSORING/MONITORING AGENCY REPORT NUMBER(S)
AFRL-RX-WP-TM-2010-4084

12. DISTRIBUTION/AVAILABILITY STATEMENT
Approved for public release; distribution unlimited.

13. SUPPLEMENTARY NOTES
PAO case number 88ABW-2009-0426, cleared 01 February 2009. Report contains color.

14. ABSTRACT

This research in support of the Air Force Research Laboratory Materials and Manufacturing Directorate was conducted at Wright-Patterson AFB, Ohio from 2 June 2005 through 1 February 2008. The research develop a comprehensive understanding of the causes of fatigue variability, especially the minimum life, in a +b titanium alloys and nickel base superalloys. A physics-based life-prediction model has been developed that provides accurate probabilistic fatigue lifetime limits in aerospace materials with respect to microstructural and extrinsic variables, and promises significant reduction in the uncertainty associated with life prediction. The modeling is based on some key findings, common to a range of aerospace material systems, in terms of the fatigue variability behavior. First, it is found that effect of microstructural and loading variables on fatigue variability is manifested as separate degree of influences on the mean fatigue behavior and the life-limiting, lower-tail behavior. Therefore, the lifetime distribution can be represented as a divergence or convergence of these two behaviors as a function of the imposed variables. Second, the life-limiting behavior is shown to be controlled by the crack growth regime, i.e., the crack initiation lifetime is negligible. This separation of mean and the crack-growth-controlled behavior is found to be promoted by the development of an array of heterogeneity scales in the material under any given nominal microstructure and loading condition. These heterogeneity scales, which are related to the underlying microstructural configurations, are suggested to produce sequential failure mechanisms in the order of decreasing heterogeneity level. These vital concepts have been developed with the help detailed investigation of the relationship of the mean and the life-limiting mechanisms to the underlying microstructural drivers. Quantitative analysis of crack initiation sites in terms of size, and spatial and crystallographic orientations of the crack initiating feature and its neighborhood were employed to support this purpose. This was also done in conjunction with the measurements of small fatigue crack growth variability in microstructurally-initiated as well as Focused Ion Beam (FIB) machined notch-initiated cracks. The probabilistic modeling approach developed here is demonstrated to have significant promise for removing the uncertainty in prediction of the limiting lifetime of fracture critical components.

15. SUBJECT TERMS
Titanium life-prediction model

16. SECURITY CLASSIFICATION OF:			17. LIMITATION OF ABSTRACT:	18. NUMBER OF PAGES	19a. NAME OF RESPONSIBLE PERSON (Monitor)
a. REPORT	b. ABSTRACT	c. THIS PAGE			Rita Scholes
Unclassified	Unclassified	Unclassified	SAR	104	19b. TELEPHONE NUMBER *(Include Area Code)* N/A

Standard Form 298 (Rev. 8-98)
Prescribed by ANSI Std. Z39-18

Physics-Based Probabilistic Fatigue Life-Prediction in Aerospace Materials

Objective

The objective of this task was to develop a physics-based, probabilistic fatigue life-prediction methodology for various aerospace materials. Specific goals were to provide a microstructural and mechanistic basis for the fatigue variability behavior in selected turbine engine alloys, and to implement this understanding in a life-prediction model.

Abstract

A physics-based life-prediction model has been developed that provides accurate probabilistic fatigue lifetime limits in aerospace materials with respect to microstructural and extrinsic variables, and promises significant reduction in the uncertainty associated with life prediction. The modeling is pivoted on some key findings, in terms of the fatigue variability behavior, common to a range of aerospace material systems. First, it is found that the effect of microstructural and loading variables on fatigue variability is manifested as separate degree of influences on the mean fatigue behavior and the life-limiting, lower-tail behavior. Therefore, the lifetime distribution can be represented as a divergence (or convergence) of these two behaviors as a function of the imposed variables. Second, the life-limiting behavior is shown to be controlled by the crack growth regime, irrespective of the microstructure or stress level, via negligible crack initiation lifetime in a critical microstructural neighborhood. This separation of mean and the crack-growth-controlled behavior is found to be promoted by the development of an array of local heterogeneity scales in the material under any given nominal microstructure and loading condition. These scales, which are related to the underlying microstructural configurations, are suggested to produce sequential realization of failure mechanisms in the order of decreasing heterogeneity level. These concepts are vital to the physics-based description of fatigue variability and particularly to probabilistic life prediction. These have been developed with the help detailed investigation of the relationship of the mean and the life-limiting mechanisms to the underlying microstructural drivers. Towards this, quantitative analysis of crack initiation sites in terms of size, and spatial and crystallographic orientations of the crack initiating feature and its neighborhood were employed. This was also done in conjunction with the measurements of small fatigue crack growth variability in microstructurally-initiated as well as Focused Ion Beam (FIB) machined notch-initiated cracks. The probabilistic modeling approach developed here is demonstrated to produce accurate predictions of the lifetime variability with respect to a host of material and extrinsic variables almost independent of the number of experiments, and shown to have significant promise for reducing the uncertainty in predicting the limiting lifetime of fracture critical components.

Publications

- S.K. Jha, J.M. Larsen, A.H. Rosenberger, “Role of Competing Mechanisms in the Fatigue Life Variability of a Nearly Fully Lamellar γ-TiAl based alloy,” Acta Materialia, Vol. 53, pp. 1293-1304, 2005.
- K.S. Ravi Chandran and S.K. Jha, “Duality of the S-N Fatigue Curve Caused by Competing Failure Modes in a Titanium Alloy and the Role of Poisson Defect Statistics, Acta Materialia, Vol. 53, pp. 1867-2179, 2005.

- [Invited] S.K. Jha, J.M. Larsen, and A.H. Rosenberger, "The role of competing mechanisms in the fatigue life variability of a titanium and a γ-TiAl based alloy," *JOM*, Vol. 57, no. 9, pp. 50-54, 2005.
- [Invited] S.K. Jha, J.M. Larsen, and A.H. Rosenberger, "Prediction of the worst-case fatigue failures in an α+β Titanium alloy," in *Materials Damage Prognosis*, J.M. Larsen, L. Christodoulou, et. al. eds., TMS publications, 2005, pp. 143-150.
- S.K. Jha, M.J. Caton, J.M. Larsen, and A.H. Rosenberger, "Superimposing mechanisms and their effect on the variability in fatigue lives of a nickel-based superalloy," in *Materials Damage Prognosis*, J.M. Larsen, L. Christodoulou, et. al. eds., TMS publications, 2005, pp. 343-350.
- C. Annis, J.M. Larsen, A.H. Rosenberger, S.K. Jha, and D.H. Annis, "RfTh, a Random Fatigue Threshold Probability Density for Ti6246," in *Materials Damage Prognosis*, J.M. Larsen, L. Christodoulou, et. al. eds., TMS publications, 2005, pp. 151-156.
- C.J. Szczepanski, A. Shyam, S.K. Jha, J.M. Larsen, T.M. Pollock, and J.W. Jones, " Characterization of the role of microstructure on the fatigue life of Ti-6Al-2Sn-4Zr-6Mo using ultrasonic fatigue," in *Materials Damage Prognosis*, J.M. Larsen, L. Christodoulou, et. al. eds., TMS publications, 2005, pp. 315-320.
- K. Polasik, S.K. Jha, M.J. Mills, J.M. Larsen, and H.L. Fraser, "The role of microstructure on fatigue life variability in β-processed Ti-6Al-4V," in *Materials Damage Prognosis*, J.M. Larsen, L. Christodoulou, et. al. eds., TMS publications, 2005, pp. 121-128.
- Shyam, C.J. Szczepanski, S.K. Jha, M.J. Caton, J.M. Larsen, T.M. Pollock, and J.W. Jones, "Ultrasonic fatigue of a nickel-base turbine disk alloy at room and elevated temperature," in *Materials Damage Prognosis*, J.M. Larsen, L. Christodoulou, et. al. eds., TMS publications, 2005, pp. 247-252.
- S.K. Jha, J.M. Larsen, and A.H. Rosenberger, "Microstructure and temperature effects on the fatigue variability behavior of an α+β titanium alloy," in *Fatigue-2006*, International Fatigue Congress, 2006.
- J. Szczepanski, S.K. Jha, J.M. Larsen, and J.W. Jones, "Fatigue crack initiation in an α+β titanium alloy," in *Fatigue-2006*, International Fatigue Congress, 2006.
- [Invited] S.K. Jha, M.J. Caton, J.M. Larsen, and A.H. Rosenberger, "A New Paradigm of Fatigue Variability Behavior and implications for life prediction," *Materials Science and Engineering A*, Vol. A468-470, pp. 23-32, 2007.
- S.K. Jha and J.M. Larsen, "Random Heterogeneity Scales and Probabilistic Description of Long-Lifetime Regime of Fatigue," *VHCF-4*, Proceedings of the Fourth International Conference on Very High Cycle Fatigue, pp. 385-396, 2007.
- J. Szczepanski, S.K. Jha, J.M. Larsen, and J.W. Jones, "The Role of Microstructure on Fatigue Lifetime Variability in an α+β Ti-Alloy," *VHCF-4*, Proceedings of the Fourth International Conference on Very High Cycle Fatigue, pp. 37-44, 2007.

- S.K. Jha, M.J. Caton, and J.M. Larsen, "Mean vs. Life-Limiting Fatigue Behavior of a Nickel-Base Superalloy," in Press, *Superalloys-2008.*
- W.J. Porter, K. Li, M.J. Caton, S.K. Jha, B.B. Bartha, and J.M. Larsen, "Microstructural Conditions Contributing to Fatigue Variability in P/M Nickel-Base Superalloys," in press, *Superalloys-2008*.
- J. Szczepanski, S.K. Jha, J.M. Larsen, and J.W. Jones, "Microstructural Influences on Very High Cycle Fatigue Crack Initiation in Ti-6246," Accepted, *Metallurgical and Materials Transactions A*, 2008.
- [Invited] S.K. Jha, J.M. Larsen, and A.H. Rosenberger, "Applying a 'Physics-Based' Description of Fatigue Variability Behavior to Probabilistic Life Prediction," in review, *Engineering Fracture Mechanics*, 2007.
- S.K. Jha, H.R. Millwater, and J.M. Larsen, "Probabilistic Sensitivity Analysis in Life-Prediction of an $\alpha+\beta$ Titanium Alloy," in review, *Fatigue and Fracture of Engineering Materials and Structures*, 2008.
- S.K. Jha, S.K. Jha, M.J. Caton, and J.M. Larsen, "The Mean Vs. Life-Limiting Fatigue Response of a Ni-Base Superalloy, Part I: Mechanisms," Prepared for submission, *Materials and Metallurgical Transactions A*.
- S.K. Jha, M.J. Caton, and J.M. Larsen, "The Mean Vs. Life-Limiting Fatigue Response of a Ni-Base Superalloy, Part II: Life-Prediction Methodology," prepared for submission, *Materials and Metallurgical Transactions A*.
- M.G. Glavicic, B.B. Bartha, S.K. Jha, and C.J. Szczepanski, "The Origins of Microtexture in Duplex Titanium Alloys," prepared for submission, *Scripta Materialia*, 2008.
- S.K. Jha, R. John, and J.M. Larsen, "Nominal versus Local Shot-Peening Effects on Fatigue Lifetime," prepared for submission, *Scripta Materialia*, 2008.

Presentations

- **[Invited]** S.K. Jha, M.J. Caton, J.M. Larsen, R. John, and A.H. Rosenberger, "Need for a new paradigm of fatigue variability behavior and implications for life prediction," TMS Annual meeting, San Antonio, TX, Mar 12-16, 2006.
- **[Invited]** S.K. Jha, M.J. Caton, J.M. Larsen, R. John, and A.H. Rosenberger, "A worst-case life prediction methodology and implications for life prediction of turbine engine components," to be presented at the Materials Life Cycle Engineering Conference, Snow Mass, CO, July, 2006.
- **[Invited]** S.K. Jha, M.J. Caton, J.M. Larsen, and A.H. Rosenberger, "Understanding fatigue variability and predicting worst-case failures in turbine engine materials," ASTM International Symposium, Dallas, Texas, 2005. (Presented by R. Morrissey)
- **[Invited]** J.M. Larsen, S.K. Jha, M.J. Caton, A.H. Rosenberger, and R. John, "A Novel Philosophy for Worst Case Fatigue Behavior of Ni-Base Superalloys at Elevated Temperature," TMS Annual Meeting, Feb 25 – March 1, 2007, Orlando, FL, 2007. (Presented by JML).

- **[Invited]** J.M. Larsen, S.K. Jha, M.J. Caton, A.H. Rosenberger, and R. John, "Worst-Case Prognosis of Advanced Turbine Engine Materials," Materials Science and Technology 2007, Detroit, MI, Sep 16 – 20, 2007. (Presented by JML).
- S.K. Jha, J.M. Larsen, and A.H. Rosenberger, "Crack Initiation/Propagation Induced Duality in Fatigue Variability of an $\alpha+\beta$ Titanium Alloy and Implications for Life Prediction," MS&T 2005, Pittsburgh, PA, Sep 25-28, 2005.
- K. Polasik, S. K. Jha, M. J. Mills, J.M. Larsen, and H.L. Fraser, "Microstructure-Fatigue Lifetime Relationship for Ti-6Al-4V," MS&T 2005, Pittsburgh, PA, Sep 25-28, 2005. (Presented by AKP).
- M.J. Caton, S.K. Jha, J.M. Larsen, and A.H. Rosenberger, "Identifying sources of fatigue variability in a nickel-based superalloy," TMS Annual Meeting, San Antonio, TX, Mar 12-16, 2006. (Presented by MJC).
- J. Szczepanski, S.K. Jha, J.M. Larsen, and J.W. Jones, TMS Annual Meeting, San Antonio, TX, Mar 12-16, 2006. (Presented by CJS).
- S.K. Jha, M.J. Caton, and J.M. Larsen, "Incorporating Fatigue Variability in a Life Prediction Approach for Nickel-Based Superaloys," Fatigue 2006, 9th International Fatigue Congress, Atlanta, GA, May 14-19, 2006.
- S.K. Jha, R. John, and J.M. Larsen, "Residual Stress Effects on the fatigue Variability Behavior of an $\alpha+\beta$ Titanium Alloy," Fatigue 2006, 9th International Fatigue Congress, Atlanta, GA, May 14-19, 2006.
- S.K. Jha, J.M. Larsen, and A.H. Rosenberger, "Implementing Microstructure and Temperature Effects on Fatigue Variability in a Mechanism-Based Life Prediction Methodology," Fatigue 2006, 9th International Fatigue Congress, Atlanta, GA, May 14-19, 2006.
- M.J. Caton, S.K. Jha, W.J. Porter, III, K. Li, A.H. Rosenberger, and J.M. Larsen, "Sources of Fatigue Variability in IN-100," Fatigue 2006, 9th International Fatigue Congress, Atlanta, GA, May 14-19, 2006. (Presented by MJC).
- W.J. Porter, III, K. Li, S.K. Jha, M.J. Caton, and J.M. Larsen, "Variability in Microstructure and its Effect on Fatigue Variability in IN-100," Fatigue 2006, 9th International Fatigue Congress, Atlanta, GA, May 14-19, 2006. (Presented by WJP).
- J. Szczepanski, S.K. Jha, J.M. Larsen, and J.W. Jones, "Fatigue Crack Initiation Mechanisms in an $\alpha+\beta$ Titanium Alloy," Fatigue 2006, 9th International Fatigue Congress, Atlanta, GA, May 14-19, 2006. (Presented by CJS).
- J.M. Larsen, R. John, S.K. Jha, M.J. Caton, et. al., "Life Prediction and Durability of High Temperature Materials," AFOSR Review, Seattle, WA, Aug 31, 2006. (Presented by RJ).
- S.K. Jha, M.J. Caton, J.M. Larsen, R. John, and A.H. Rosenberger, "Fatigue variability and mechanism-based life prediction of turbine engine materials," Propulsion Safety and Affordable Readiness (P-SAR) Conference, Jacksonville, FL, Mar 28-30, 2006. (Presented by JML).

- M.J. Caton, S.K. Jha, K. Li, W.J. Porter, and J.M. Larsen, "Identifying sources of fatigue variability in a powder processed nickel-based superalloy for improved life prediction," Propulsion Safety and Affordable Readiness (P-SAR) Conference, Jacksonville, FL, Mar 28-30, 2006. (Presented by MJC).
- S.K. Jha, M.J. Caton, and J.M. Larsen "Physically based simulations to test a new theory of fatigue variability behavior," Materials Science & Technology – 2006, Cincinnati, OH, Oct 15-19, 2006.
- M.J. Caton, O.N. Senkov, S.K. Jha, and L. Selegue "Mechanical and fatigue properties of a super-high strength developmental Al-Zn-Mg-Sc alloy for use in cryogenic applications," Materials Science & Technology – 2006, Cincinnati, OH, Oct 15-19, 2006. (Presented by MJC).
- J. Szczepanski, S.K. Jha, J.M. Larsen, and J.W. Jones "Characterization of fatigue crack initiation in an $\alpha+\beta$ titanium alloy," Materials Science & Technology – 2006, Cincinnati, OH, Oct 15-19, 2006. (Presented by CJS).
- S.K. Jha, J.M. Larsen, and A.H. Rosenberger, "The Mean vs. Life-Limiting Behavior in Fatigue of an $\alpha+\beta$ Titanium alloy," TMS Annual Meeting, Feb 25 – March 1, 2007, Orlando, FL, 2007.
- S.K. Jha, M.J. Caton, and J.M. Larsen, W.J. Porter, K. Li, and A.H. Rosenberger, "Implementing a Physics-Based Description of Fatigue Variability in Probabilistic Life Prediction: IN-100 Example," TMS Annual Meeting, Feb 25 – March 1, 2007, Orlando, FL, 2007.
- S.K. Jha, H.R. Millwater, and J.M. Larsen, "Probabilistic Sensitivity Analysis in Life Prediction of an $\alpha+\beta$ Titanium Alloy," TMS Annual Meeting, Feb 25 – March 1, 2007, Orlando, FL, 2007.
- M.J. Caton, S.K. Jha, and J.M. Larsen, "Effect of Dwell-Loading and Grain Size on the Fatigue Variability Behavior of Nickel-Based Superalloys," TMS Annual Meeting, Feb 25 – March 1, 2007, Orlando, FL, 2007. (Presented by MJC).
- H.R. Millwater, A. Bates, E. Vazquez, S.K. Jha, and J.M. Larsen, Propulsion-Safety and Affordable Readiness Conference, P-SAR, Mar 13 – 15, 2007, San Diego, CA, 2007. (Presented by HRM).
- S.K. Jha and J.M. Larsen, "Random Heterogeneity Scales and Probabilistic Life Prediction in the Long Lifetime Regime of Fatigue," VHCF-4, 4th International Conference on Very High Cycle Fatigue, Ann Arbor, MI, Aug 19-22, 2007.
- C.J. Szczepanski, S.K. Jha, J.M. Larsen, and J.W. Jones, "The Role of Microstructure on the Fatigue Lifetime Variability of the $\alpha+\beta$ Titanium Alloy, Ti-6Al-2Sn-4Zr-6Mo," VHCF-4, 4th International Conference on Very High Cycle Fatigue, Ann Arbor, MI, Aug 19-22, 2007. (Presented by CJS).
- S.K. Jha, M.J. Caton, and J.M. Larsen, "Probabilistic Fatigue Life Prediction of the Nickel-Based Superalloy IN100," Materials Science and Technology 2007, Detroit, MI, Sep 16 – 20, 2007.

- M.J. Caton, S.K. Jha, J.M. Larsen, W.J. Porter, and K. Li, "Role of Grain Size on the Fatigue Variability of Nickel-Based Superalloys Under Dwell Loading," Materials Science and Technology 2007, Detroit, MI, Sep 16 – 20, 2007. (Presented by MJC).
- C.J. Szczepanski, S.K. Jha, J.M. Larsen, and J.W. Jones, "Relating Microstructural Variability to Fatigue Lifetime Variability in an $\alpha+\beta$ Titanium Alloy," Materials Science and Technology 2007, Detroit, MI, Sep 16 – 20, 2007. (Presented by CJS).
- S.K. Jha, M.J. Caton, and J.M. Larsen, "Separation of Mean and Life-Limiting Behavior: A "Physics-Based" Description of Fatigue Variability," ASTM Symposium on Fatigue and Fracture Mechanics, Tampa, FL, Nov 14-16, 2007.
- S.K. Jha, R. John, D.J. Buchanan, and J.M. Larsen, "Incorporating Residual Stress in Life Prediction of an $\alpha+\beta$ Titanium Alloy," TMS Annual Meeting, New Orleans, LA, Mar 9 – 13, 2008.
- S.K. Jha, M.J. Caton, and J.M. Larsen, "Predicting the Effect of Dwell Time on the Probabilistic Fatigue Lifetime Limit," TMS Annual Meeting, New Orleans, LA, Mar 9 – 13, 2008.
- C.J. Szczepanski, S.K. Jha, J.M. Larsen, and J.W. Jones, "Microtexturing Effects on Fatigue Lifetime of Ti-6246," TMS Annual Meeting, New Orleans, LA, Mar 9 – 13, 2008. (Presented by CJS).
- S.K. Jha and J.M. Larsen, "Random Heterogeneity Scales Produce the Mean vs. Life-Limiting Behavior in Fatigue: A Study on an a+b Titanium Alloy," Propulsion Safety and Affordable Readiness (P-SAR) Conference, Myrtle Beach, SC, Mar 18 – 20, 2008. (Presented by JML).

Report outline

The research under this task is summarized in the following chapters, which represent a few selected publications resulting from this work.

Chapter I

A NEW PARADIGM OF FATIGUE VARIABILITY BEHAVIOR AND IMPLICATIONS FOR LIFE PREDICTION

S.K. Jha[1*], M.J. Caton, and J.M. Larsen
US Air Force Research Laboratory, Wright-Patterson AFB, OH 45431, USA
[1]Universal Technology Corporation, Dayton, OH 45432, USA
Published in: *Materials Science and Engineering A*, 2007.

ABSTRACT

The treatment of the fatigue variability behavior has traditionally been based on the understanding of the mean-lifetime behavior. With reference to two turbine engine materials, an $\alpha+\beta$ titanium alloy and a nickel-based superalloy, it is shown that the traditional approach may not accurately describe the fatigue variability behavior of these materials. Decreases in stress level, or microstructural change directed at increasing the mean lifetime, were found to affect mean and worst-case (life-limiting) fatigue behavior differently, and these differences could not be accounted for in the traditional understanding. In particular, the life-limiting mechanism was controlled by crack growth although the mean-lifetime response was increasingly dominated by crack initiation with decreasing stress level. A new paradigm of fatigue variability was therefore suggested, in which the total uncertainty in lifetime breaks down into the variability in (1) the worst-case mechanism and that in (2) the classical, mean-lifetime governing response. The effects of microstructure and temperature on the fatigue variability behavior were studied with respect to the new paradigm and found to have a very systematic effect on the worst-case and the mean behavior, depending on the degree of influence of these variables on the crack initiation and the growth regime.

Keywords: Fatigue variability, $\alpha+\beta$ titanium alloy, nickel-base superalloy, life-limiting behavior, microstructure, probability of failure

1.0 INTRODUCTION

Fatigue lifetime variability behavior is generally described in terms of variability about the overall mean behavior [1-3]. The life prediction approach of fracture critical turbine engine components has also been governed by the conventional understanding of fatigue variability [4,5]. The minimum book life, or the limiting-lifetime, is taken as the extrapolation of the variability about the overall mean behavior at some given set of conditions corresponding to a predetermined probability of failure (POF), typically taken as 1 in 1000 [4]. As a result, there is large degree of uncertainty associated with the limiting-lifetime prediction and it is estimated that a significant number of components may be discarded while still possessing a considerable fraction of their useful life [5]. A more accurate predicted life may require a re-evaluation of the traditional approach to fatigue variability, especially with respect to its applicability to life prediction.

In this paper, the fatigue variability behavior of two common turbine engine materials is discussed. These were: the $\alpha+\beta$ titanium alloy, Ti-6Al-2Sn-4Zr-6Mo (Ti-6-2-4-6) and a powder metallurgy (P/M) processed nickel-based superalloy. There are few studies of fatigue variability of titanium alloys, although their mean fatigue behavior has been widely studied, and correlations between microstructure and loading variables vs. the mean behavior have been established in many cases [6-9]. In $\alpha+\beta$ titanium alloys, depending on the microstructure, the mean lifetime

has been related to the equiaxed α size, and lamellar α/β colony size [7-9]. Decreasing the controlling microstructural unit is known to increase the mean lifetime [9], especially at lower stress levels. It is also well known in titanium alloys that, crack initiation has increased contribution to the total lifetime as the stress level is decreased [10,11]. The relationship of these variables to the fatigue lifetime-variability, however, has not been widely addressed.

The fatigue behavior of P/M nickel-based superalloys has also been reported in many studies [3, 12-18]. These materials are known to fail from crystallographic crack initiation [17,18], as well as processing related constituent particles [17-20] and voids [12,13,15,16]. The treatment of fatigue variability behavior of these materials has been largely focused at obtaining the lifetime distribution from variation in the given microstructural feature as well as, in some cases, the variation in the crack initiation and crack growth rates about the mean response [3, 14-16]. From a design-life perspective, a more important problem may be the competition between mechanisms and their ranking in terms of likelihood of occurrence, as addressed in some studies [21, 22].

Recently, it was shown that, the competition between mechanisms, and the interplay between the number density of relevant microstructural features and the specimen volume, can produce a duality in the S-N fatigue behavior [23]. In a different material [24], the competition, and the sequence of occurrence of mechanisms, was shown to produce a superposition of variability in two mechanisms at the same stress level. These and other studies [25] point to growing evidence that the fatigue variability behavior may not follow the same trend as the mean response. It is crucial to capture and incorporate these fatigue variability responses for reliable life prediction, as it appears this behavior cannot be accounted for in the traditional, mean-based framework.

2.0 MATERIALS AND EXPERIMENTAL PROCEDURE

The materials in this study were an $\alpha+\beta$ titanium alloy, Ti-6-2-4-6 and a P/M processed nickel-based superalloy. Two heats of the Ti-6-2-4-6 alloy with constant composition but different optical microstructures were considered. These were designated as the pancake and the disk microstructure and are shown in Fig. 1 (a) and (b), respectively. As shown, both microstructures had a duplex structure with equiaxed primary α (α_p) grains in a transformed β matrix. These however, differed significantly in terms of their crystallographic texture as shown in Fig. 2.

The microstructure of the nickel-based superalloy is shown in Fig. 3. The γ - primary γ' structure is revealed in Fig. 3(a) and the secondary γ' morphology is shown in Fig. 3(b). Since the tertiary γ' precipitates were very fine, they are not resolved at this magnification. The median γ grain size was about 4 μm.

Fatigue specimens were electro-discharge machined in the circumferential orientation from the forgings of the two heats of the titanium alloy. The final machining step involved low stress grinding. Subsequently, each specimen was electropolished (to remove approximately 50 μm from the surface) to eliminate the surface residual stress and to produce a uniform surface condition. Specimens had round-bar geometry with a uniform gage length of about 12.5 mm and a diameter of about 4 mm. The superalloy specimens were also extracted in the circumferential orientation from a pancake forging of the material. For the elevated temperature experiments, a

cylindrical, button-head specimen geometry similar to the one described in [26] was used. The gage length was about 15.2 mm and the diameter was about 5 mm.

The fatigue tests were conducted using an MTS 810 servo hydraulic test system equipped with a 458 controller. The experiments were performed in load-control and in lab air. The Ti-6-2-4-6 experiments were performed at room temperature and 260ºC. The temperature of 650 ºC was employed for the superalloy. The stress ratio was 0.05 for all tests, and the frequencies were 20 Hz for the titanium alloy and 0.333 Hz for the superalloy. A resistance-heated furnace with dual zone temperature control was used for the high temperature tests, and control thermocouples were welded to two locations near the gage of the sample so that the temperature was maintained within ± 2ºC of the set point. A high temperature extensometer was used to record the stress – strain behavior throughout the tests.

Small-crack growth was monitored using the acetate replication technique. Cracks initiating from starter notches, as well as those naturally initiating, were studied. Starter notches were machined using the Femtosecond laser at the University of Michigan, the details of which can be found elsewhere [27]. Additionally, in some samples, notches were machined using a Focused Ion Beam (FIB). Replicas were recorded at predetermined cycle intervals at the static load of 60% of the maximum load in a cycle.

Fractography and orientation imaging microscopy (OIM) were performed in a Cambridge S360FE scanning electron microscope. The microscope was equipped with a TSL OIM system. For imaging, the accelerating voltage of 15 kV, and the probe current of 100 pA was used. For OIM, the accelerating voltage and the probe current of 20 kV and 10 nA were employed. The sample was tilted at 70º with respect to the horizontal axis for OIM, and the working distance was 25 mm. The sample was moved in steps in automated stage control to scan a large area in a single session.

3.0 FATIGUE VARIABILITY BEHAVIOR OF THE α+β TITANIUM ALLOY

3.1 Mean vs. the Life-Limiting Behavior

The fatigue variability behavior of the Ti-6-2-4-6 pancake microstructure at 25ºC is shown in Fig. 4 (a). The mean-lifetime behavior is also superimposed in the plot. Clearly, the mean behavior followed the classical response to the decrease in stress level, which is attributed to the increasing contribution of the crack initiation regime to the total lifetime [10,11]. At the same time, the life-limiting behavior had a different response, being relatively insensitive to change in stress level. The minimum lifetime also remained almost unaffected with respect to σ_{max}, as illustrated in Fig. 4(b). The result of these different responses of the lower-tail behavior and the mean lifetime was that the separation between the minimum and mean lifetimes increased with decreasing σ_{max}, causing an increase in the total lifetime-variability (up to 500 X). This indicates that the mean and the lower-tail behavior may be governed by different mechanisms. Another consequence of this type of response was that the lifetime corresponding to the POF of 0.1% (based on the extrapolation of the total variability) decreased with decreasing stress level except at σ_{max} = 820 MPa. This is also shown in Fig. 4(b). As discussed earlier, these fatigue variability responses cannot be accounted for by the mean-life fatigue based understanding and call for an alternate paradigm of fatigue variability behavior.

The separation of the worst-case mechanism, and the mechanism dominating the mean lifetime with decreasing stress level was more evident when the experimental points were plotted

as a Cumulative Distribution Function (CDF). This is shown in Fig. 5. The lognormal distribution function was assumed. A detailed discussion is provided elsewhere [25]. As shown, at the higher stress level (σ_{max} = 1040 MPa), the CDF agreed well with the data. However at the lower stress levels, experimental points exhibited a step-like shape with respect to the CDF, as illustrated for σ_{max} = 860 MPa in Fig. 5. This suggests that the variability in total fatigue lifetime results from a superposition of a worst-case and a long-life mechanism (designated as Type I and Type II respectively).

3.2 Total Variability vs. Variability within Mechanisms

Small-crack growth experiments with different starting notch sizes were conducted to determine the contributions of crack-size regimes to the total variability. The results are presented in Fig. 6. As shown, no small-crack effect and almost insignificant variability in crack growth behavior was observed when the starting notch dimension (length x depth) was 20 μm x 25 μm or larger, and these small-crack growth data matched with the long-crack behavior. However, a significant small-crack effect was seen when the crack initiated naturally across an equiaxed α grain of size about 4 μm. The maximum contribution to the total lifetime variability is, therefore, expected to originate from crack initiation and early small crack growth (on the order of < 20 – 30 μm).

Figure 4(a) indicates the increasing contribution of crack initiation to the mean lifetime (dominated by the Type II mechanism) as the stress level is decreased. However, the Type I lifetimes were up to two orders of magnitude smaller. The limiting small-crack growth curves and the limits on the crack initiation sizes were used deterministically to predict the range in the crack growth lifetimes presented in Fig. 7. This figure clearly shows that the range in the Type I lifetimes was related to small crack growth starting from the equiaxed α size scale. Therefore, it can be suggested that the separate response of the mechanisms with decreasing stress level was caused by the increasing crack initiation lifetime of the Type II failures, while the Type I mechanism was controlled by small-crack growth.

3.3 Simulation of Variability in the Type I mechanism

The lifetimes related to the variability in the crack growth rates and the crack initiation sizes were simulated using the Monte Carlo method. The distributions in the crack initiation size and the small-crack growth parameters m and c are presented in Fig. 8. The parameters, m and c, of the crack growth equation are correlated [16,28] as shown in Fig. 8(c). These were therefore sampled from their joint probability density using the algorithm described in [28]. Further details of the simulation can be found elsewhere [29]. The simulated lifetimes at σ_{max} = 860 MPa are shown in Fig. 9. As shown, these lifetimes had the same range of values as the experimental Type I lifetimes. It is to be noted that the Type I failures are taken as those comprising the left part of the step when the data are plotted in the CDF space (see Fig. 5). The simulated lifetimes are compared to the Type I and Type II distributions in Fig. 9 (b) at the σ_{max} of 860 MPa. A reasonable agreement between the two is evident. This shows that the uncertainty in the worst-case mechanism was governed purely by the variability in crack growth lifetime starting from the relevant microstructural size scale.

The statistics of the simulated lifetimes are compared with the experimental Type I failures with respect to the stress level in Fig. 10. As shown, the predicted mean lifetimes were in excellent agreement with the experiment (Fig. 10(a)). The standard deviations of the simulated

lifetimes (Fig. 10(b)), although under-predicted, were similar to that of the Type I failures. This under-prediction may be due to the limited small-crack data used as input, therefore, the possible under-estimation of the variability in the crack growth behavior. The simulated and the experimental minimum lifetimes (Fig. 10(c)) were also in reasonable agreement. Inclusion of additional small-crack data is expected to further improve the predictions. These simulations however, confirm the observed behavior that the minimum lifetimes may not vary significantly within the range of stress levels considered (see Fig. 4).

3.4 Effect of Microstructure and Temperature

The fatigue variability behavior of the pancake and the disk microstructure are compared in Fig. 11 (a) and (b) at the σ_{max} levels of 860 and 820 MPa, respectively. As shown, at both stress levels, microstructure had a strong influence on the Type II mechanism but almost no effect on the Type I failure distribution. This led to a decrease in the mean lifetime of the disk material. Since the variability in the Type I mechanism is controlled by crack growth, and given the similar equiaxed α size in the two cases, the very weak response of the worst-case mechanism to microstructure can be attributed to the very similar crack growth behavior of the two microstructures [30]. Due to the dominance of the crack initiation regime in the Type II mechanism, the shift with microstructure may be related to a decrease in the crack initiation lifetime of the disk microstructure. It is not surprising that the crack initiation regime was significantly more sensitive to microstructure than the crack growth [31].

The effect of temperature on the lifetime variability of the two microstructures is shown in Fig. 12 at σ_{max} = 860 MPa. Clearly, the increase in temperature caused a further shift in the Type II mechanism towards smaller lifetimes, as illustrated. However, the Type I lifetimes were not significantly affected by temperature. This was, once again, due to the similar crack growth behavior of the material between room temperature and 260°C [30].

Figures 11 and 12 show that microstructure and temperature had a very systematic influence on the fatigue variability behavior, depending on the degree of sensitivity of crack initiation and growth regimes to these variables. This caused the mean (biased towards the crack initiation controlled, i.e., Type II, mechanism) and the worst-case behavior (crack growth controlled, Type I) to respond very differently to microstructure and temperature.

3.5 An Alternate Paradigm of Fatigue Variability

The vital understanding that follows from the preceding discussion is that, the mean and the worst-case behavior have separate response to operating variables. Therefore, an attempt to increase the mean lifetime (for e.g., by microstructure modification, decreasing the stress level, or decreasing the temperature) may not produce the same effect on the life-limiting behavior. In Ti-6-2-4-6, this seems to be related to the crack growth vs. the crack initiation control of the life-limiting and the mean behavior respectively. An alternate paradigm is proposed that accounts for this dual response of fatigue variability. This is illustrated in Fig. 13. The total lifetime-variability is due to superposition of variability in the worst-case mechanism and in the long-life mechanism. Further, the uncertainty in the worst-case mechanism is controlled by the variability in crack growth lifetime from equiaxed α size scale. This paradigm can be implemented in a life prediction approach, shown in Fig. 9(b) for σ_{max} = 860 MPa. As discussed previously, the worst-case and the long-life mechanisms are plotted as separate distributions in this figure. The simulated lifetimes based on the crack growth and the crack initiation size variability is also shown for comparison. Since failure can occur by either one of the mechanisms, life prediction

can be based on the variability in the worst-case mechanism, i.e., Type I. As illustrated (Fig. 9(b)), this may significantly reduce the uncertainty associated with the traditional approach to life prediction.

4.0 FATIGUE VARIABILITY OF THE NICKEL-BASED SUPERALLOY

4.1 Mean vs. the Life-Limiting Behavior

The fatigue variability behavior of the nickel-based superalloy at 0.33 Hz, 650°C, and the stress ratio, R of 0.05 is presented in Fig. 14. As shown, there was a significant increase in the mean lifetime with decreasing σ_{max}, but the worst-case, as well as the minimum lifetimes, did not change appreciably. This was similar to the response of the titanium alloy and indicated that the mean and the lower-tail behavior were governed by different mechanisms, which continued to diverge with decreasing σ_{max}. The experimental points are plotted in the CDF space in Fig. 14(b). Once again, while the CDF agreed well with data at σ_{max} = 1200 MPa, the agreement broke down at lower stress levels.

Characterization of the failures revealed that the life-limiting distribution was related to failure from surface non-metallic particles. The long-life distribution consisted of the surface-void and the subsurface-non-metallic particle related failures. This is illustrated by Figs. 15 (a) and (b). Unlike the titanium alloy, in this case failure was controlled by the processing related microstructural features. However, the nature of fatigue variability was the same. The separation into the worst-case and the mean-lifetime dominating mechanisms in the superalloy material may be a function of the number density and the size distribution of the relevant microstructural features, and also the surface area vs. the volume of the sample [23]. It is also to be noted that the three competing mechanisms (i.e., failure from (i) surface-non metallic particle, (ii) subsurface non-metallic particle, and (iii) surface-void) are realized, in order of their likelihood to cause failure, in order to produce the observed probabilities of occurrence of each (Fig. 14(a)). For example, depending on the stress level, the subsurface non-metallic particle failure can occur only after all possible conditions for the surface non-metallic particle failure have been exhausted in a given sample although all mechanisms may be operating simultaneously.

4.2 Role of Small and Long Crack Growth in the Life-Limiting Mechanism

In order to determine the contribution of crack growth in the life-limiting mechanism, variability in the small crack-growth behavior of naturally initiated cracks was measured and compared to the long-crack behavior obtained from C-T samples. This is presented in Fig. 16. As shown, the variability in the long-crack growth regime was not very significant. On the other hand, a larger degree of variability was seen in the small-crack regime. The limiting small-crack growth curves, along with the observed range of crack initiation sizes of the life-limiting failures, were used to make deterministic estimates of the bounds on the crack growth lifetimes. The limiting crack growth lifetimes, shown in Fig. 17, described the range in the worst-case lifetimes. As in the case of the titanium alloy, this suggests that the life-limiting failures is controlled purely by crack growth from the relevant microstructural feature.

4.3 Distinction and Similarities between the Behaviors of the Two Materials

Although the titanium alloy and the superalloy failed by different mechanisms, the nature of their fatigue variability behavior was very similar and can be described by the proposed paradigm. In both materials, at higher stress levels, fatigue variability could be described by a single-mode CDF. With decreasing stress level, in both materials, a separation between the

worst-case mechanism and the conventionally expected mean-dominating behavior was seen. Although speculative at this point, in the titanium alloy this response may be produced by activation of heterogeneous deformation mechanisms as the stress level is decreased [32-34] or when the microstructural modification is aimed at increasing the mean lifetime. In the superalloy, the effect of the heterogeneity in terms of the spatial distribution of processing related features seems to be more active at lower stress levels, causing the separation between the life-limiting and the mean behavior. In both materials, the uncertainty in the lifetimes of the worst-case mechanism can be described by the variability in small-crack growth from the relevant microstructural size scale.

5.0 CONCLUSIONS

The following primary conclusions can be drawn from this study:

- The fatigue variability behavior of the $\alpha+\beta$ titanium alloy and the nickel-based superalloy could not be accurately described by the conventional understanding, i.e., based on the mean behavior.
- An alternate paradigm was proposed in which the mean behavior is dominated by a different mechanism than the one controlling the life-limiting behavior.
- The mean-lifetime and the worst-case behavior responded differently to a change in microstructure and stress level therefore, affecting the total lifetime-variability.
- The life-limiting behavior in both materials was controlled by the variability in crack growth lifetimes starting from the relevant microstructural size scale.

Acknowledgements

This work was performed at the Air Force Research Laboratory, Materials and Manufacturing Directorate, Wright-Patterson Air Force Base, OH. The partial financial support of the Defense Advanced Research Project Agency (DARPA) under DARPA orders M978, Q588, P699, and S271 with Dr. Leo Christodoulou as the program manager is gratefully acknowledged. We acknowledge Mr. Phil Buskohl and Ms. Lindsey Selegue for their assistance with the replication-based small-crack growth experiments. We also wish to acknowledge Dr. Amit Shyam, Mr. Chris Szczepansi, Prof. Wayne Jones, and Prof. Tresa Pollock for assistance with the Femtosecond-laser machining.

References

1. E.A. DeBartolo and B.M. Hillberry, *Int. J. Fatigue*, Vol. 23, p. S49, 2001.
2. R. Tryon and A. Dey, *J. Aerospace Engng*., Oct 2001, p. 120, 2001.
3. A. de Bussac and J. C. Lautridou, *Fatigue Fract. Engng. Mater. Struct*., Vol. 16, p. 861, 1993.
4. B.A. Cowles, *Mater. Sci. Engng*., Vol. A103, p. 63, 1988.
5. L. Christodoulou and J.M. Larsen, *JOM*, Mar 2004, p. 15, 2004.
6. D.F. Neal and P.A. Blenkinsop, *Acta Metall*., Vol. 24, p. 59, 1976.
7. J.A. Hall, *Int J. Fatigue*, Vol. 19, p. S23, 1997.
8. G. Lutjering, *Mater. Sci. Engng*., Vol. A263, p. 117, 1997.

9. Y. Mahajan, H. Margolin, *Metall. Trans.*, Vol. 13A, p. 257, 1982.

10. J. Ruppen, D. Eylon, and A.J. McEvily, *Metall. Trans. A*, Vol. 11A, p. 1072, 1980.

11. H. Yokoyama, O. Umezawa, K. Nagai, and T. Suzuki, *ISIJ International*, Vol. 37, p. 1237, 1997.

12. J.M. Hyzak and I.M. Bernstein, *Metall. Trans.* Vol. 13A, p. 33, 1982.

13. J.M. Hyzak and I.M. Bernstein, *Metall. Trans.* Vol. 13A, p. 45, 1982.

14. A. Bruckner-Foit, H. Jackels, and U. Quadfasel, *Fatigue Fract. Engng. Mater. Struct.* Vol. 16, p. 891, 1993.

15. J. Luo and P. Bowen, *Acta Materialia*, Vol. 51, p. 3521, 2003.

16. J. Luo and P. Bowen, *Acta Materialia*, Vol. 51, p. 3537, 2003.

17. T.P. Gabb, J. Telesman, P.T. Kantzos, P.J. Bonacuse, and R.L. Barrie, *NASA/TM-2002 211571*, 2002.

18. T.P. Gabb, P.J. Bonacuse, L.J. Ghosn, J.W. Sweeny, A. Chatterjee, and K.A. Green, *NASA/TM-2000-209418*, 2000.

19. D.A. Jablonski, *Materials Sci. Engng.* Vol. 48, p. 189, 1981.

20. E.S. Huron and P.G. Roth, In: *Superalloys 1996*, 1996.

21. A. de Bussac, *Fatigue Fract. Engng. Mater. Struct*. Vol. 17, p. 1319, 1994.

22. M.T. Todinov, *Computers and Structures*, Vol. 79, p. 313, 2001.

23. K.S. Ravi Chandran and S.K. Jha, *Acta Materialia*, Vol. 53, p. 1867, 2005.

24. S.K. Jha, J.M. Larsen, and A.H. Rosenberger, *Acta Materialia*, Vol. 53, p. 1293, 2005.

25. S.K. Jha, J.M. Larsen, A.H. Rosenberger, and G.A. Hartman, *Scripta Materialia*, Vol. 48, p. 1637, 2003.

26. M.J. Caton, S.K. Jha, J.M. Larsen, and A.H. Rosenberger, In: *Superalloys 2004*, 2004.

27. A. Shyam, C.J. Torbet, S.K. Jha, J.M. Larsen, M.J. Caton, C.J. Szczepanski, T.M. Pollock, and J.W. Jones, In: *Superalloys 2004*, 2004.

28. C.G. Annis, In: *Probabilistic aspects of life prediction*, ASTM STP 1450, W. S. Johnson, and B.M. Hillberry, Eds., ASTM International, West Conshohocken, PA, 2004.

29. S.K. Jha, J.M. Larsen, and A.H. Rosenberger, In: *Fatigue 2006*, 9th International Fatigue Congress, May 14 – 19, Atlanta, GA, 2006.

30. S.K. Jha, J.M. Larsen, and A.H. Rosenberger, to be published.

31. S. Suresh, *Fatigue of Materials*, Cambridge University Press, 1991.

32. A.S. Beranger, X. Feaugas, and M. Clavel, *Mater. Sci. Eng.*, Vol. A172, p. 31, 1993.

33. X. Feaugas and M. Clavel, *Acta Materialia*, Vol. 45, p. 2685, 1997.

34. D.L. McDowell, K. Gall, M.F. Horstememyer, and J. Fan, *Engng. Fract. Mech.*, Vol. 70, p. 49, 2003.

Figures

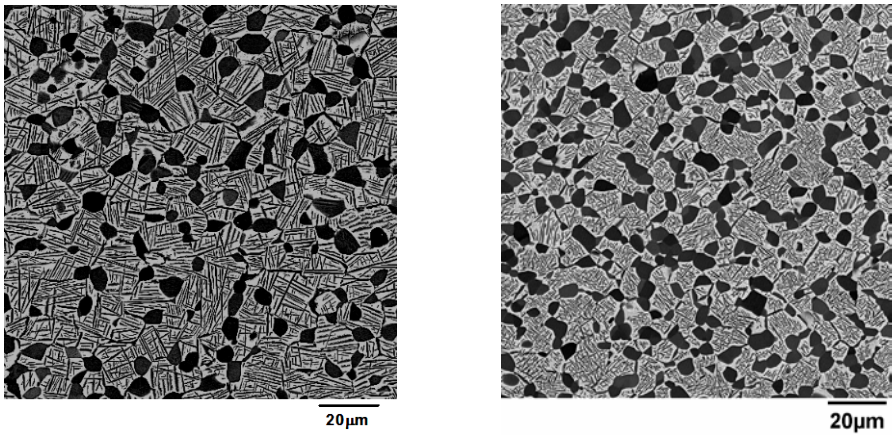

(a) (b)

Figure 1. Microstructures of the Ti-6-2-4-6 alloy; (a) the pancake microstructure, and (b) the disk microstructure.

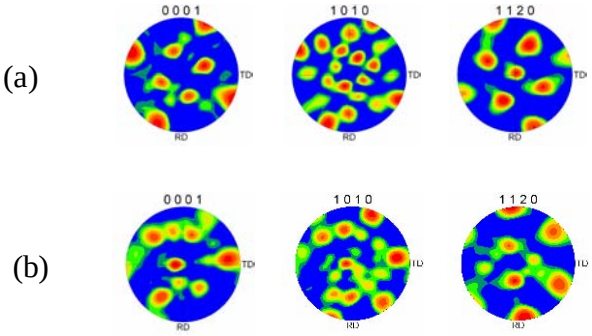

Figure 2. Crystallographic texture of the two microstructures; (a) pancake and (b) disk.

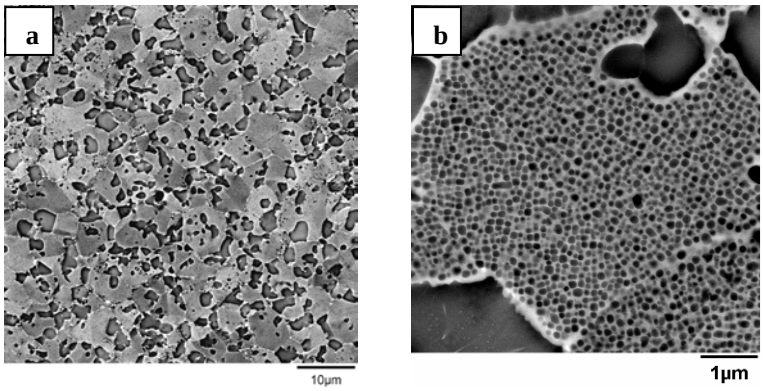

Figure 3. Microstructure of the nickel-based superalloy; (a) the γ-primary γ' structure, and (b) the secondary γ' structure.

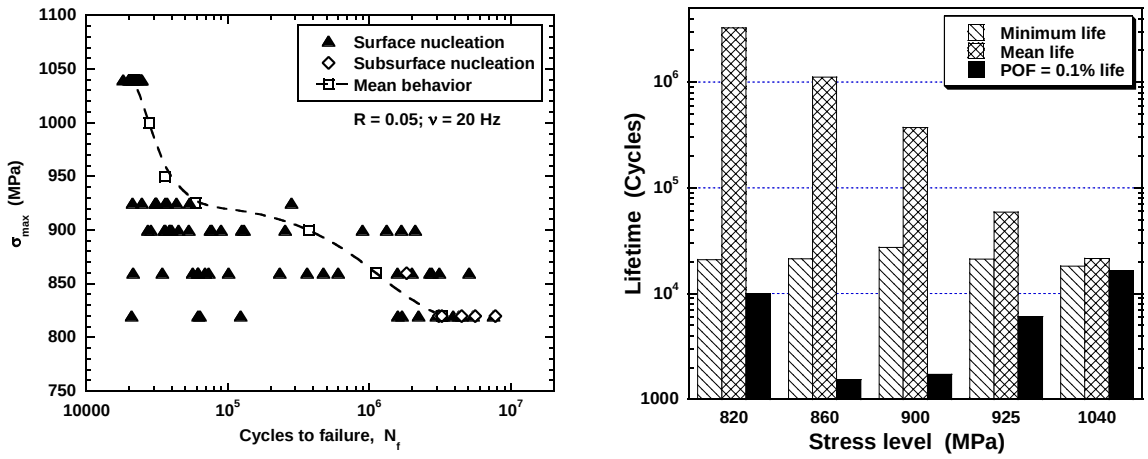

(a) (b)

Figure 4. Fatigue variability behavior of the Ti-6-2-4-6 alloy at 25°C; (a) mean vs. the life-limiting behavior, and (b) comparison of the B0.1 lifetime with the minimum and the mean lifetime.

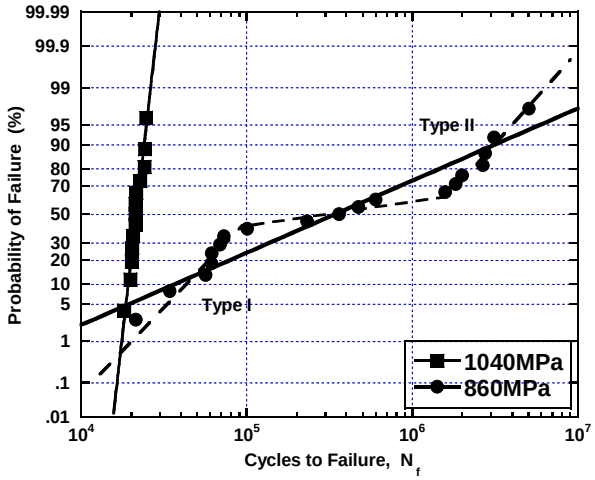

Figure 5. Experimental points plotted in the CDF space showing the step-like behavior at 860 MPa but a good agreement with the CDF at 1040 MPa.

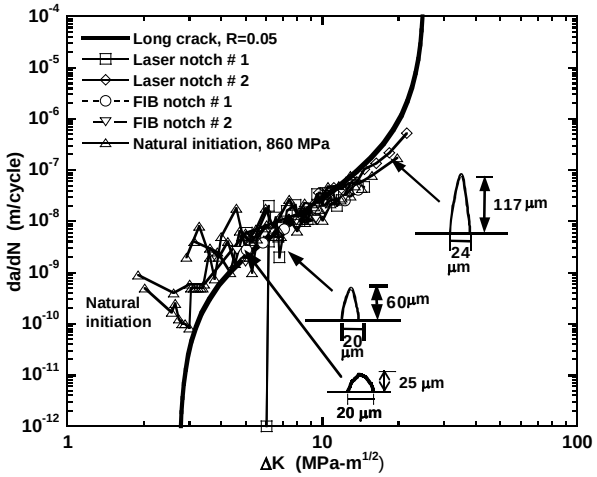

Figure 6. Small-crack growth behavior from notches and naturally initiated cracks in Ti-6-2-4-6.

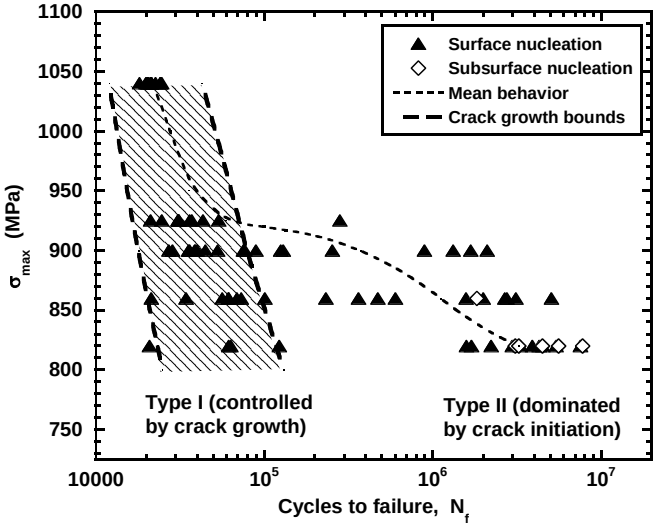

Figure 7. The deterministic range in crack growth lifetimes based on the limiting small-crack growth curves and the limits on the crack initiation sizes.

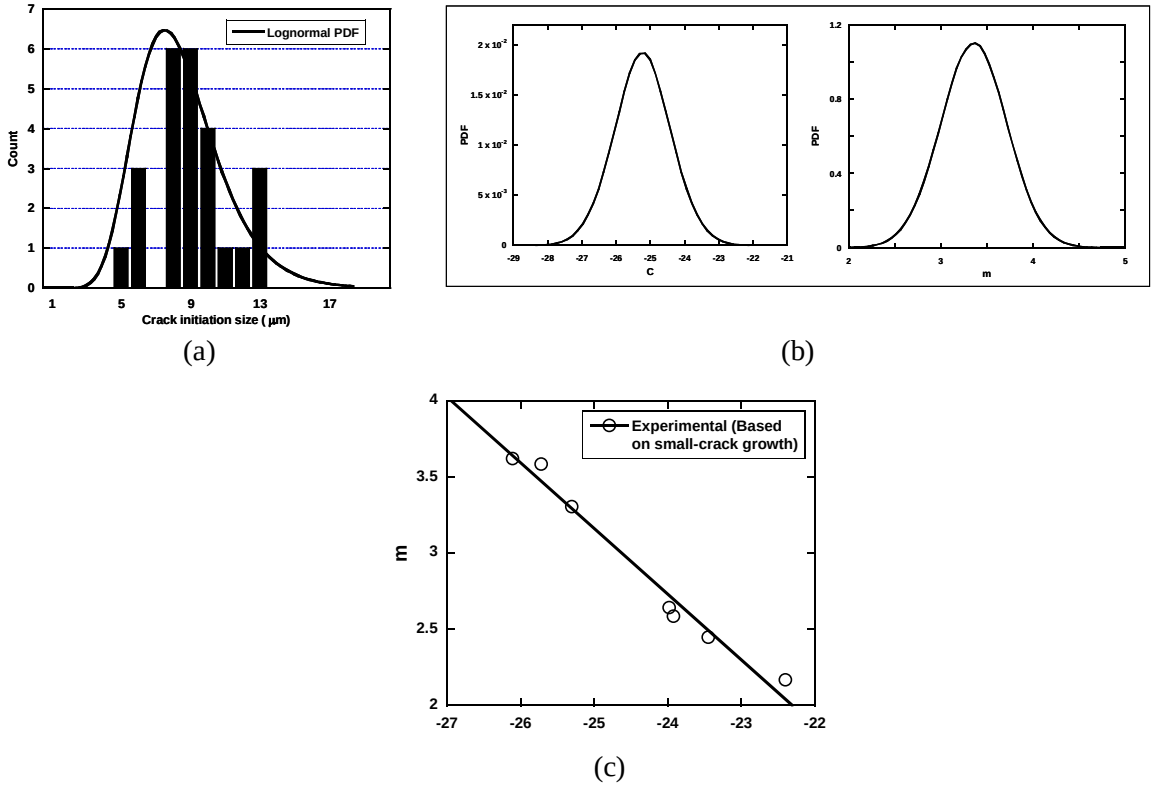

(a) (b)

(c)

Figure 8. Inputs to the Monte Carlo Simulation; (a) Crack initiation size distribution, (b) variability in crack growth behavior, and (c) correlation between crack growth parameters.

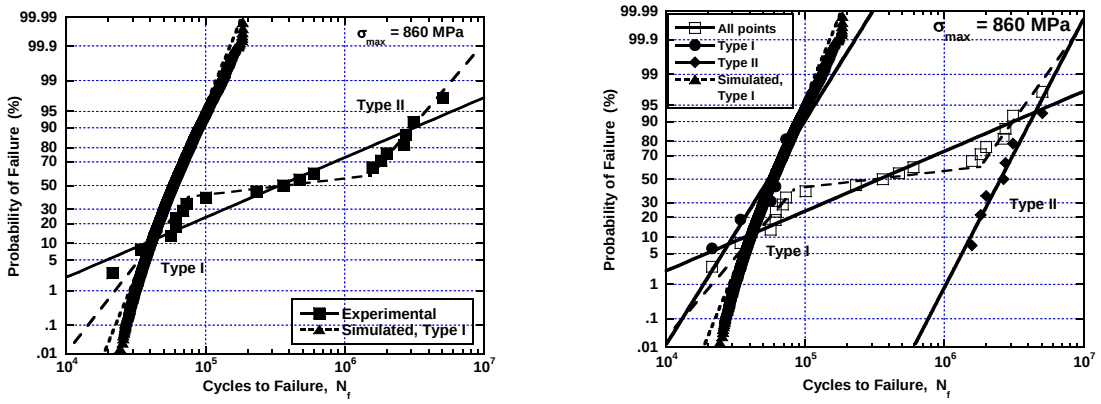

(a) (b)

Figure 9. Simulated vs. experimental lifetimes; (a) comparison of the simulations with the total lifetime distribution, and (b) comparison of variability in the simulated lifetimes and the experimental Type I distribution.

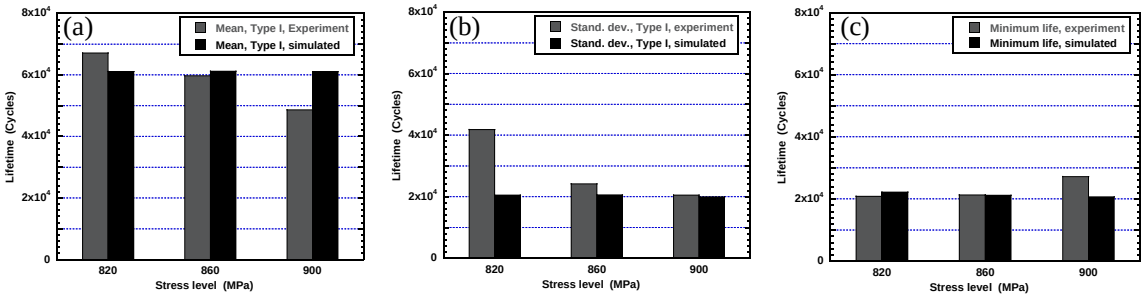

Figure 10. Comparison of the (a) mean, (b) the standard deviation, and (c) the minimum lifetime of the simulations and experimentally observed Type I failures.

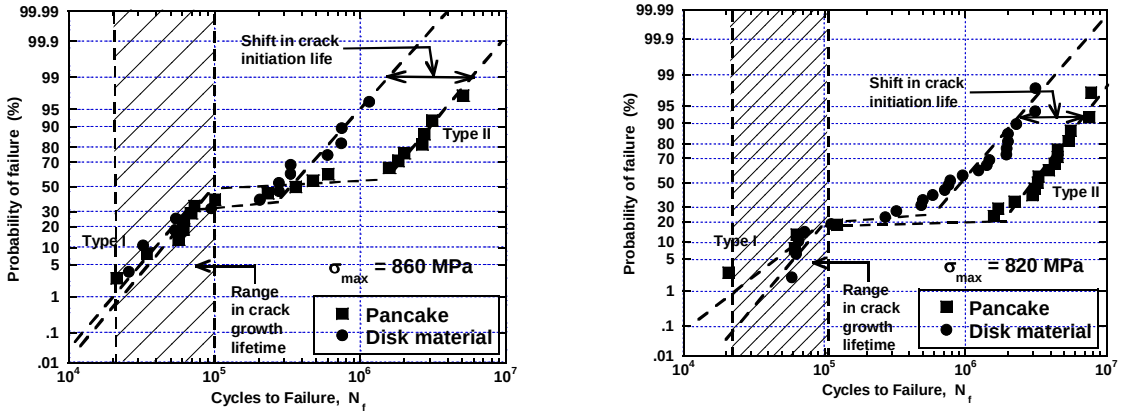

Figure 11. Effect of microstructure on the fatigue variability behavior of Ti-6-2-4-6; (a) σ_{max} = 860 MPa, and (b) σ_{max} = 820 MPa.

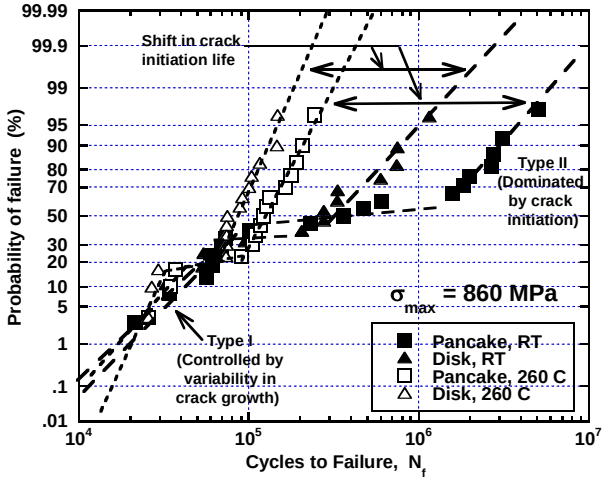

Figure 12. Effect of temperature on the fatigue variability behavior of Ti-6-2-4-6.

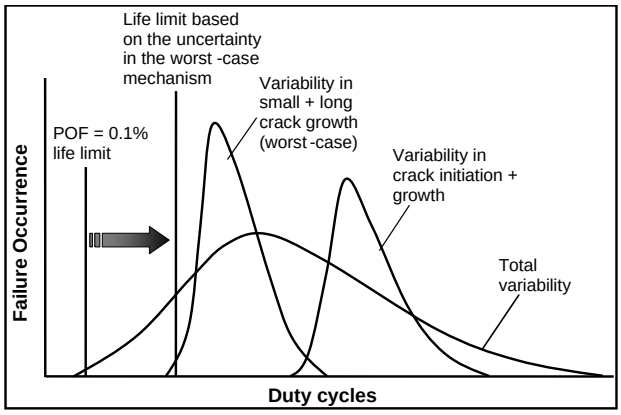

Figure13. Illustration of the proposed paradigm of fatigue variability behavior.

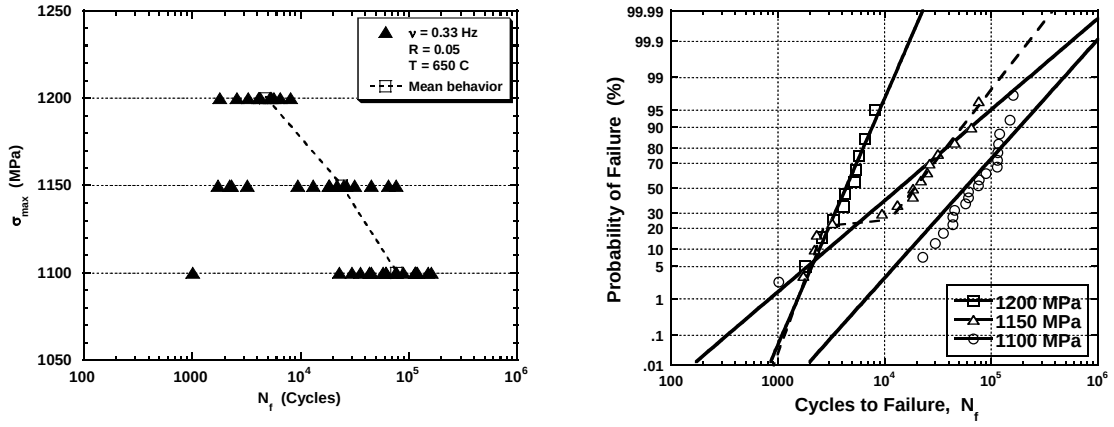

(a) (b)

Figure14. Fatigue variability behavior of the nickel-based superalloy at 650°C; (a) Mean vs. the life-limiting behavior, and (b) Experimental points plotted in the CDF space.

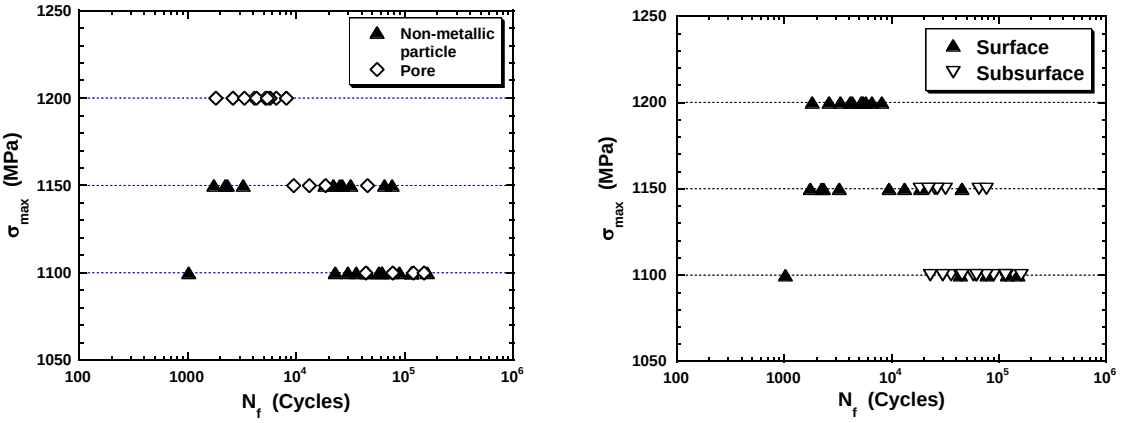

(a) (b)

Figure 15. Competing failure mechanisms in the Ni-based superalloy; (a) Surface vs. subsurface initiated failures, and (b) non-metallic particle vs. void related failures.

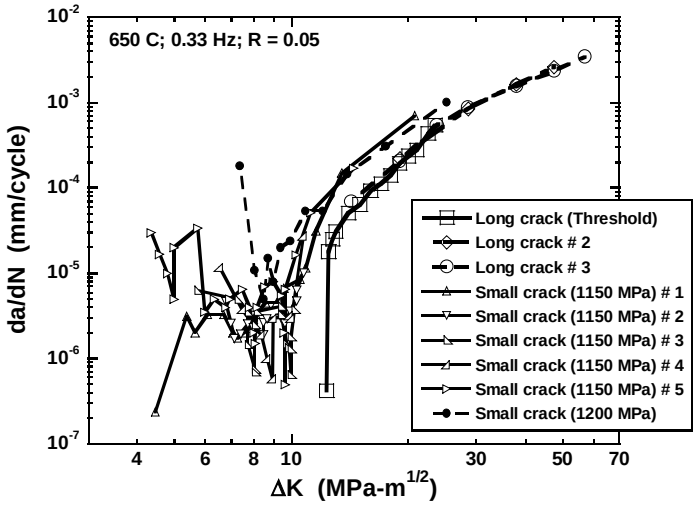

Figure 16. Variability in the small and the long crack behavior of the nickel-based superalloy.

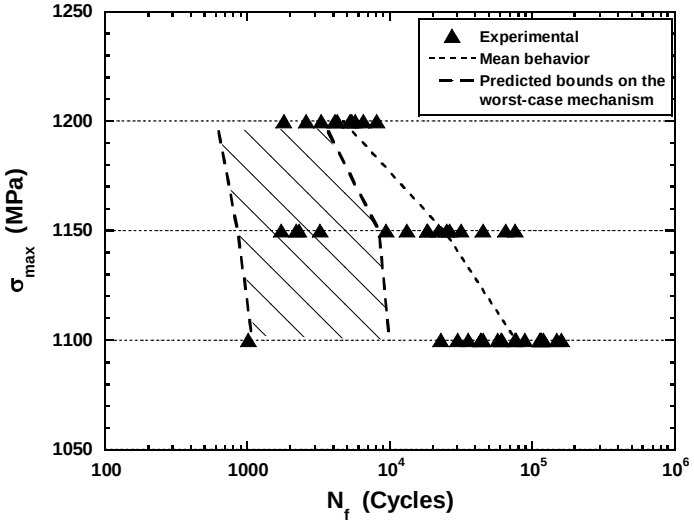

Figure 17. Deterministic range in the crack growth lifetimes in the superalloy material based on the limiting small crack growth curves and the observed range of crack initiation sizes of the life-limiting mechanism.

Chapter II

RANDOM HETEROGENEITY SCALES AND PROBABILISTIC DESCRIPTION OF THE LONG-LIFETIME REGIME OF FATIGUE

S.K. Jha* and J.M. Larsen
US Air Force Research Laboratory, Wright-Patterson Air Force Base, OH 45433, USA
*Universal Technology Corporation, Dayton, OH 45432, USA
Published in: *VHCF-4*, 2007

Abstract

The long-lifetime fatigue regime is suggested to be a probabilistic realization of sequentially occurring mechanisms. We associate these mechanisms with the development of a ranking of heterogeneity scales in the material, with decreasing probability of occurrence in the order of increasing scale, at any given loading condition. The underlying drivers for these heterogeneity levels are an array of randomly occurring microstructural configurations. With respect to the $\alpha+\beta$ titanium alloy, Ti-6Al-2Sn-4Zr-6Mo (Ti-6-2-4-6), we identify four microstructural configurations producing different degrees of heterogeneous behavior. At lower stress levels, these configurations present probabilities of failure by a crack-growth-controlled, life-limiting mechanism, and a group of long-lifetime mechanisms. This description of the long-lifetime regime seems to explain the increased incidence of subsurface failures with decreasing stress level, as well as the microstructural neighborhoods involving crack initiation in short and long-lifetime mechanisms and those related to surface and subsurface failures.

Keywords: Heterogeneity scales, Microstructural configuration, Probabilistic description, fatigue variability, Ti-6Al-2Sn-4Zr-6Mo, long-lifetime regime, life-limiting mechanism.

1.0 INTRODUCTION

Characterization and understanding of the fatigue behavior in the long-lifetime regime is essential to meet the demand for increased durability of gas turbine engine components [1], as well as, realizing safe operation in the ultra-long cycle regime in many current and emerging applications [2, 3]. In particular, there is a need for a quantitative physics-based analysis of long-lifetime fatigue [4] in order to remove empiricism from life-prediction and management approaches in fracture critical applications [4, 5].

There has been an increased interest in the very high cycle fatigue (VHCF) regime in the recent years [6, 7]. The capability to conduct fatigue tests by ultrasonic excitations has enabled significantly faster experimentation and characterization of behavior beyond 10^7 cycles [6-9]. It is widely accepted that the conventional fatigue limit does not extend to longer lifetimes [10-12]. Often, depending on the material, the long-lifetime regime is accompanied by a step in the stress vs. lifetime (S-N) behavior, which is attributed to a switch in the crack initiation mechanism at lower stress levels [10-12]. In most cases, this change in mechanism has been reported to be associated with a shift from surface to subsurface crack initiation [12-14]. In particular, subsurface crack initiation has been related to non-metallic particles in many studies [10, 12, 13]. This behavior has been explained through existence of multiple thresholds corresponding to initiation of fatigue by each mechanism [11].

The above descriptions of fatigue in the long-lifetime regime seem to relate to the average behavior. Therefore, the understanding of the effect of microstructure and loading variables on fatigue lifetime in this regime has been largely deterministic. A probabilistic description of the long-lifetime behavior appears attractive, given the variable nature of fatigue, but perhaps more so, from a life-prediction perspective. This is owing to an increasing need in the aircraft industry for move towards probabilistic life-prediction, especially, physics-based methodologies [5]. This will remove the large degree of uncertainty in life prediction that might occur in traditional, uncertainty-factor-based design approaches [14]. A probabilistic understanding of fatigue behavior in the long-lifetime regime may therefore, naturally lend itself to emerging life-prediction and life-management practices [5].

Towards a probabilistic description, the competition between mechanisms, in which the final failure in any given loading regime is suggested to occur by the mechanism that produces the shortest lifetime, has been recognized in several studies [11, 12]. Its effect on producing separation of life-limiting and the mean-dominating behavior in the fatigue variability response [15-17] and causing dual S-N curves [18] has been reported recently. Besides the relatively known population of grains and microstructural features, random microstructural neighborhoods and their interaction with the fatigue variability response are relatively unexplored.

Here, we discuss a probabilistic approach to describing the long-lifetime fatigue behavior, and the effect of microstructure and loading variables on the long-lifetime regime of the $\alpha+\beta$ titanium alloy Ti-6-2-4-6. By long-lifetime we mean lifetimes in the range of 10^6 to 10^7 cycles which are not in the very high cycle fatigue (VHCF) regime in the strictest sense, but the same concepts are applicable beyond 10^7 cycles. We show that the long-lifetime fatigue is a result of fatigue variability behavior arising due to sequential probability of occurrence of mechanisms, in order of decreasing level of underlying heterogeneous deformation. Our emphasis has been on identifying the randomly occurring microstructural configurations associated with the heterogeneous response and their relationship to fatigue variability behavior at lower stress levels.

2.0 MATERIALS AND EXPERIMENTAL PROCEDURE

The materials in this study were two similar microstructures of the $\alpha+\beta$ titanium alloy, Ti-6-2-4-6. These are shown in Fig. 1 (a) and (b) respectively. We designate these as microstructures A and B, as indicated. The microstructures differed slightly in terms of the primary-α structure, in that there was a small increase in the volume fraction of equiaxed-α in microstructure B, along with occasional clusters of a few equiaxed-α grains. The lath-α size in microstructure B was much smaller than in microstructure A, as evident from Fig. 1. In terms of texture, reported in [17], the differences between the two microstructures were more apparent. Particularly, there was greater tendency for the basal and the prismatic poles to be parallel to the loading axis in microstructure B [17].

Some of the experimental procedures in this study have been reported in [15, 17]. The crack initiation facet angles, with respect to the loading axis, were measured using the MeX^{TM} (a trademark of Alicona Imaging GmbH) 3D image analysis program. Stereo-image pairs at relative tilt of 7° were recorded for this purpose using a Lecia S360FE Scanning Electron Microscope. The crack initiation neighborhoods in selected samples were analyzed by sectioning the crack-initiation region using focused ion beam (FIB) machining. A FEI-NOVA^{TM} dual beam FIB system was used for this purpose. A Ga ion beam was employed at the accelerating voltage

of 30 kV and the current of 9.3 nA. The FIB sections were made either parallel or perpendicular to the fracture surface. The sectioning step-size was such as to preserve part of the crack initiating grain. The sectioned planes were then characterized by Electron Back Scattered Diffraction (EBSD) to determine the orientation of the crack initiating grain and the surrounding neighborhood. The inverse pole figure (IPF) plots and maps were constructed using the TSL^{TM} analysis software.

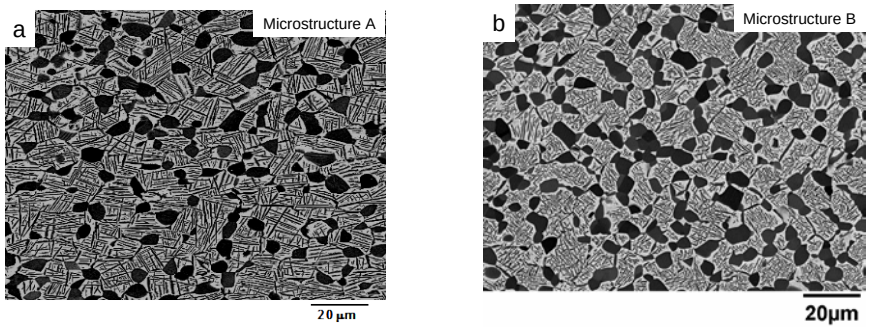

Figure 1. Back-scattered electron (BSE) images of (a) microstructure A and (b) microstructure B of Ti-6-2-4-6.

Probabilistic Description of the Long-Lifetime Regime

The observed long-lifetime fatigue response, producing two-stage S-N curves [11, 12] or failures (in the $10^7 - 10^9$ cycles range) by appearance of a different mechanism such as subsurface-inclusion based crack-initiation [7, 10], can be suggested to be a special case of a more general fatigue variability behavior. In particular, we propose that nominally elastic loading produces a ranking of heterogeneity levels in a material, even under the same loading condition. By heterogeneity levels we imply the scale or intensity of localized plastic deformation as caused by randomly existing microstructural neighborhoods. Borrowing the concepts from statistical-physics [19], higher the level of heterogeneity, the smaller is the probability of its occurrence in a sample. It also follows that, for a given crack initiation location (surface or subsurface), the higher the rank of the heterogeneity associated with a mechanism, the shorter is the lifetime.

The above description supposes that deformation can be concentrated in several random microstructural configurations. In a later section, we identify these configurations in Ti-6-2-4-6. The incidence of a given lifetime-range, therefore, may be less dependent on reaching the threshold for a damage accumulation method [11], but controlled by the probability of a microstructural configuration that would produce the necessary heterogeneity level for crack initiation and early propagation. This suggests that, the behavior in the long-lifetime regime corresponds to probabilistic realizations of sequential failure mechanisms, signifying the possibility of both short and long-lifetimes for given microstructure and loading variables.

Long-Lifetime Regime in Ti-6-2-4-6

The fatigue variability behaviors of microstructures A and B of Ti-6-2-4-6 at room temperature are presented in Fig. 2 (a). The deterministic crack growth lifetime limits are superimposed in the figure. The calculations of crack growth bounds were based on the limiting small crack growth curves, shown in Fig. 2(b), and the range in the observed crack initiation sizes [20]. As illustrated in the figure, power-law fits to the small crack data representing the fastest and the slowest crack growth rates were taken as the limiting curves. The crack initiation

sizes were measured from the fracture surface and corresponded to the crack initiation facet present at the origin of the crack [20]. The crack growth behaviors of the two microstructures were similar. Therefore, the calculated lifetime bounds can be considered applicable to both cases.

Figure 2 indicates that, in both microstructures, the mean-lifetime behavior (designated as Type II in the figure) diverged from the crack-growth-controlled life-limiting behavior (designated as Type I) as the stress level was decreased. In [15-17] we describe this behavior by a bimodal probability density. This separation produced up to 500X variability in lifetime at the same stress level. The long-lifetime fatigue regime could, therefore, be a manifestation of decreased probability of occurrence of a microstructural configuration in the specimen surface to enable a purely crack-growth-controlled mechanism. Other mechanisms in the sequence can emerge with varying probabilities, producing much longer lifetimes. However, the latter mechanisms need not be related only to subsurface crack initiation, as evident in Fig. 2(a). According to the suggested probabilistic description, these longer-lifetime mechanisms might be, related to either a smaller heterogeneity scale (therefore, more frequently distributed) at the surface or a larger heterogeneity level (therefore, unlikely to occur at the surface) occurring in the subsurface.

It is also to be noted that the transition from surface to subsurface failure is not abrupt but gradual, with increasing probability of subsurface mechanism occurring with decreasing stress. Szczepanski, et al. [21] show that this trend continues into the 10^7 – 10^9 cycles regime.

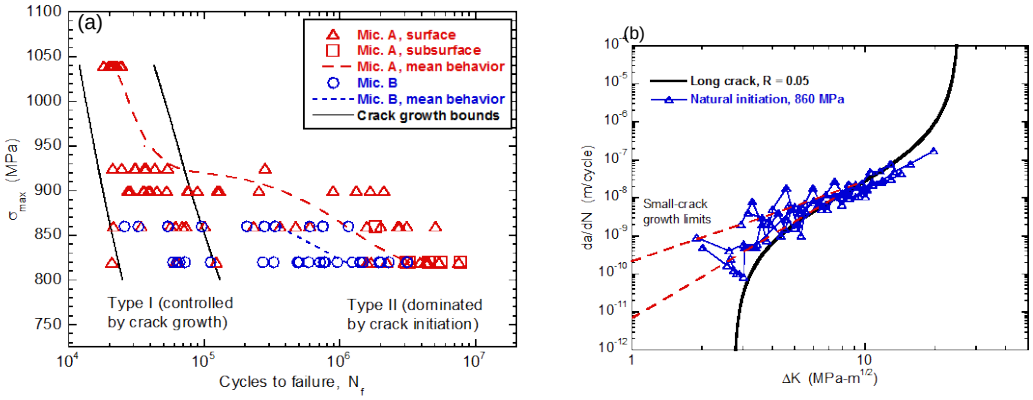

Figure 2. Divergence of the mean-dominating mechanisms from the crack-growth-controlled life-limiting behavior in Ti-6-2-4-6; (a) fatigue variability behavior of microstructures A and B and (b) The small crack growth rate limits used in the calculation.

Different Heterogeneity Scales

Here we attempt to reveal the possible heterogeneous configurations underlying the life-limiting and the long-lifetime (or the mean-dominating) mechanisms. At moderate temperatures, slip in the α phase is considered as the primary deformation mode in α+β titanium alloys [22, 23]. The soft deformation modes are known to be slip in a prismatic <a> system, followed by the basal <a> slip [22]. The deformation in the c-direction of the HCP crystal is accounted by <c+a> slip, which is a significantly harder slip mode [23, 24] when compared to the <a> modes. Although the slip mechanisms in the lamellar α/β colonies are not fully understood, deformation is thought to be accomplished by either prismatic slip parallel to the α/β interface or basal slip

across the interface [22, 24]. The later is made possible by the Burger's orientation relationship in the lamellar region: $(0001)_\alpha$ // $\{110\}_\beta$ and $<11\bar{2}0>_\alpha$ // $<111>_\beta$.

Heterogeneity Neighborhoods Associated with Surface Crack Initiation

Typical surface crack initiation regions in Type I (life-limiting) and Type II (mean-lifetime dominating) mechanisms at 860 MPa are shown in Fig. 3(a) and (b) respectively. The crack initiated across an equiaxed-α grain, producing a facet at the crack origin in both mechanisms, as shown. In some cases (especially in Type II failures) more than one facet was seen. Clearly, any differences between the underlying microstructural configurations in the two cases cannot be conclusively ascertained from the fracture surfaces.

A comparison of the surface crack initiation size distribution and the nominal equiaxed-α size distribution revealed that the crack initiation sizes were displaced slightly to the right of the nominal distribution of the equiaxed α [20]. However, the critical facet size was not in the extreme right tail, especially considering that the measured facet area usually represents the largest plane across the grain as opposed to random sections in a nominal measurement [25]. Also, there was no clear trend in the crack initiation size with respect to the lifetime [20]. These results seem to reinforce the important roles of the orientation of the crack initiating grain (besides the size) and the local neighborhood in crack initiation.

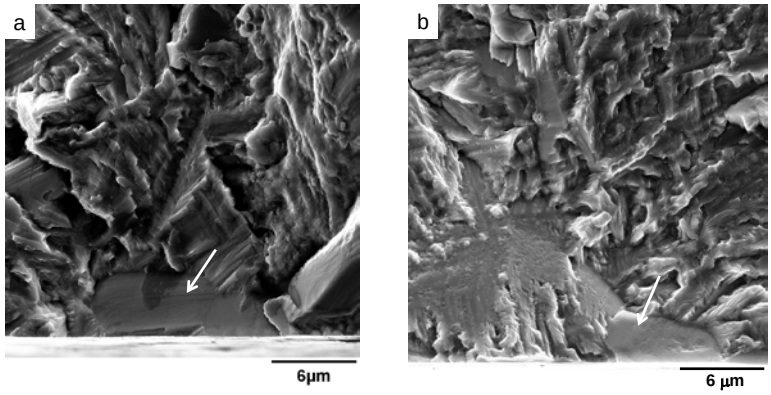

Figure 3. Typical crack initiation morphology in (a) a Type I mechanism tested at 860 MPa that failed in 72,977 cycles and (b) a Type II mechanism tested at 860 MPa and having the lifetime of 2,755,245 cycles.

In Fig. 4, the angle of the crack initiation facet normal with the loading axis (indicated as θ in the figure) is plotted with respect to lifetime for the two microstructures of Ti-6-2-4-6. The data points correspond to the applied stress levels of 860 and 820 MPa. As shown, irrespective of lifetime, surface crack initiation facets in microstructure A were at an angle of about 35 - 45° from the loading axis. The spread in the angles was slightly larger in microstructure B. Figure 4 indicates that, in both Type I and Type II surface crack initiation, these facets were oriented for close to maximum shear, i.e., slip deformation.

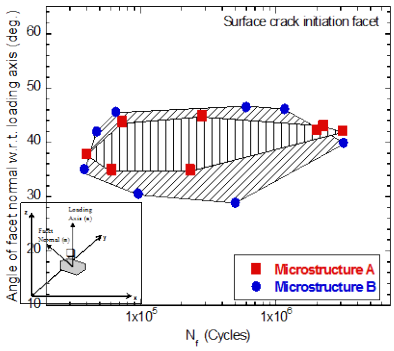

Figure 4. Crack initiation facet angle with respect to the loading axis.

Examples of FIB sections of the crack initiation region in a Type I and a Type II mechanism are shown in Figs. 5 and 6 respectively. The crack origin in a sample tested at 860 MPa that failed in 61,162 cycles (Type I) is shown in Fig. 5(a). The crack initiation facet is indicated in the figure. The facet angle with respect to the loading axis was 35.02°. In this case, the FIB surface was parallel to the fracture surface. The Inverse Pole Figure (IPF) map (in the loading direction) from the FIB sectioned plane is shown in Fig. 5(b). The crack initiating equiaxed-α grain is identified in the figures. The IPF map indicates that the crack initiating grain had a close to basal orientation with respect to the loading axis. This would mean that, in Type I failures, the crack initiation facet may be formed by a <c+a> hard slip mechanism.

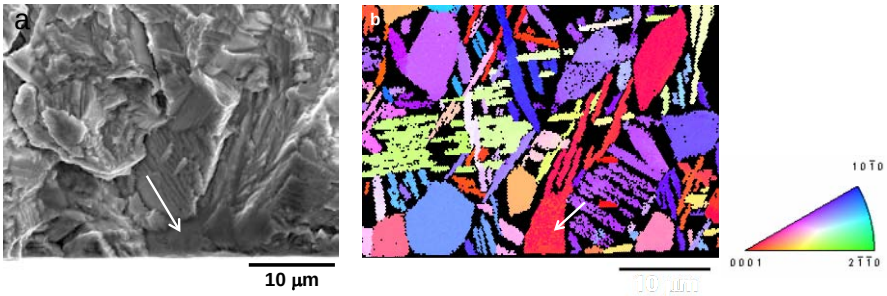

Figure 5. FIB sectioning and OIM analysis of crack initiation region in a Type I failure; (a) the crack initiation region and (b) IPF map, in the loading direction, of the FIB plane (machined parallel to the fracture surface).

The crack initiation region in a Type II failure at 860 MPa is shown in Fig. 6(a). The lifetime in this case was 1,996,709 cycles. The crack initiation facet is indicated. The facet angle with respect to the loading axis was 42.33°. In this sample, the FIB section was made perpendicular to the fracture surface, at about 2 µm from the sample edge, as indicated by the dashed line. Only a part of the crack initiating α grain was sectioned through, as illustrated. The partially sectioned crack initiating α grain is indicated by the arrow. The IPF map, in the direction of the loading axis, is shown in Fig. 6(b). Clearly, in this case, the crack initiating α grain does not have a basal orientation with reference to the loading axis, unlike the Type I mechanism.

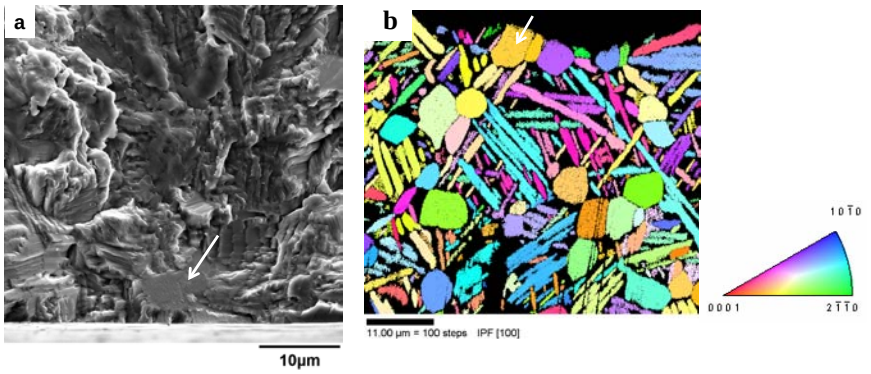

Figure 6. Analysis of the crack initiation region in a Type II failure; (a) fracture surface showing the crack initiation region, (b) IPF map of the FIB plane in the loading direction.

The orientation of crack initiating α grain in three Type I, and a Type II failure, measured by the procedure described above, are plotted in stereographic triangles in Fig. 7. The Schmid Factor (SF) contour lines [24] are superimposed in these figures. The SF contours for prismatic <a>, basal <a>, 1st order pyramidal <c+a>, and 2nd order pyramidal <c+a> are shown in Figs. 7 (a), (b), (c), and (d) respectively. Firstly, as expected from the IPF maps, the Type I points (indicated by the circular symbol) plot close to the basal pole. Furthermore, Figs. 7(a) and (b) indicate that the crack initiating α-grains, in the Type I mechanism, were not in the high SF regions for either prismatic <a> or basal <a> slip. On the other hand, Figs. 7(c) and (d) indicate that these points were very close to maximum SF for either 1st order or 2nd order pyramidal <c+a> slip (both being significantly harder slip modes compared to the prismatic <a> and the basal <a> slip). The crack initiating grain in the Type II mechanism (indicated by the square symbol in Fig. 7) was oriented close to maximum SF for the soft, basal <a>, slip (Fig. 7(b)).

From the argument of different heterogeneity levels, it is known that an α grain oriented for hard slip, surrounded by soft grains or colonies presents a location of significant stress concentration [22, 23]. This kind of microstructural configuration can be considered to be a higher ranked heterogeneity scale than a favorably oriented primary-α, as in the Type II mechanism.

The poles representing the α lath (in lamellar colonies) and the primary-α grains, neighboring the crack initiating α grain in the two mechanisms, were also plotted in stereographic triangles. The purpose was to determine the possible deformation characteristics of the neighborhood in relation to the crack initiating grain that would highlight further differences between the two mechanisms. This is shown in Figs. 8 and 9 for Type I and Type II mechanisms respectively. The contour lines representing SF for prism <a> and basal <a> slip are superimposed in Fig. 8 (a) and (b) respectively. In Fig 8, neighboring grains from the three Type I samples, as in Fig. 6, are plotted. The lath-α is represented by the circular symbol and the equiaxed-α grain is shown by the square symbol. In the Type I mechanism (Fig. 8), almost all neighboring grains from the three samples were away from the hard <c+a> slip mode (i.e., away from the basal orientation). It is also striking that none of the neighboring poles, in the Type I mechanism, plot near the $(2\bar{1}\bar{1}0)$ plane (Fig. 8).

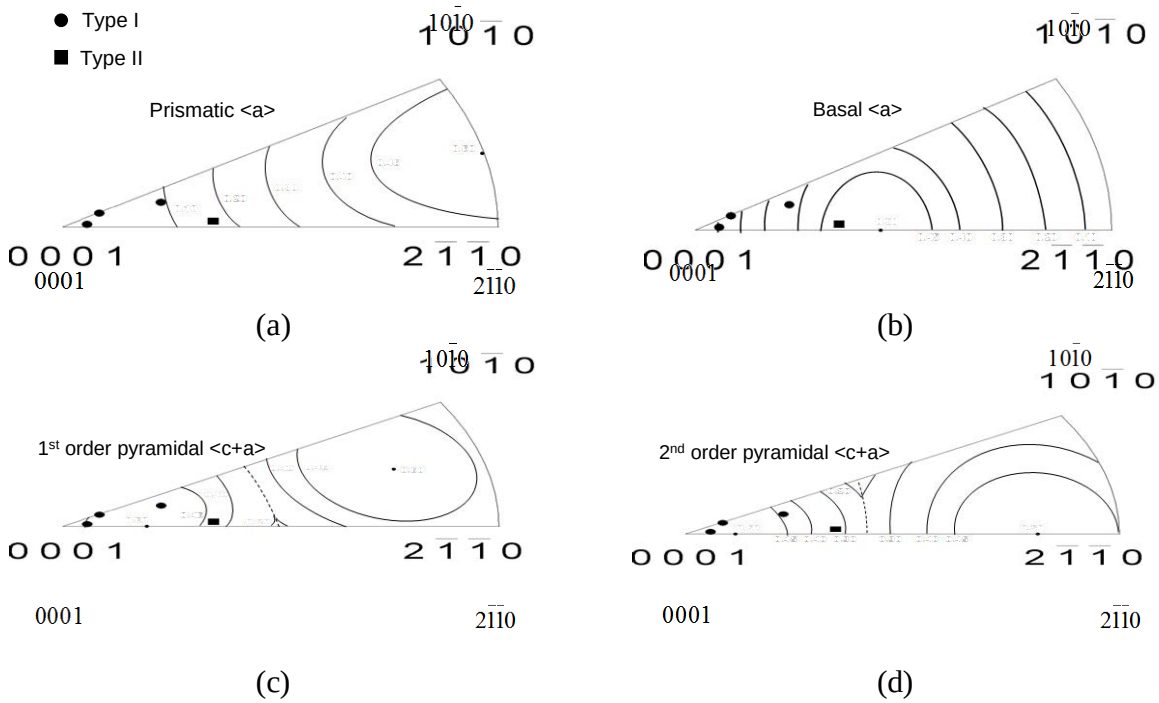

Figure 7. Deformation mechanisms of crack initiating primary-α grain in Type I and Type II mechanisms with the help of SF contour maps for (a) prismatic <a> slip, (b) basal <a> slip, (c) 1st order pyramidal <c+a> slip, and (d) 2nd order pyramidal <c+a> slip.

As stated before, slip in lamellar colonies is said to occur by prismatic <a> mode (in α-lath) along the interface, or basal <a> slip across the colony due to alignment of $(0001)_\alpha$ and $(110)_\beta$ slip planes per the Burger's relationship [22]. Accordingly, only one out of the three possible prismatic <a> slip systems can be active in the lamellar phase [22]. Therefore, high SF for prismatic <a> slip is a necessary but not the sufficient condition for slip. However, all of the three basal <a> systems can be active, provided the α-lath is oriented for the basal slip [22]. Figure 8(b) indicates that a majority of the neighboring lath-α, in the Type I mechanism, plot between SF of about 0.35 and 0.5 for basal <a> slip, implying that these neighboring colonies were oriented for easy deformation mode. The remainder of α laths (total of 7) shows high (between about 0.4 and 0.5) SF for prismatic <a> slip, as indicated by Fig. 8(a). However, in order to confirm that these neighboring colonies were "soft", it needs to be ascertained if the prismatic planes in these laths are parallel to the α/β interface. Figures 8 (a) and (b) also indicate that most of the neighboring primary-α (square symbols) grains, in the Type I mechanism, were oriented for either prismatic <a> or basal <a> slip. Although it remains to be verified if the prismatic <a> systems in laths with high SF for that slip are parallel to the α/β interface, it appears that the microstructural neighborhood in Type I mechanism consists of a hard primary-α grain surrounded by soft lamellar colonies and primary-α. This is also consistent with suggestions in other studies [22, 23] that this kind of configuration presents enhanced stress concentration at the basal-oriented primary-α due to strain incompatibility with the easily deforming neighborhood. Crack initiation in the Type I mechanism can be suggested to occur by cracking across a pyramidal plane in a close to basal-oriented primary-α that is surrounded by "easy-slip" colonies and equiaxed-α grains.

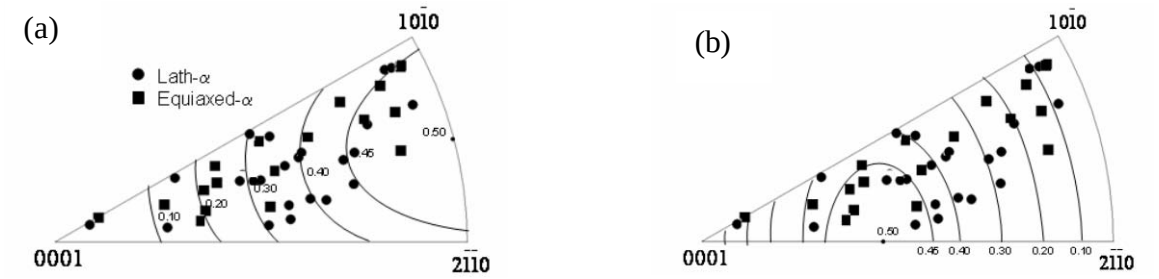

Figure 8. Possible slip behavior of lath and equiaxed α neighboring the crack initiating grain in Type I failures; (a) prismatic <a> contour map and (b) basal <a> contour map.

The poles of lath-α and primary-α neighboring the crack initiating grain in the Type II mechanism are plotted in Fig. 9. The closed circles represent the lath-α and the closed squares indicate the equiaxed-α grains. In this case, again, almost all neighboring α laths and grains are away from the hard, basal orientation. There is an equal mix of lath-α with high SF for basal <a> and those with high SF for prismatic <a> slip. We haven't determined if the ones oriented for prismatic <a> slip satisfy the condition for easy deformation of the colony. It is, therefore, hard to draw conclusions towards the extent to which these neighboring colonies and grains played a role in crack initiation in the Type II mechanism. It seems clear, however, that in the Type II surface initiated failures, crack initiated by slip accumulation in a (or a few) favorably oriented (for basal <a> slip) α grain(s). This is similar to the conventional slip band cracking mechanism that is associated with the creation of surface steps [11].

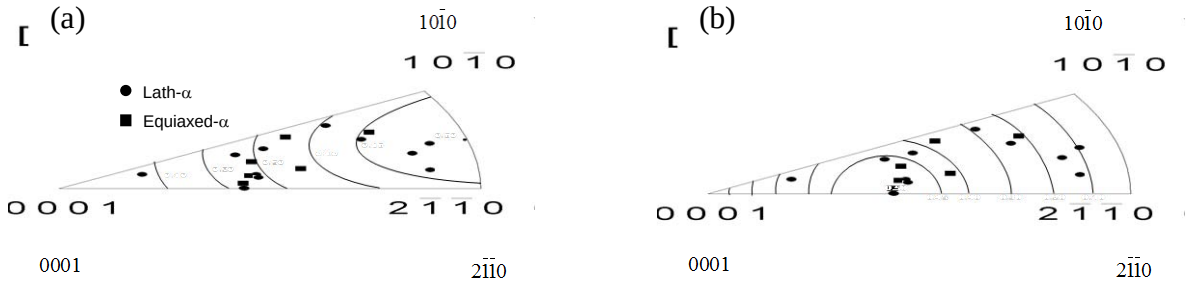

Figure 9. Possible slip mechanisms of lath and equiaxed-α neighboring the crack initiating grain in a Type II failure; (a) prismatic <a> SF contours and (b) basal <a> SF contours.

Heterogeneity Scales Associated with Subsurface Crack Initiation

As shown in Fig. 2(a), in addition to surface crack initiation, the mean-dominating (Type II) distribution also comprised of the subsurface initiated mechanism. Two different kinds of subsurface crack initiation characteristics were observed. Examples of these are presented in Figs. 10 and 11. In the first (Fig. 10(a)), the crack initiation facet appeared to correspond to a cluster of equiaxed α and lamellar α/β colonies producing a continuous, relatively large crack initiation facet. The angle of this facet with respect to the loading axis was measured at multiple locations (labeled in Fig. 10(a)). The measurements are shown in Fig. 10(b) and indicate that the angles were very similar at each of the locations, confirming that the crack initiation facet is continuous. The average angle with respect to the loading axis was about 44° suggesting that the facet was formed due to continuous slip in a microstructural cluster that included equiaxed-α and lamellar colonies. We have not yet analyzed the crystallographic direction of the facet

constituents with respect to the loading axis. However, it can be suggested that the slip planes of the constituent phases in the facet were aligned.

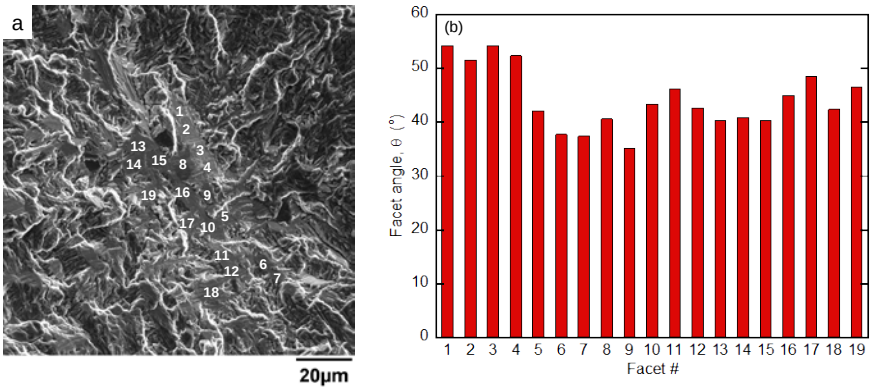

Figure 10. Subsurface crack initiation by a cluster producing continuous facet plane (σ_{max} = 820 MPa, N_f = 3,088,204); (a) the crack origin and (b) facet angles at the locations labeled in (a).

The second subsurface crack initiation characteristic observed in Ti-6-2-4-6 is shown in Fig. 11(a). In this case, we observe a cluster of equiaxed-α grain facets, over a relatively large region, at the crack origin. Szczepanski, et al [22] have also identified this as the predominant subsurface crack initiation mechanism at ultrasonic loading frequencies. The angles of these facets, with respect to the loading axis, are shown in Fig. 11(b). Once again, all facets belonging to the cluster were oriented similarly and the angles were in the range of about 31-53°, i.e., close to maximum shear. Szczepanski and coworkers [22] have determined that most of the facet-forming equiaxed-α grains were close to basal <a> slip orientation. The lifetimes in this subsurface crack initiation configuration were generally longer than the one shown in Fig. 10.

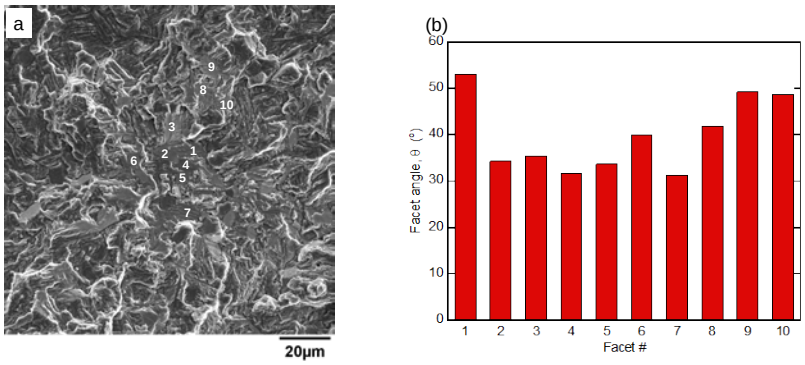

Figure 11. Subsurface crack initiation by a primary-α cluster (σ_{max} = 820 MPa, N_f = 4,487,636); (a) the crack origin and (b) facet angles.

Ranking of Heterogeneity Scales

Based on the above discussion, in Ti-6-2-4-6, at least 4 heterogeneity levels can be identified. The underlying microstructural configurations are schematically illustrated in Fig. 12. In the order of decreasing intensity of deformation accumulation, these are: (i) Cluster of equiaxed-α and lamellar α/β colonies with aligned slip planes and oriented for close to maximum shear, (ii) Cluster of equiaxed-α grains, each similarly oriented for basal <a> slip, (iii) A hard equiaxed-α (oriented for pyramidal <c+a> slip) surrounded by soft lamellar colonies and

primary-α, and (iv) A (or a few) favorably oriented (for basal <a>) equiaxed-α grain(s). It follows from our earlier argument that, the probability of occurrence of these configurations will decrease in the order of increasing scale of heterogeneity.

Recognizing the difference between the free surface and the subsurface location with respect to fatigue, the four heterogeneous configurations in Fig. 12 can be arranged into at least 8 possible failure mechanisms. However, due to decreasing probability of occurrence with increasing heterogeneity level, it seems that only 4 mechanisms (2 surface-initiated and 2 subsurface) were observed in the given number of tests. The ranking of heterogeneity levels and the associated probabilities seems to explain the observation that the two surface-initiated mechanisms corresponded to two relatively smaller scale configurations (Fig. 12).

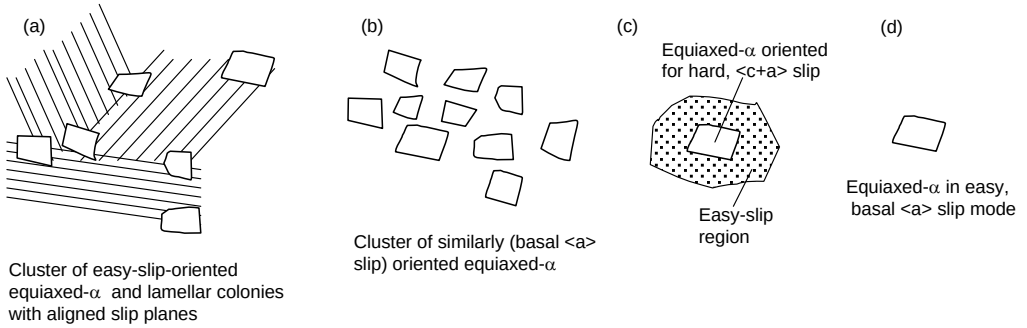

Figure 12. Illustration of randomly occurring microstructural configurations in Ti-6-2-4-6 producing a ranking of heterogeneity scales.

The ranking of heterogeneity scales and their interaction with surface and the subsurface location can be suggested to produce the following sequence of mechanisms in this study: (i) surface initiated failure from a hard primary-α (Fig. 12(c)), (ii) surface crack initiation in a (or a few) favorably oriented primary-α (Fig. 12(d)), (iii) subsurface crack initiation from a cluster of equiaxed-α and lamellar colonies (Fig. 12(a)), and (iv) subsurface crack initiation from an equiaxed-α cluster (Fig. 12(d)). It is to be noted that, the probabilities of occurrence of any given level of heterogeneous deformation will decrease with decreasing stress level, implying a continued shift towards failures by higher ranked random microstructural configurations. This may explain the increased incidence of subsurface initiated failures with decreasing stress level. However, the occurrence of the surface initiated mechanism in the very long-lifetime regimes cannot be ruled out. In those regimes, surface failures can be realized by higher ranked heterogeneity scales, for example, by a cluster of similarly oriented primary-α. Although the probability of occurrence of such mechanism at the surface will decrease for a larger scale of associated microstructural configuration, this ought to be accounted for from a life-prediction perspective. The probabilistic description of the long-lifetime regime discussed here also explains the observations that the long-lifetimes occur either by surface failures from a small heterogeneity scale (as in a favorably oriented primary-α) or by subsurface failures from a large heterogeneity scale (as in clusters with aligned slip planes). Finally, it can be emphasized that the present probabilistic description of long-lifetime regime provides a physical-basis for fatigue variability by accounting for randomly occurring microstructural scales. As such, it may be very advantageous in reducing the uncertainty in lifetime prediction [16, 17].

3.0 CONCLUSIONS

The following primary conclusions can be drawn from this study:

- The long-lifetime regime in Ti-6-2-4-6 could be described as a probabilistic realization of surface-crack-growth controlled mechanism or mean-lifetime dominating mechanisms.
- Four randomly occurring microstructural configurations were identified, which were related to different heterogeneity scales at the same loading condition.
- The surface short-lifetime mechanism occurred by cracking along, or near, pyramidal planes in an equiaxed-α oriented for hard, <c+a> slip.
- The surface long-lifetime mechanism occurred by slip in a favorably oriented (for basal <a> slip) primary-α grain.
- The subsurface long-lifetime mechanisms occurred in the region of larger microstructural configurations than the surface failures.
- The probabilistic description of the long-lifetime regime appeared to explain the increasing incidence of subsurface mechanism with decreasing stress level, as well as the heterogeneity scales associated with surface and subsurface failures.

Acknowledgements

This work was performed at the Air Force Research Laboratory, Materials and Manufacturing Directorate, Wright-Patterson Air Force Base, OH. The financial support of the Air Force Office of Scientific Research (AFOSR) through the AFOSR task no. 92ML02COR with Dr. Victor Giurgiutiu as the program manager is gratefully acknowledged. We are also grateful for the partial financial support of the Defense Advanced Research Project Agency (DARPA) under DARPA orders M978, Q588, P699, and S271 with Dr. Leo Christodoulou as the program manager. We acknowledge Mr. Phil Buskohl and Ms. Lindsey Selegue for their assistance with the replication-based small-crack growth experiments. We also wish to acknowledge Dr. Mike Caton, Dr. Andy Rosenberger, and Dr. Reji John for very helpful discussions.

References

1. J.C. Williams and E.A. Starke, Jr., "Progress in Structural Materials for Aerospace Systems," *Acta Materialia*, 51 (2003), 5775-5799.
2. C. Bathais and P.C. Paris, *Gigacycle Fatigue in Mechanical Practice* (CRC Press, 2004).
3. C.L. Muhlstein, E.A. Stach, and R.O. Ritchie, "Mechanism of Fatigue in Micron-Scale Films of Polycrystalline Silicon for Microelectromechanical Systems," *Applied Physics Letters*, 80 (2002), 1532-1534.
4. B.A. Cowles, "High Cycle Fatigue in Aircraft Gas Turbines – An Industry Perspective," *International Journal of Fracture*, 80 (1996), 147-163.
5. L. Christodoulou and J.M. Larsen, "Using Materials Prognosis to Maximize the Utilization Potential of Complex Mechanical Systems," *JOM*, (2004), 15-19.
6. S. Stanzl-Tschegg and H. Mayer, Eds., *Proceedings of the International Conference on Fatigue in the Very High Cycle Regime*, Institute of Meteorology and Physics, Vienna, Austria, 2001.

7. Y. Murakami, M. Takada, and T. Toriyama, "Super-long life tension-compression fatigue properties of quenched and tempered 0.46% carbon steel," *International Journal of Fatigue*, 16 (1998), 661-667.

8. H. Mayer, M. Papakyriacou, R. Pippan, and S. Stanzl-Tschegg, "Influence of Loading Frequency on the High Cycle Fatigue Properties of AlZnMgCu1.5Al Alloy," *Materials Science & Engineering A*, 314A (2001), 48-54.

9. A. Shyam, C.J. Torbet, S.K. Jha, J.M. Larsen, M.J. Caton, C.J. Szczepanski, T.M. Pollock, and J.W. Jones, *Superalloys-2004*, Proceedings of the 10th International Conference on Superalloys, T. M. Pollock, et al., Eds., 2004, 259-268.

10. K. Tanaka and Y. Akiniwa, "Fatigue Crack Propagation behavior Derived from S-N Data in Very High Cycle Fatigue," *Fatigue and Fracture of Engineering Materials and Structures*, 25 (2002), 775-784.

11. H. Mughrabi, "On 'Multi-Stage' Fatigue Life Diagrams and the Relevant Life-Controlling Mechanisms in Ultrahigh-Cycle Fatigue," *Fatigue and Fracture of Engineering Materials and Structures*, 25 (2002), 755-764.

12. S.K. Jha and K.S. Ravi Chandran, "An Unusual Fatigue Phenomenon: Duality of the S-N Fatigue Curve in the β-Titanium Alloy Ti-10V-2Fe-3Al," *Scripta Materialia*, 48 (2003), 1207-1212.

13. Q.Y. Wang, C. Bathais, N. Kawagoishi, and Q. Chen, "Effect of Inclusion on Subsurface Crack Initiation and Gigacycle Fatigue Strength," *International Journal of Fatigue*, 24 (2002), 1269-1274.

14. J.W. Lincoln, "Risk Assessment of an Aging Military Aircraft," *Journal of Aircraft*, 22 (1985), 687-691.

15. S.K. Jha, J.M. Larsen, A.H. Rosenberger, and G.A. Hartman, "Dual Fatigue Failure Modes and Consequences on Probabilistic Life Prediction," *Scripta Materialia*, 48 (2003), 1637-1642.

16. S.K. Jha, J.M. Larsen, and A.H. Rosenberger, "The Role of Competing Mechanisms in the Fatigue Life Variability of a Nearly-Fully Lamellar γ-TiAl based Alloy," *Acta Materialia*, 53 (2005), 1293-1304.

17. S.K. Jha, M.J. Caton, and J.M. Larsen, "A New Paradigm of Fatigue Variability Behavior and Implications for Life Prediction," *Materials Science and Engineering A*, article in press, DOI: 10.1016/j.msea.2006.10.171 (2007).

18. K.S. Ravi Chandran and S.K. Jha, "Duality of the S-N Fatigue Curve Caused by Competing Failure Modes in a Titanium Alloy and the Role of Poisson Defect Statistics," *Acta Materialia*, 53 (2005), 1867-1881.

19. K.H. Hoffmann and M. Schreiber, Eds., *Computational Statistical Physics*, Springer, 2001.

20. S.K. Jha, J.M. Larsen, and A.H. Rosenberger, "Microstructure and Temperature Effects on the Fatigue Variability Behavior of an α+β Titanium Alloy and Implications for Life Prediction," *Fatigue-2006*, Proceedings of the 9th International Fatigue Congress, Atlanta, GA, 2006.

21. C.J. Szczepanski, S.K. Jha, J.M. Larsen, and J.W. Jones, "The Role of Microstructure on Fatigue Lifetime Variability," *VHCF-4*, Proceedings of the 4th Very High Cycle Fatigue Conference, Ann Arbor, MI, 2007.

22. J.R. Mayeur, "*Three Dimensional Modeling of Titanium-Aluminum Alloys with Application to Attachment Fatigue*," Masters Thesis, Mechanical Engineering, Georgia Institute of Technology, 2004.

23. V. Hasija, S. Ghosh, M.J. Mills, and D. Joseph, "Deformation and Creep Modeling in Ti-6Al Alloys," *Acta Materialia*, 51 (2003), 4533-4549.

24. H. Tan, H. Gu, C. Laird, and N.D.H. Munroe, "Cyclic Deformation Behavior of High Purity Titanium Single Crystals: Part I. Orientation Dependence of Stress–Strain Response," *Metallurgical and Materials Transactions A*, 29A (1998), 507-512.

25. J.E. Spowart, B. Maruyama, and D.B. Miracle, "Multi-scale Characterization of Spatially Heterogeneous Systems: Implications for Discontinuously Reinforced Metal-Matrix Composite Microstructures," *Materials Science and Engineering A*, A307 (2001), 51-66.

Chapter III

A "PHYSICS-BASED" DESCRIPTION OF FATIGUE VARIABILITY BEHAVIOR IN PROBABILISTIC LIFE PREDICTION

S.K. Jha*, J.M. Larsen, and A.H. Rosenberger
US Air Force Research Laboratory
AFRL/MLLMN, 2230, 10th Street, Suite 1
Wright-Patterson Air Force Base, OH – 45433

*Universal Technology Corporation
1270 N. Fairfield Road
Dayton, OH – 45432

To be published in: *Engineering Fracture Mechanics*, 2008.

ABSTRACT

We describe fatigue lifetime variability as a separation/overlap of a crack-growth-controlled life-limiting mechanism and a mean-lifetime dominating behavior. We implement this description through a bimodal probability density representing the superposition of the crack-growth and the mean-lifetime dominating densities. Using the α+β titanium alloy Ti-6Al-2Sz-4Zr-6Mo, it is shown that the effect of microstructure, temperature, and loading variables have different influences on the life-limiting (worst-case) vs. the mean-lifetime behavior. We suggest that this behavior may be related to the development of different deformation heterogeneity levels in the material at any given loading condition, which appears to present some probability of a predominantly crack-growth controlled mechanism controlling the worst-case behavior. Based on the new description of fatigue variability, a procedure is presented for predicting the probability of failure from a relatively small number of experiments. This description appears to explain the fatigue variability trends reported in other studies and is shown to be especially relevant for reducing the uncertainty in prediction of useful fatigue lifetime for fracture-critical structures.

Keywords: Fatigue variability, life prediction, life-limiting mechanism, probability of failure, α+β titanium, Ti-6Al-2Sn-4Zr-6Mo, crack initiation, crack growth, worst-case fatigue

1.0 INTRODUCTION

Traditional descriptions of the variability in fatigue lifetime behavior are often guided primarily by a material's mean-lifetime response, and fatigue variability is characterized as a distribution about the overall mean-lifetime behavior [1, 2]. This is illustrated schematically in Fig. 1. In such approaches, the lifetime probability-density is typically based on a deterministic understanding of the mean-fatigue relationship to operating variables and is often derived from the probability distribution of variables in these relationships [3, 4]. An implicit assumption in this description (Fig. 1) is that the tails of the fatigue variability behavior result from random deviations from the overall mean behavior and have the same response to the operating variables as the mean. However, a sufficient number of experiments may not be always available to verify this trend. Often, the uncertainty in lifetime is observed to increase with decreasing stress level (Fig. 1) and is attributed to greater contribution of the crack initiation regime in the total lifetime [5].

The current approach to probabilistic life-management of fracture-critical turbine engine components also seems to be driven by the above understanding of fatigue variability [1, 2]. As illustrated for a given loading in Fig. 1, the lower-tail, and therefore the book-life, is derived by extrapolation of variability with respect to the mean to an acceptable level of risk (typically taken as 1 in 1000 probability of development of a pre-defined level of damage) [6]. As such, this approach appears to present significant uncertainty in life-prediction [6]. Due to the underlying description of fatigue variability, this approach may also produce physically counterintuitive predictions with respect to operating variables. For example, due to increased uncertainty in lifetime with decreasing stress level, lower useful-lifetimes may be predicted at lower stress levels, as illustrated for the $\alpha+\beta$ titanium alloy Ti-6Al-2Sn-4Zr-6Mo (Ti-6-2-4-6) in Fig. 2((a) and (b)) [7, 8]. The experimental points are plotted with respect to the lognormal cumulative distribution function (CDF) (shown by broken lines) in Fig. 2(a). As the stress level was decreased, the mean lifetime significantly increased (Fig. 2(a)), which is attributed to increased contribution from the crack initiation regime in $\alpha+\beta$ titanium alloys [9]. The increase in the mean corresponded to a shift in the upper-tail behavior to the right (Fig. 2(a)). On the other hand, the life-limiting behavior or the lower-tail in Fig. 2(a) was very weakly affected by stress level. This produced increased separation between the crack initiation-dominated, mean-response, and the life-limiting behavior, as illustrated by the bar graph in Fig. 2(b). However, since the increased variability is attributed only to the deviation from the overall mean fatigue response, the present understanding allows for arbitrarily increasing the scale of the lifetime-distribution function, therefore, resulting in a significantly lower design lifetime (the 1 in 1000, or the B0.1 lifetime shown in Fig. 2(b)) at lower stress levels.

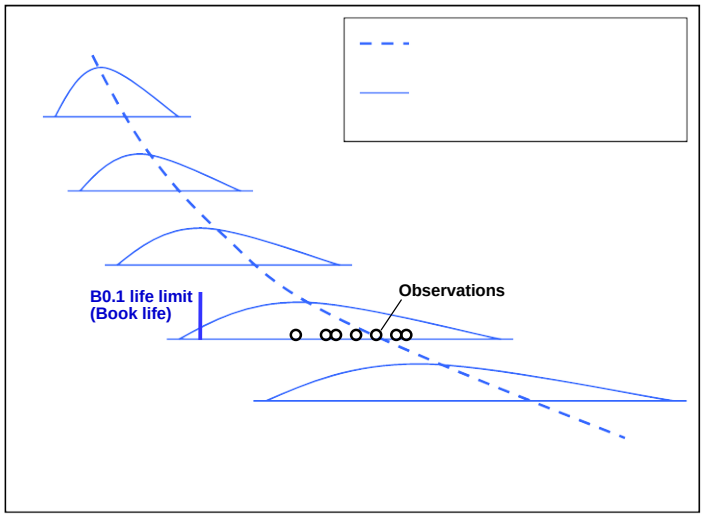

Figure 1. Illustration of the traditional description fatigue variability behavior the corresponding life-prediction approach.

The same arguments can also be applied to the observed decrease in lifetime variability with an increase in the operating temperature [8] or by seeding a material with non-metallic particles which produces uniformly distributed crack initiation sites [10, 11]. In the traditional description of fatigue variability, if the lifetime uncertainty in these cases is described only as deviations with respect to the mean behavior, it is possible to predict significantly lower B0.1 design lifetimes at the room temperature than at the elevated temperature. Similarly, a lower

B0.1 limiting lifetime may be predicted in a relatively defect-free material, when compared to increased defect content. These conclusions can be reasoned statistically, but from a physical standpoint one expects a greater risk of failure at elevated temperature and in the presence of defects.

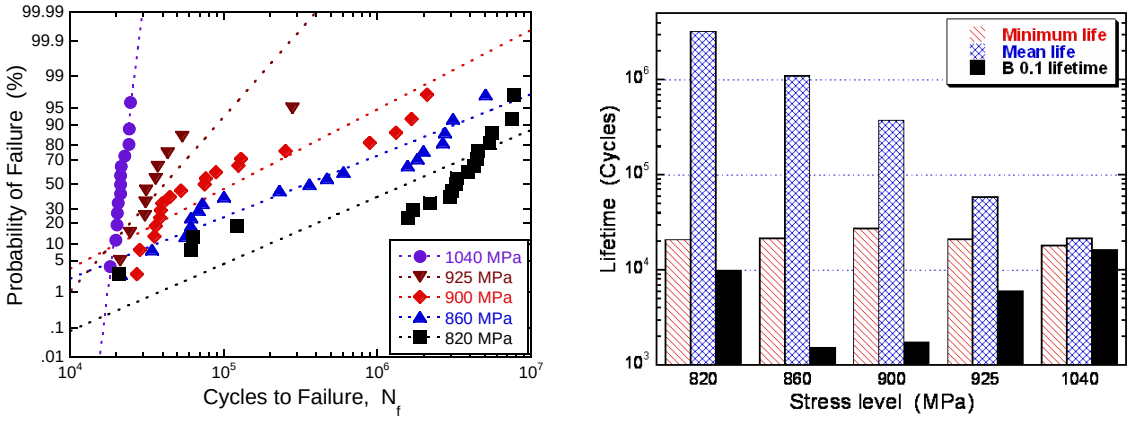

(a) (b)

Figure 2. Illustration of the separate response of tails and the mean of the fatigue variability behavior of Ti-6-2-4-6; (a) CDF vs. experiment and (b) Illustration of physically counterintuitive B0.1 lifetime w.r.t. stress level when based on the traditional description of fatigue variability.

Questions raised in this paper are firstly, whether it is physically accurate to describe the tails of fatigue variability as an extrapolation of deviations from the expected mean behavior. Secondly, can an increase in variability with decreasing stress level (or with respect to microstructure and other variables) be accommodated simply by broadening the lifetime probability density? Our earlier studies [7, 8, 12, 13] suggest that a continual increase in the scale of the lifetime density is not physically plausible without being accompanied by a breakdown or some sort of separation of mechanisms.

We have discovered the so called separation of mechanisms as a function of microstructure and loading variables in several structural materials including Ti-6-2-4-6 [7, 8], γ-TiAl based alloys [12], and nickel-based superalloys [13]. This kind of response was also seen in a separate study on a β-titanium alloy [14]. These studies appear to point to an alternate theory of fatigue variability wherein the microstructure and external variables may produce different response of the mean-lifetime behavior and the life-limiting behavior in certain loading regimes. In this paper we implement this description of fatigue variability by a bimodal probability density representing superposition of these dual mechanisms with reference to the α+β titanium alloy, Ti-6-2-4-6. We examine the effect of microstructure and external variables on the life-limiting and the mean-dominating peaks of the bimodal density. A procedure for calculating the fatigue variability density of Ti-6-2-4-6, with respect to microstructure and loading variables from limited number of experiments is presented. This description is then applied in a fracture mechanics based life-prediction methodology for this material. In the end, the possible physics behind the separation of mechanisms is discussed.

2.0 MATERIALS AND EXPERIMENTAL PROCEDURE

2.1 Materials

The Ti-6-2-4-6 material considered in this study was in the forged condition. Two different microstructures, designated as microstructures A and B, were produced. The microstructural details have been provided elsewhere [8]. Both microstructures consisted of a mixture of equiaxed (or globular) primary-α phase and lamellar α/transformed-β colonies. The two microstructures appeared nominally equivalent using scanning electron microscopy, although microstructure B had a shorter length of lath-α and a slight tendency for clustering of the equiaxed-α grains. The global textures of the two microstructures (measured on a plane normal to the loading axis) were very different [8], with a greater tendency of the basal and the prismatic poles to be parallel to the loading axis in microstructure B.

2.2 Experimental Procedure

The microstructure was characterized using a LEICA field-emission scanning electron microscope (SEM). The texture was measured by Orientation Imaging Microscopy (OIM) of nominal sections in the two microstructures. The OIM scans were conducted in step-wise automated stage control to enable measurement from a relatively large area. A TSL™ (trademark of the EDAX Company) OIM camera and associated software were used for data collection and analysis. The size distribution of microstructural phases was measured using the ImagePro™ image analysis program.

The Ti-6-2-4-6 specimens were extracted in the circumferential orientation from the two circular forging heats (microstructures A and B) of the material. Room temperature (RT) testing was performed using cylindrical specimens having a uniform gage section of about 12.5 mm length and 4 mm diameter. For the elevated temperature (260°C) tests, a cylindrical button-head specimen geometry [13] with the same gage section was used. The final machining step was low stress grinding (LSG), and each specimen was subsequently electropolished to remove approximately 50 μm from the surface in order to eliminate the LSG-induced residual stress and produce a uniform surface.

The fatigue tests were conducted at RT and 260°C using an MTS servo-hydraulic test system with a 646 controller. The tests were performed in load control at the frequency of 20 Hz and a stress ratio ($\sigma_{min}/\sigma_{max}$) of 0.05. For the elevated temperature tests, an electric resistance furnace was mounted on the test frame, and a high-temperature button-head gripping assembly was used in conjunction with a standard water-cooled hydraulic collet-grip system. Temperature-control thermocouples were welded outside of the specimen gage section to maintain the test temperature at the specimen. A clip gage was used with a few RT tests to record the stress-strain behavior. A high temperature extensometer was used with the elevated temperature tests to obtain the stress-strain loops at frequent intervals during the test.

Small-crack growth experiments were also performed on round-bar specimens. The crack growth rate was monitored using the acetate replication technique, and the test was interrupted at predetermined cycle intervals to obtain the replica. The specimen was held at the load of 60% of the maximum load to partially open the crack during replication. The crack lengths were measured in an Olympus™ optical microscope. The fracture surface analysis and crack initiation mechanisms were studied in a LECIA field emission SEM. The crack initiation sizes were measured using the ImagePro™ program.

3.0 RESULTS AND DISCUSSION

3.1 A new description of fatigue variability behavior

As discussed in section 1, the traditional description of fatigue variability appears inadequate in describing the increased variability observed with decreasing stress level or the non-proportional responses of the mean and the tails of the behavior. It was also noted, that probabilistic life predictions (for example the B0.1 lifetime) with respect to microstructure and loading variables do not appear to show physically plausible trends when based on the traditional description. In the following, we discuss a new, perhaps more physics-based, description of fatigue variability behavior that may account for these trends.

The alternate description of fatigue variability is illustrated with respect to the $\alpha+\beta$ titanium alloy Ti-6-2-4-6. The stress vs. total lifetime behavior of microstructure A at RT is shown in Fig. 3. The deterministic range in crack growth lifetimes is also shown in the plot. The lower-bound crack-growth lifetime corresponded to upper limits of the crack initiation size and the small crack growth rate [8]. Similarly, the upper-bound lifetime was calculated from lower limits on the crack initiation size and the small crack growth rate [8]. The small crack growth behavior at 860 MPa is presented in Fig. 4. As shown, the upper and lower limits on crack growth behavior were taken as power-law segments fit to data representing the fastest and the slowest growth rate respectively. As indicated in Fig. 4, these limiting crack growth curves were taken to be the $\pm 3\sigma$ points in deriving the probability densities of the crack growth parameters discussed in section 3.2.1.

Figure 3 indicates that the mean-lifetime and the life-limiting response tend to overlap with the crack growth range at the higher stress levels. With decreasing stress level, the mean behavior separated from the crack-growth-controlled (life-limiting) behavior, producing increased lifetime variability at lower stress levels. In Ti-6-2-4-6, this separation can be attributed to increased dominance of crack initiation lifetime in the mean behavior [9] as the stress level is decreased.

The experimental points are plotted in the CDF space in Fig. 5 using the lognormal probability density. Only two stress levels are shown for clarity (other stress levels are given in Fig. 2(a)). The calculated crack growth ranges at both stress levels are also shown. At the higher stress level, a very good agreement of data with the CDF is seen, which relates to the overlap of higher stress level behavior with the crack growth range. This agreement broke down as the stress level was decreased, as illustrated by the 860 MPa points in the figure. The step-like shape in the data with respect to the CDF at the lower stress level can be shown to result from superposition of at least two mechanisms [7] at the same stress level. These mechanisms are designated as Type I and Type II in the figure. From Fig. 5, the Type I or the life-limiting behavior is controlled by crack growth. The Type II mechanism, which can be suggested to be controlled by crack initiation in Ti-6-2-4-6, dominates the mean behavior, as evident from Fig. 3.

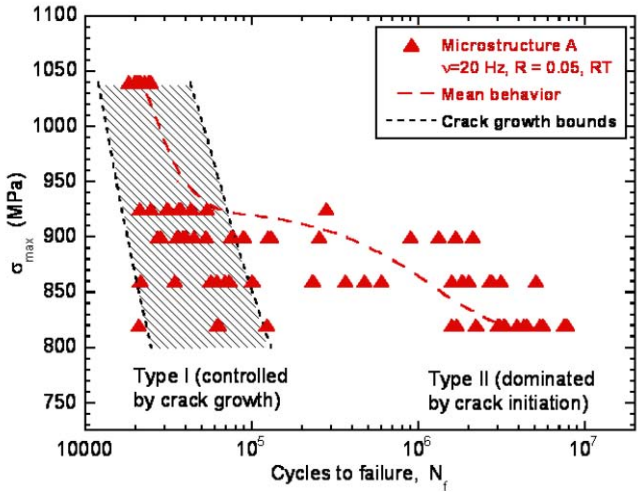

Figure 3. Stress vs. lifetime behavior of microstructure A at RT showing the separation of crack initiation dominated behavior (Type II) from the crack growth controlled mechanism (Type I) with decreasing stress level.

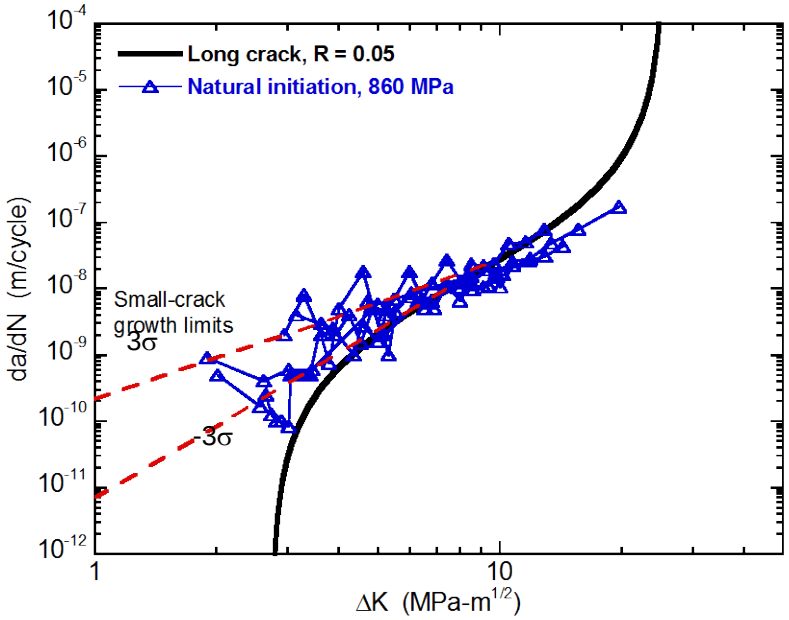

Figure 4. Small-crack growth variability in microstructure A at 860 MPa and the crack growth limits used in the deterministic calculations.

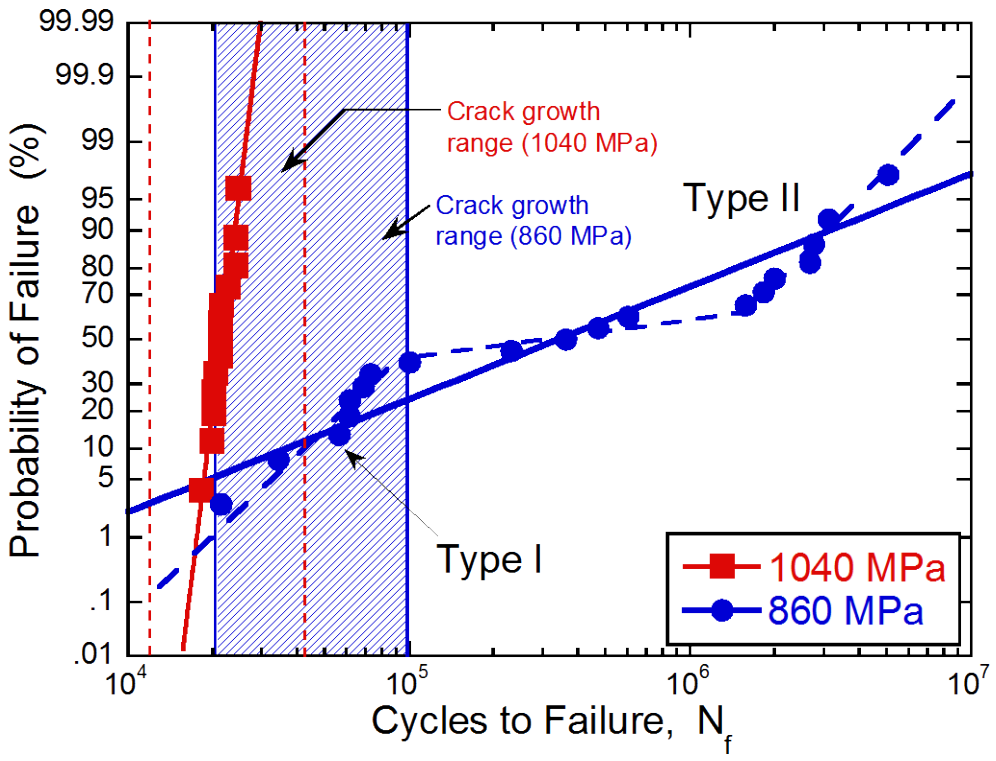

Figure 5. Experimental points plotted in the CDF space showing the breakdown in agreement with the CDF at lower stress levels.

Based on the preceding discussion, we propose that fatigue variability behavior can be described as separation (or overlap) of a life-limiting response and a mean-lifetime dominating behavior. This is schematically illustrated in Fig. 6. Although only the effect of stress level is illustrated in this figure, the influence of microstructure, temperature, and loading variables can also be described in terms of separate effects of these variables on the life-limiting and the mean-dominating densities, consequently affecting the total variability.

3.2 Implementing the description

The proposed description of fatigue variability can be implemented by a bimodal probability density representing the superposition of a crack growth related peak and a mean-lifetime dominated peak. The total density, $f_t(x)$, can be expressed as [7, 12]:

$$f_t(x) = p_l f_l(x) + p_m f_m(x) \tag{1}$$

where, $f_l(x)$ and $f_m(x)$ are the life-limiting density and the mean-lifetime dominating density, respectively. These probability densities are weighted by the probability of occurrences, p_l and p_m, of individual responses such that $p_l + p_m = 1$. Here $f_l(x)$ and $f_m(x)$ are taken as the lognormal density function which is given by [15]:

$$f_{l,m}(x) = \frac{1}{xS\sqrt{2\pi}} e^{-\left(\frac{\ln x - M}{S\sqrt{2}}\right)^2} \tag{2}$$

where, M and S are the mean and the standard deviation respectively of the natural logarithm of the random variable.

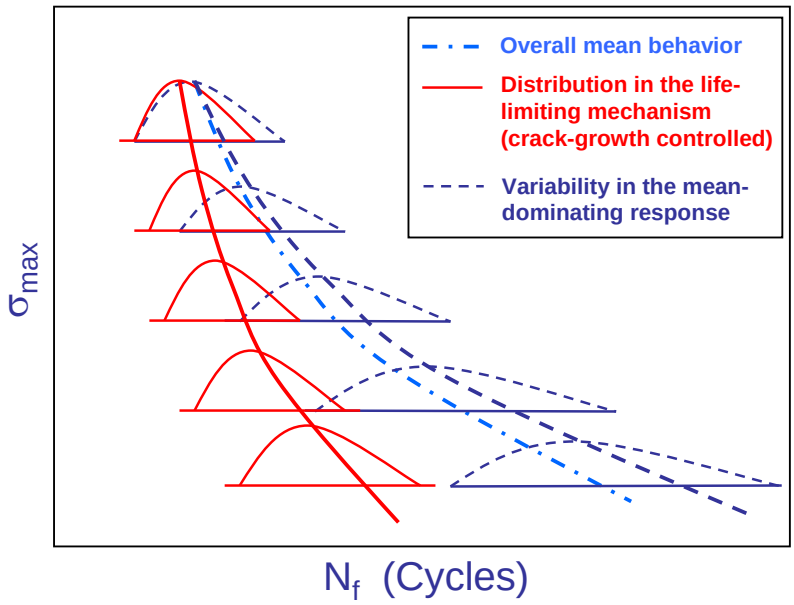

Figure 6. Schematic illustration of the proposed description of fatigue variability behavior with respect to stress level.

3.2.1 On deriving the total probability density, $f_t(x)$

Life-limiting peak

Following the earlier discussion, the life-limiting density ($f_l(x)$) can be obtained by simulating the crack growth lifetime, provided the variability in the small + long crack growth rates and the size distribution in the critical microstructural unit are known. We performed multiple small crack growth experiments using an acetate replication technique to obtain the variability in the small crack growth regime. This was illustrated in Fig. 4. In this material, most of the variability in growth rates was found to occur in the early stages of crack growth, typically less than the crack length of about 30 μm [8, 16]. The variability in the small crack regime was described by the probability densities of the crack growth parameters c and m when the crack growth rate is given by [17]:

$$\frac{da}{dN} = e^{c}\Delta K^{m} \tag{3}$$

where, a is the crack size, N is cycles, and ΔK is the stress intensity factor range. The parameters c and m were assumed to be normally distributed [17] and their densities are shown in Fig. 7. In order to obtain these densities, power-law segments were fit to the small crack growth data and the ±3σ limits (where σ is one standard deviation) on the parameters c and m was taken to correspond to the small crack curves showing the maximum and the minimum average growth rates respectively (Fig. 4). The variables c and m are correlated [8] and were, therefore, sampled from their joint probability density in the subsequent lifetime simulation.

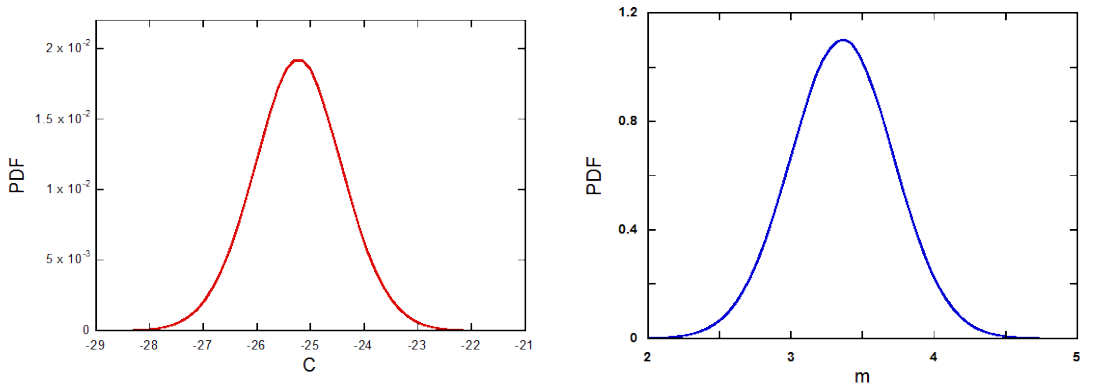

(a) (b)

Figure 7. Probability densities of the crack growth variables, (a) c and (b) m.

Crack initiation in the life-limiting mechanism in Ti-6-2-4-6 occurred within a (or a few) globular α grain(s) [18] at the specimen surface. The mean-dominating behavior was comprised of a mixture of surface and subsurface initiated failures [8]. These mean-behavior-contributing mechanisms had overlapping lifetimes and acted as a group in terms of their response to operating variables [8].

The surface replica of a small-crack growth specimen with microstructure A, recorded at N = 20,000 cycles, is shown in Fig. 8(a). The stress level was 860 MPa. The crack initiating equiaxed-α grain (about 4 μm in surface length) is indicated at the center of the crack. One or more crack-initiation facet(s) are typically created at the fracture surface, as shown in Fig. 8(b). The sample is shown at an SEM tilt angle of 45° in this figure. The distribution in the crack-initiation facet size is compared to the nominal equiaxed α grain size distribution in Fig. 9. The lognormal probability density function provided a good fit to the distributions. Although the crack initiation sizes appear to be slightly displaced with respect to the nominal equiaxed α size distribution, it is to be noted that the facet size measured on the fracture surface usually represents the largest plane across a grain [19]. The nominal distribution obtained from a metallographic section may therefore underestimate the true 3-D particle size [19]. The crack initiation size distribution along with the small-crack growth variability was employed to simulate the crack growth lifetime density ($f_l(x)$) using the Monte Carlo analysis method.

Mean-dominating peak

It may be possible to derive the mean-lifetime dominating peak, $f_m(x)$, from only a few total lifetime tests at a given stress level. This is shown for the Ti-6-2-4-6 alloy in Fig. 10. Four failure points were randomly selected at each stress level, as shown in the figure. The mean of $\text{Log}(N_f)$ based on 10 – 19 tests at these stress levels is also plotted. The randomly selected points tend to fall near the mean behavior (Fig. 10). For illustration purposes we consider the stress level of 860 MPa. In order to screen for points that may belong to the life-limiting mechanism we superimpose the simulated crack growth density at 860 MPa on the plot (Fig. 10). The points falling under the crack growth peak, within $\pm 3\sigma$ of the mean crack growth lifetime, were classified as due to the life-limiting mechanism. The maximum likelihood estimate method [15] was then used with the remaining points to obtain the parameters of the mean-dominating (or Type II) density.

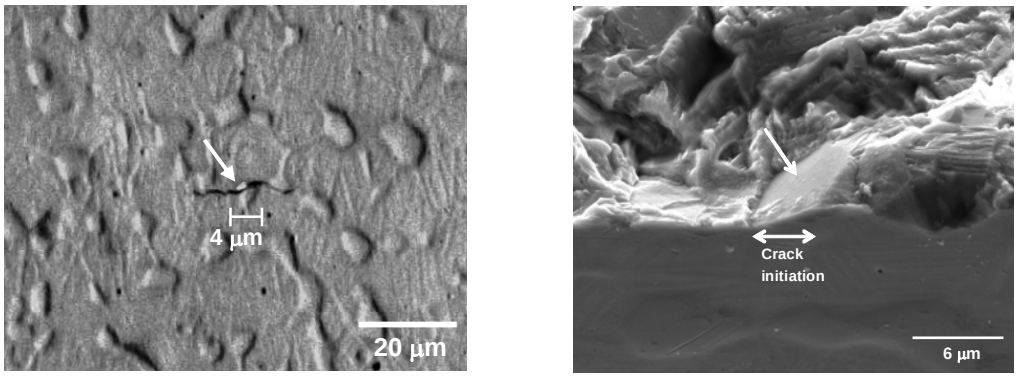

(a) (b)

Figure 8. Crack initiation microstructural unit in Ti-6-2-4-6; (a) surface replica at N = 20,000 of a sample cycled at σ_{max} = 860 MPa with N_f =39,864 and (b) the corresponding crack initiation facet in the fracture surface.

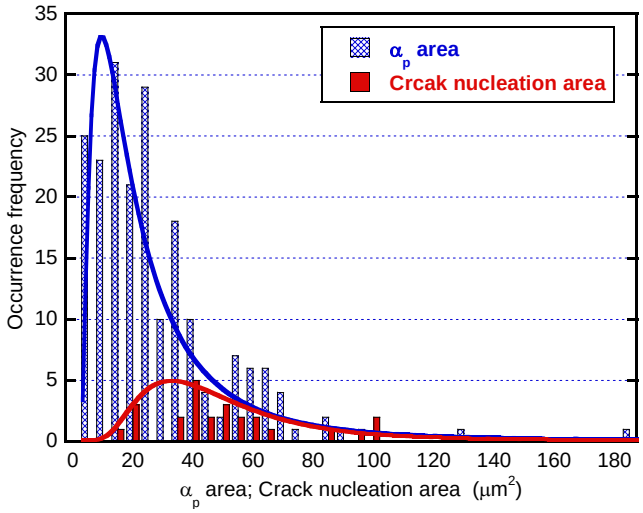

Figure 9. Nominal equiaxed α size distribution compared to the crack initiation facet size distribution in microstructure A.

The crack growth (life-limiting) and the mean-dominating density at 860 MPa are shown in Fig. 11. These can be weighted by the respective probabilities, p_l and p_m, to obtain the total density, $f_t(x)$. This is shown in Fig. 12(a) for a range of values for p_l. Clearly, the heights of the individual peaks in the total density are very sensitive to p_l and p_m (Fig. 12(a)). However, in the proposed description, the lower-tail of the density or the limiting lifetime (for example, B0.1) does not vary significantly with the probability of occurrence of mechanisms but is dependent on the parameters of the crack growth density. This is discussed further in section 3.4. The CDFs corresponding to $f_t(x)$ are shown in Fig. 12(b). Note that the ordinate is linear in this figure. Expectedly, the probability, p_l, has significant influence on the height of the step in the CDF but has a weak effect on the lower-tail behavior (Fig. 12(b)). The experimental points at 860 MPa, plotted in Fig. 12(b), are in reasonable agreement with the calculated bimodal density for p_l = 0.533 (which was the experimentally observed probability of occurrence).

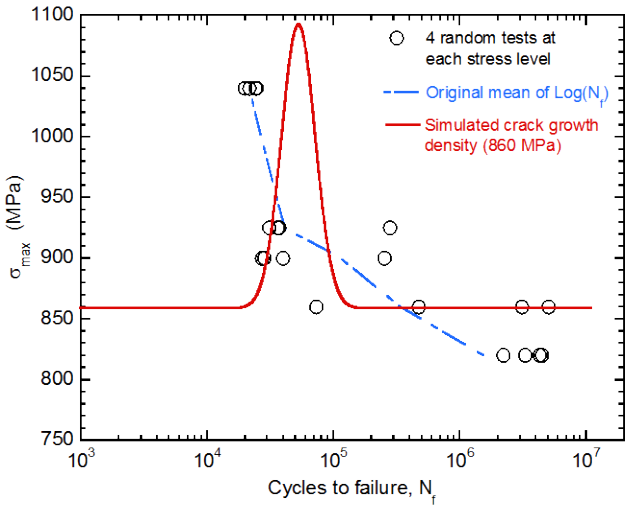

Figure 10. Illustration of a method to derive the mean-dominating probability density, $f_m(x)$.

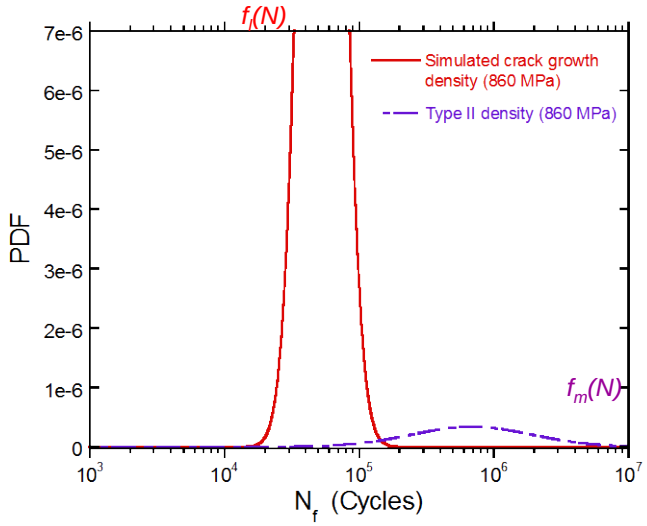

Figure 11. Calculated life-limiting and mean-dominating densities, $f_l(x)$ and $f_m(x)$.

3.3 Understanding the effect of microstructure and loading variables on fatigue variability

The proposed description of fatigue variability behavior may be particularly useful in evaluating the effect of microstructure, temperature, and other loading variables on lifetime variability. In case of Ti-6-2-4-6, the crack initiation and the crack growth regimes have different sensitivities to these variables. Therefore, the variables affect the life-limiting (crack growth) and the mean-dominating (crack initiation) densities to different degrees causing their increased separation / overlap. Other variables in this study, besides the stress level, were microstructure and temperature.

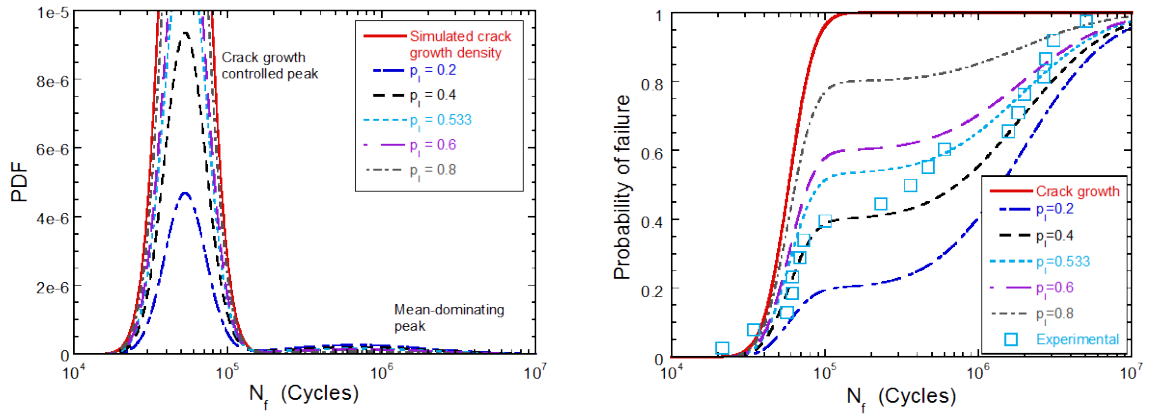

Figure 12. The proposed description of fatigue variability behavior; (a) predicted bimodal densities with respect to p_l and (b) Effect of probability, p_l on the CDFs.

The crack growth behavior of Ti-6-2-4-6 was similar in both microstructural conditions [20]. Also, an increase in the test temperature to 260°C had almost no effect on crack growth rates [20]. This is consistent with reports [21] on other α+β titanium alloys. Secondly, the surface crack initiation facets corresponded to globular α grains in both microstructures. Although we did not perform small crack experiments at 260°C, the variability in the small crack regime was assumed to be the same as that at room temperature. Therefore, at a given stress level, the crack growth density was similar for the two microstructures and temperatures. We randomly selected 4 samples in each microstructure and temperature condition to derive the respective mean-dominating densities using the procedure described in section 3.2.1.

The proposed description was applied to study the effect of stress level, microstructure, and temperature on lifetime variability of Ti-6-2-4-6. The effect of stress level is illustrated in Fig. 13 (a and b). The calculated probability densities are plotted for different stress levels in Fig. 13(a). The probability, p_l, used in the calculation are indicated in each case. In this figure, p_l is based on the experimental observation. Besides the probabilities p_l and p_m, the peak heights are also very sensitive to their location and width, due to the requirement of the probability density function to integrate to unity. The change in peak heights with respect to stress level can, therefore, be attributed to p_l and the shift in their locations. Figure 13 (a) clearly illustrates an increase in the overlap between the mean-dominating (crack-initiation) peak and the life-limiting (crack growth) peak of the total density as the stress level is increased. At the highest stress level, 1040 MPa, it can be suggested that the two individual densities of the bimodal description are indistinguishable and the total fatigue variability can be described by the crack growth density. The corresponding calculated CDFs are compared to experiment in Fig. 13(b). The experimental points show reasonable agreement with the calculated CDFs at these stress levels, although some discrepancy can be seen at higher stresses and for longer lifetimes in some cases. Note that the same small crack behavior and variability in growth rates measured at 860 MPa was used at all stress levels. A part of the discrepancy can be attributed to this assumption. Incorporation of more small-crack data in lifetime simulation is expected to further improve the agreement. Nevertheless, the predicted densities capture the effect of stress level on the tails and the total fatigue variability behavior. This indicates that the increased variability with decreasing stress level can be understood in terms of a stronger response of the mean-dominating peak to stress level and, therefore, increased separation from the life-limiting peak.

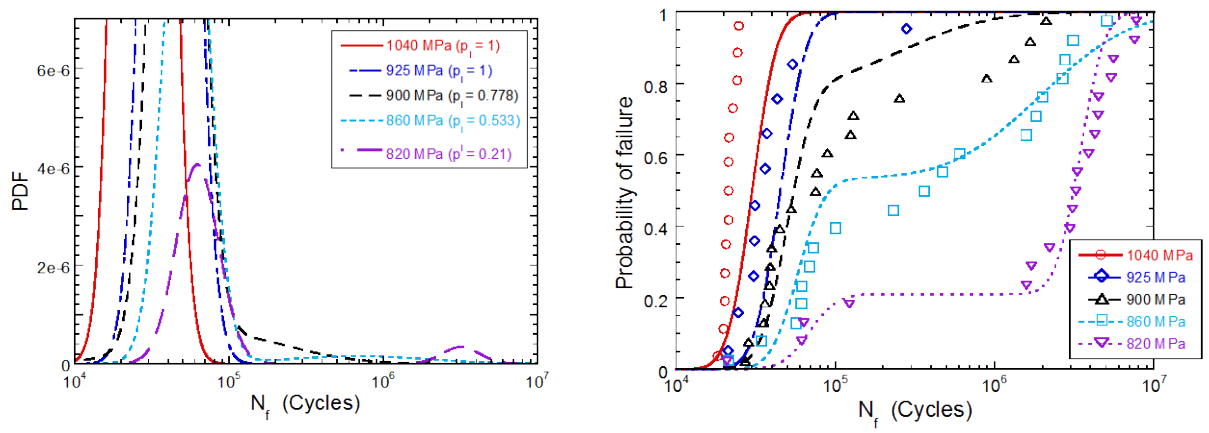

(a) (b)

Figure 13. Predicted fatigue variability behavior with respect to stress level; (a) calculated bimodal PDFs and (b) the corresponding CDFs compared to experiment.

Figure 14 shows that the effect of microstructure and temperature on fatigue variability can also be readily understood in terms of the sensitivity of crack growth and crack initiation regimes to these variables. The predicted total probability density with respect to microstructure and temperature at 860 MPa is presented in Fig. 14(a). The figure illustrates that the mean-dominating and the life-limiting peaks shift according to the sensitivity of crack initiation and crack growth to these variables, affecting the total lifetime variability. For example an increase in temperature to 260°C has a strong influence on the crack initiation lifetime, affecting the crack initiation density significantly. Since the crack growth behavior was almost unaffected by temperature, the crack growth controlled peak did not exhibit much change. The overall effect of this dual response was a decrease in the total variability with increase in temperature (Fig. 14(a)). The proposed description therefore allows for predicting the effect of these variables on lifetime distribution. The calculated CDFs with respect to microstructure and temperature are plotted in Fig. 14(b). As shown, these demonstrate reasonable agreement with the experimental points, considering the assumptions made in using the small crack growth data and a relatively limited number of experimental observations.

Besides providing an understanding and prediction of the effect of microstructure and other operating variables on fatigue variability, perhaps more importantly, the proposed description may also supply a more physics-based framework for life-prediction and reliability estimates. It follows from this description that the tails of the fatigue variability behavior are not simply a deviation from the mean behavior. In particular, the response of the lower-tail to operating variables differs from the response of the mean. From a life-prediction perspective, this would indicate that an observed decrease in total lifetime variability cannot be automatically construed as increased limiting (or B0.1) lifetime and vice versa.

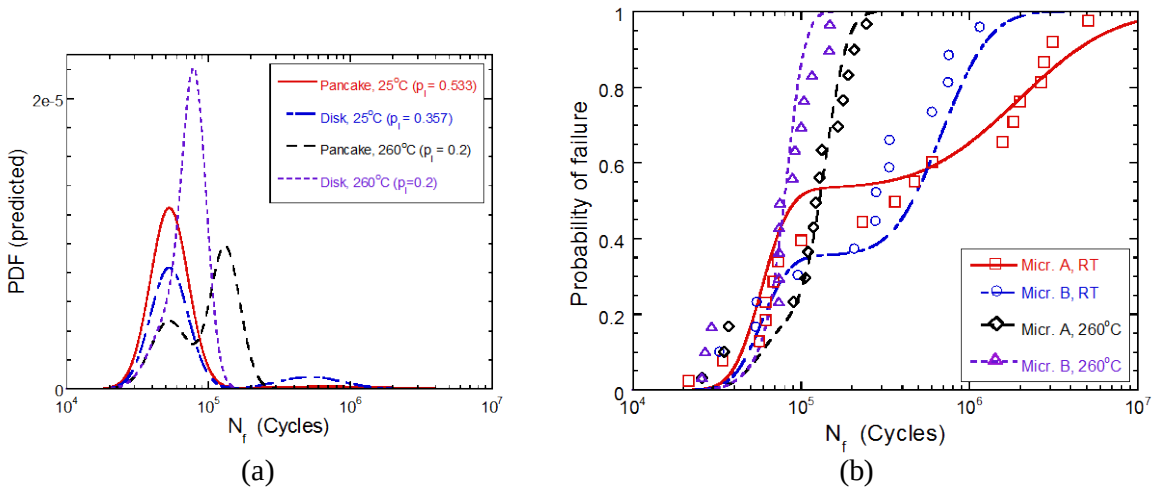

Figure 14. Applying the bimodal density in understanding the effect of microstructure and temperature on fatigue variability; (a) calculated PDFs and (b) the corresponding CDFs compared to experiment.

3.4 Applying the description in a Life Prediction Methodology

A salient factor to the application to life prediction is the understanding that fatigue variability arises from separate responses of a crack growth controlled life-limiting mechanism and a mean-dominating behavior to operating variables. Since failure can occur by either one of the mechanisms, life-prediction can be based on the worst-case mechanism, i.e., the crack growth density in the bimodal description.

The response of the proposed lifetime density with respect to probabilities, p_l and p_m, of the superimposing behaviors was presented in Fig. 12(a). The B0.1 lifetimes derived from this bimodal probability density are plotted with respect to p_l in Fig. 15 and, as shown, appear to have a power-law relationship to p_l. The predicted B0.1 lifetime was not very sensitive to the probability of occurrence of the respective mechanisms within a range of values for p_l ($p_l \geq 0.2$) and asymptotically approached the B0.1 lifetime predicted from the crack growth density (Fig. 15). The prediction based on the crack growth density can therefore be considered as the conservative limiting lifetime. The proposed description of fatigue variability therefore leads to life-prediction based on the crack growth density.

The life prediction methodology is graphically illustrated in Fig. 16 for microstructure A at the stress level of 860 MPa. The predicted bimodal description is compared to the traditional description of fatigue variability in the bottom plot of Fig. 16. The traditional description was derived from the four random points at 860 MPa shown in Fig. 10 using the MLE estimates of the parameters. As discussed previously, the underlying assumption in this description is that tails of the fatigue variability behavior can be described as an extrapolation of variability with respect to the overall mean response. As such, the lower-tail behavior in this case exhibits extreme conservatism with respect to the proposed description (Fig. 16, bottom plot). The corresponding CDFs are plotted in the top plot of Fig. 16. The experimental points belonging to the Type I mechanism are plotted as separate distributions in the figure and show reasonable agreement with the calculated crack growth CDF. As expected, the B0.1 lifetime derived from the bimodal description is similar to the B0.1 life (vertical lines in the bottom plot) based solely

on the crack growth density. When compared to the traditional description of fatigue variability we find a significant reduction in uncertainty with life-prediction as evident from the figure.

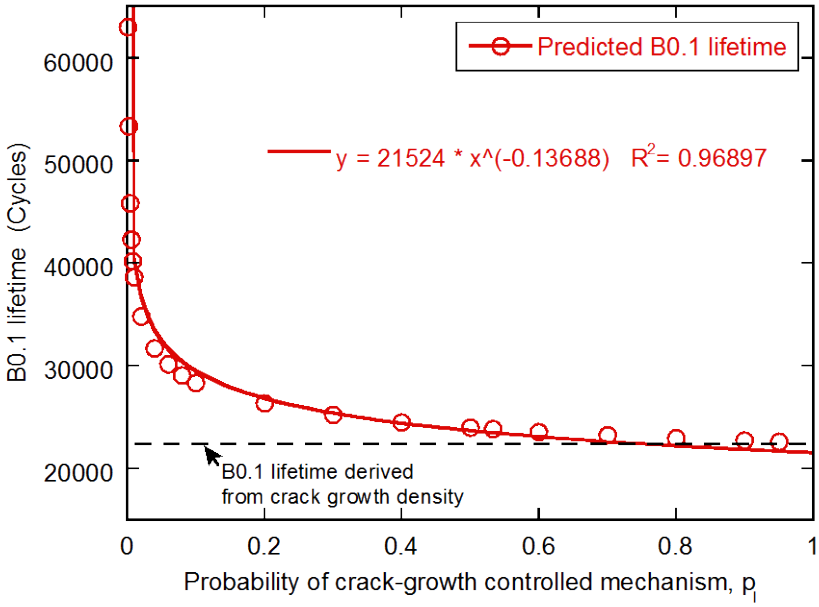

Figure 15. The B0.1 lifetimes predicted by the proposed description of fatigue variability as a function of the probability, p_I.

Although in the present instance the traditional description provided significantly conservative B0.1 lifetime, it also follows from the above discussion that a case may arise when the mean-based description produces a non-conservative prediction relative to the bimodal density. For example, this can occur when the traditional description is deduced from a limited number of points that are biased towards the Type II mechanism. In either case, the proposed description of fatigue variability may produce a more accurate design lifetime.

3.4.1 Resolving the Observed Fatigue Variability Trends

The fatigue variability description developed here appears to resolve the observed trends in total variability as a function of loading variables and microstructural constituents [10, 11] for the purpose of life-prediction. In particular, a life-prediction methodology based on the bimodal density seems to mitigate the physically counterintuitive scenarios that we alluded to previously. For example, although lower defect content increases the mean lifetime, it often produces increased lifetime variability due to non-uniform spatial distribution of initiation sites and increased scale of the crack initiation size distribution [10, 11]. Similarly, in the present study we find an increase in variability with decrease in temperature from 260°C to RT (Fig. 14). If the tails of the fatigue variability behavior are considered to be an extrapolation of variability from the mean lifetime, the material with lower defect content, or at the lower temperature, may be predicted to have lower limiting lifetime for a given probability of failure. This is illustrated for the present Ti-6-2-4-6 alloy in Fig. 17. In the proposed description, however, the lower-tail has a different behavior than the mean of the fatigue variability response, and increased variability with decreased defect content or temperature is attributed to separate response of mean-dominating mechanism from the life-limiting behavior. Therefore, the limiting probabilistic lifetime at the lower temperature (or under lower defect content) is dependent on the crack growth density and

is expected to be at least the same, if not higher, at RT (or in an unseeded material) than at 260°C (or a seeded condition) as shown in the figure.

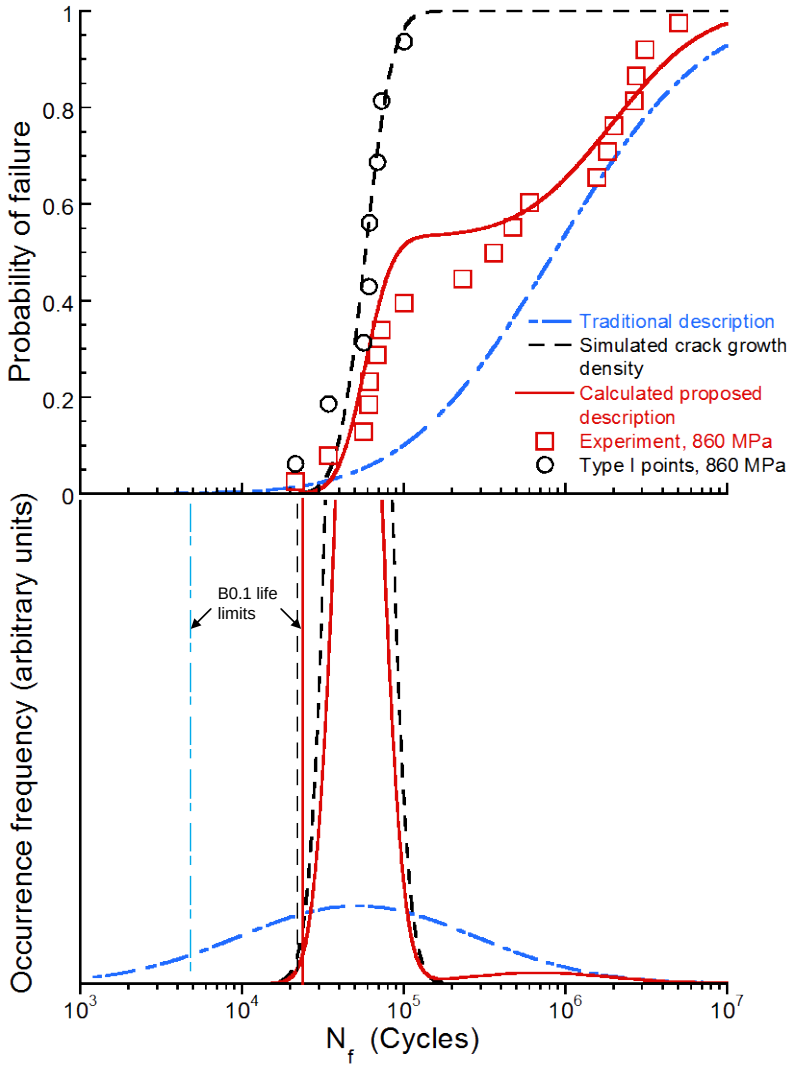

Figure 16. Illustration of the life-prediction methodology based on the proposed fatigue variability description.

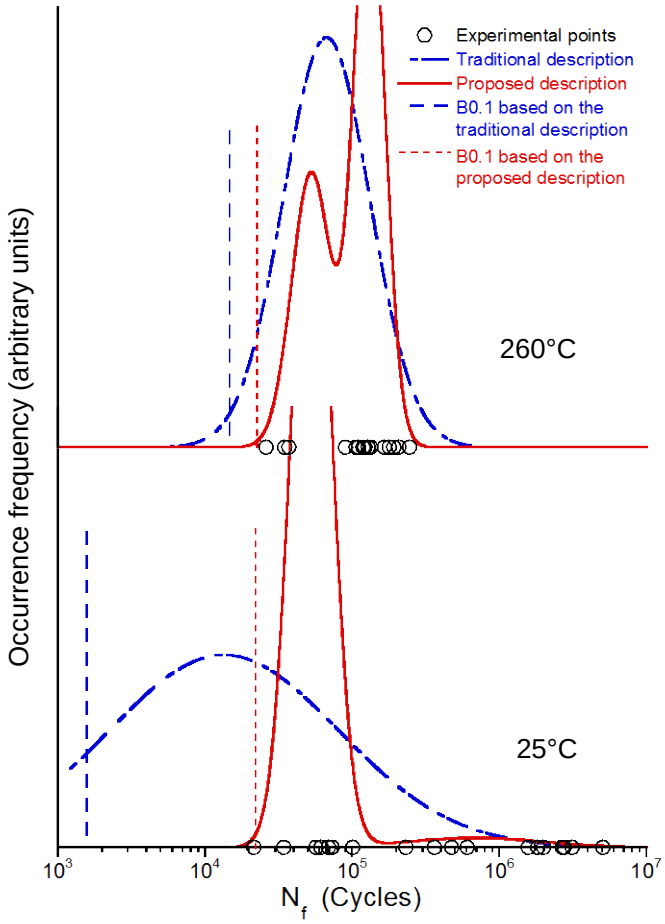

Figure 17. Illustration of the effect of temperature on the B0.1 lifetime in the traditional and proposed description of fatigue variability.

3.5 Possible Theory of Separation of Mechanisms

We suggest that the separation of mean-dominating and life-limiting behaviors may be related to development of different heterogeneity levels in a material at the same loading condition. Analogies can be drawn from disorder – order related second order transitions that are seen in several physical systems including ferromagnetism [22] and earthquake dynamics [23, 24], and it may be possible to apply the statistical physics based theories from these fields to fatigue variability behavior.

At the highest stress level (1040 MPa), Ti-6-2-4-6 may be considered to produce a relatively homogeneous deformation response to applied stress. As such, the life-limiting and the mean-dominating behaviors seem to completely overlap, and a single mode of failure is observed. At the lower stress level, heterogeneity levels are generated in the material due to local plasticity. The localized deformation can be attributed to several factors, from favorable crystallographic orientation of a grain [25] or collection of grains [26] to clustering of microstructural phases [14] and grain boundary disorientation [27]. These factors are, of course, material and loading dependent. If the underlying physics of fatigue variability is similar to the statistical-physics systems mentioned above, several of these factors can be suggested to be operational at a given applied stress causing a ranking of heterogeneity levels. It is also known

that some of the initial stress concentration may decay with cycles due to, for example, slip transfer to less favorably oriented regions [29], causing relatively more uniform distribution in deformation with time. It can be speculated that this evolution of heterogeneity levels presents a finite probability of crack initiation in randomly-occurring critical microstructural neighborhoods within the initial cycles, causing a crack growth controlled mechanism. The mean-dominating behavior, on the other hand, is suggested to be realized by damage accumulation at a much smaller and, therefore, more frequently distributed heterogeneity scale than the life-limiting mechanism. As shown previously, this is dominated by crack initiation lifetime in Ti-6-2-4-6. These mechanisms can be suggested to operate in sequence, and the mean-behavior is realized only after the life-limiting mechanism is not encountered. Clearly, the probability of occurrence of the crack growth controlled mechanism will vary depending on the material and external variables, but we suggest it is important to account probabilistically for this theoretical possibility and incorporate it in life-prediction.

4.0 CONCLUSIONS

The following main conclusions can be drawn from this study:

- Variability in total fatigue life is controlled by the combination of a crack-growth-controlled, life-limiting mechanism and a mean-dominating behavior which is governed by crack initiation in Ti-6-2-4-6.
- This description can be implemented by a bimodal probability density representing superposition of the crack growth and mean-dominating densities. The bimodal density can be calculated from simulated crack growth density and few total lifetime tests.
- The proposed description can prove very useful in understanding the effect of microstructure, temperature, and other variables on fatigue variability.
- In the limiting case, the B0.1 lifetime obtained from the bimodal-density approaches the B0.1 lifetime derived solely from the crack growth density, thereby providing a fracture mechanics basis for a worst-case life-prediction methodology.
- The seemingly counterintuitive effects of defect content, temperature, and loading variables on probabilistic life-prediction can be resolved in the proposed description of fatigue variability.

ACKNOWLEDGEMENTS

This work was performed at the Air Force Research Laboratory, Materials and Manufacturing Directorate, Wright-Patterson Air Force Base, OH. The financial support of the Air Force Office of Scientific Research (AFOSR) through task no. 92ML02COR with Dr. Victor Giurgiutiu as the program manager is gratefully acknowledged. The financial support of the Defense Advanced Research Project Agency (DARPA) under DARPA orders M978, Q588, P699, and S271 with Dr. Leo Christodoulou as the program manager is also gratefully acknowledged. We acknowledge Mr. Phil Buskohl and Ms. Lindsey Selegue for their assistance with the replication-based small-crack growth experiments, and wish to acknowledge Dr. Mike Caton and Dr. Reji John for very helpful discussions.

REFERENCES

1. K.S. Chan and M.P. Enright, *Journal of Engineering for Gas Turbines and Power*, Vol. 124, pp. 889-885, 2006.
2. R. Tryon and A. Dey, *J. Aerospace Engng.*, p. 120, 2001.
3. H. Yokoyama, O. Umezawa, K. Nagai, and T. Suzuki, *ISIJ International*, Vol. 37, p. 1237, 1997.
4. J.W. Lincoln, *Journal of Aircraft*, Vol. 22, 1985.
5. J.N. Yang and W.J. Trapp, *AIAA Journal*, Vol. 12, pp. 1623-1630, 1974.
6. L. Christodoulou and J.M. Larsen, *JOM*, Mar 2004, p. 15, 2004.
7. S.K. Jha, J.M. Larsen, A.H. Rosenberger, and G.A. Hartman, *Scripta Materialia*, Vol. 48, p. 1637, 2003.
8. S.K. Jha, M.J. Caton, and J.M. Larsen, *Materials Science and Engineering A*, article in press, DOI: 10.1016/j.msea.2006.10.171, 2007.
9. J. Ruppen, D. Eylon, and A.J. McEvily, *Metall. Trans. A*, Vol. 11A, p. 1072, 1980.
10. T.P. Gabb, J. Telesman, P.T. Kantzos, P.J. Bonacuse, and R.L. Barrie, *NASA/TM-2002 211571*, 2002.
11. J. Huang, J.E. Spowart, and J.W. Jones, *Fatigue Fract. Engng. Mater. Struct.*, Vol. 29, pp. 507-517, 2006.
12. S.K. Jha, J.M. Larsen, and A.H. Rosenberger, *Acta Materialia*, Vol. 53, p. 1293, 2005.
13. M.J. Caton, S.K. Jha, J.M. Larsen, and A.H. Rosenberger, in *Superalloys 2004*, 2004.
14. K.S. Ravi Chandran and S.K. Jha, *Acta Materialia*, Vol. 53, p. 1867, 2005.
15. W.Q. Meeker and L.A. Escobar, in *Statistical Methods for Reliability Data*, Wiley Series in Probability and Statistics, 1998.
16. S.K. Jha, J.M. Larsen, and A.H. Rosenberger In: *Fatigue 2006*, International Fatigue Congress, Atlanta, GA, 2006.
17. C.G. Annis, In: *Probabilistic aspects of life prediction*, ASTM STP 1450, W.S. Johnson, and B.M. Hillberry, Eds., ASTM International, West Conshohocken, PA, 2004.
18. S.K. Jha, J.M. Larsen, A.H. Rosenberger, and G.A. Hartman, ASTM, STP 1450, W.S. Johnson, and B.M. Hillberry, Eds., ASTM International, West Conshohocken, PA, 2004.
19. R.L. Fullman, *Trans. AIME*, Vol. 197, p. 447, 1953.
20. S.K. Jha, J.M. Larsen, and A.H. Rosenberger, unpublished research, Air Force Research Laboratory, Dayton, OH.
21. NASA Technical Report, NASA/TM 2001-210830.

22. K.H. Hoffman and M. Schreiber, Eds., Computational Statistical Physics, Springer Publ., pp.211-226, 2002.

23. J.B. Rundle, D.L. Turcotte, R. Shcherbakov, W. Klein, and C. Sammis, *Review of Geophysics*, Vol. 41, pp. 1019, 2003.

24. D. Sornette, Proceedings of the National Academy of Sciences of the United States of America (PNAS), Vol. 99, Suppl. 1, 2522-2529, 2002.

25. P. Lukas, M. Klesnil, and J. Polak, Mater. Sci. Engng, Vol. 15, pp. 229-245, 1974.

26. C.J. Szczepanski, S.K. Jha, J.M. Larsen, and J.W. Jones, In Press, VHCF-4, Proceedings of the 4th international conference on very high cycle fatigue, Ann Arbor, MI, 2007.

27. D.L. Davidson, R. Tryon, M. Oja, K.S. Ravi Chandran, TMS Annual Meeting, San Antonio, TX, 2006.

28. X. Feaugas and M. Clavel, *Acta Materialia*, Vol. 45, pp. 2685, 1997.

Chapter IV

THE MEAN VS. LIFE-LIMITING FATIGUE RESPONSE OF A Ni-BASE SUPERALLOY, PART I: MECHANISMS

S.K. Jha[1], M.J. Caton, and J.M. Larsen
US Air Force Research Laboratory, Wright-Patterson AFB, Dayton, OH 45431, USA
[1]Universal Technology Corporation, Dayton, OH 45432, USA

To be published in: *Metallurgical and Materials Transactions A*, 2008

ABSTRACT

The fatigue variability behavior of a powder metallurgy (P/M) nickel-based superalloy, IN100, was studied from the perspective of the useful-lifetime prediction. We found that the stress level produced separate effects on the mean-fatigue behavior and the life-limiting (or the worst-case) response. The fatigue variability behavior could therefore be described as the separation (or overlap) of mean-lifetime dominating mechanisms, and a life-limiting mechanism. In the present IN100 material, this separation of responses is suggested to be related to the different levels of heterogeneity induced by the number density and the size distribution of constituent particles vs. those of voids, and the sequence of selection of the failure modes. Furthermore, and perhaps of greater implication, in Part II we show that the life-limiting mechanism can be described in terms of the variability in small crack growth from the relevant microstructural size. We also demonstrate that the above description of fatigue variability leads to a probabilistic life-prediction method based on crack-growth with the potential of significantly reducing the uncertainty with the current approach wherein the lower-tail of fatigue variability is often described as the extrapolation of deviation from the expected mean-response.

Keywords: Fatigue variability, Nickel-based superalloy, Microstructure, Life prediction, Life-limiting mechanism, Mean-dominating behavior, Crack initiation, Crack growth, Probability of failure

1.0 INTRODUCTION

The traditional approach to life management of fracture-critical turbine-engine components has been largely empirical in nature [1, 2]. Typically the decision for retirement is based on an extrapolation of the "failure" (defined as the development of a predetermined level of damage) database accumulated in field, during maintenance and non-destructive inspection, as well as in the laboratory to an acceptable probability of failure (taken as 1 in 1000, or the B0.1 lifetime). Due to a large degree of uncertainty associated with this approach, a majority of the components may be retired with significant part of their useful lifetime remaining unutilized [1, 2]. One approach to this problem is to engineer improvements in the accuracy of damage characterization that will decrease the width of the "failure" lifetime distribution [3, 4]. A more significant impact on the uncertainty in life-prediction may, however, be realized by a paradigm shift in the description of fatigue variability itself towards a more physics-based theory [1]. In the present study therefore, we seek to determine the physical basis of the uncertainty in fatigue-lifetime behavior and its dependence on microstructure and loading variables. This will enable a more accurate and physics-based probabilistic life prediction method.

The fatigue variability behavior of superalloy materials has been studied by other researchers [5 - 12]. These materials are known to fail by crack initiation from processing related

void [5, 6, 9, 10, 13, 14], non-metallic constituent particle [11, 12-15], as well as from purely crystallographic crack initiation [11, 12]. Hyzak and Bernstein [5, 6] studied the effect of different types of constituent particles and void on crack initiation with respect to temperature and strain amplitude. They reported a change in the crack initiation mode from the one controlled by constituent particle and void at elevated temperature to crystallographic at room temperature. Further, at elevated temperatures they observed the void-initiated failures at higher strain ranges and the constituent particle-related failures at lower strain ranges. They also found a transition strain level below which the failure initiation switched from the specimen surface to the subsurface. This was attributed to crack initiation and crack growth dominated mechanisms at lower and higher strain ranges respectively. Several researchers have developed probabilistic descriptions of fatigue behavior of Nickel-based superalloys [7 - 10] to predict the lifetime distribution. De Bussac and Lautridou [7] modeled the failure from surface-inclusion or void to obtain a distribution in lifetime with respect to the critical size of the microstructural feature. In their work, the pore and the inclusion were treated equivalently in terms of their potential of failure initiation. Bruckner-Foit and coworkers [8] modeled the lifetime distribution for non-metallic inclusion initiated failures from a component surface. They included the variability in crack initiation as well as crack growth in their analysis. More recently, Luo and Bowen [9, 10] extended these models to incorporate the distribution in crack initiation and propagation from both pores and inclusions to describe the lifetime variability of a P/M Nickel-based superalloy. They considered only the surface failure mechanism and treated pore and non-metallic inclusion equivalently [9, 10]. These models seem to describe the specific problem in each study well, although some authors acknowledge that these may not address fatigue variability in the broadest sense.

The common aspects among the above studies can be listed as follows: (i) these tend to not account for the competition between different failure mechanisms at the same loading condition, and (ii) the sequence or the ranking of mechanisms in terms of their potential for causing failure is not addressed. One limitation of the above studies can be that these seem to be directed at determining the lifetime distribution from given size distribution of microstructural feature. This has also been the emphasis of fatigue variability studies on other materials [16-18]. For this purpose, the material is often seeded to introduce controlled levels and size distribution of particles [11]. This is an important problem and the results provide useful insights into the lifetime-variability, and in some cases [7, 9, 10] may completely describe the fatigue behavior. However, this also seems to suggest that the approach to the fatigue variability behavior has been to describe it as the distribution about the mean-lifetime behavior resulting from the deviation of input variables from their mean-values. Based on our study we argue that this conventional description of fatigue variability may tend to ignore some very important effects such as the response of the lower-tail with respect to these variables, which may be separate from the mean-response. Especially from the design-life perspective, a more encompassing problem might be the general case of interplay between different degrees of heterogeneity, and the procedure or the sequence of selection of mechanisms under given material characteristics and loading condition. As we show later in the paper, the mean-behavior and the lower-tail or the worst-case behavior (which is more pertinent for life-prediction) may be driven by different mechanisms. It is possible that due to the impracticality of testing large number of samples, and depending on the material and test condition, only a special case (that is dominated by the mean-response) of the general fatigue variability behavior may be observed. An alternate theory of fatigue variability

that may encourage a greater understanding of the lower-tail behavior may therefore be crucial in this regard.

There are some studies that address the issues stated above. De Bussac [19] modeled the competition between surface and subsurface initiation in terms of the probability of finding the critical size feature in these locations, although no distinction was made between the pore and the inclusion related crack initiation. Also, the selection between the surface and the subsurface mechanism was invoked only on the basis of the inclusion or pore size and the effect of the sequence in which a given failure mechanism is considered was ignored. For example, besides the inclusion / pore size considerations, the surface and the subsurface failures are sequential and the former is expected to occur only after all conditions for the latter are not met. Todinov [20] recognized the ranking of the lifetimes of failure from different microstructural features and based his formulation of the cumulative lifetime distribution on this relationship between various modes. A crack initiation probability was assigned to each group of features [20]. Yi and coworkers [21] in their study on a cast Al-Si alloy also performed a similar analysis that was based on ranking of pores in terms of size ranges. An alternate approach can be to rank the mechanisms rather than the average lifetime. Besides allowing for the effects of competing mechanisms, this will also account for the physically plausible case that two different mechanisms may produce similar lifetimes, although one may remain dormant unless the condition for the other is not experienced.

In a recent paper, Jha, Larsen, and Rosenberger [22], we show that the microstructure and test conditions have separate and significantly different influence on the life-limiting and the mean-fatigue behavior of an $\alpha+\beta$ titanium alloy, which correlates with the effect on the observed lifetime distribution. Chandran and Jha [23] modeled the competition between the surface and the subsurface failure in a beta titanium alloy by accounting for the different propensities of occurrence of the mechanisms. These and other studies [24, 25] indicate that an extrapolation of the variability about the mean behavior, while safe in some cases, may lead to excessively conservative design-life prediction in others. In the present study we address these issues with reference to the IN100 material and attempt to develop an improved understanding of the general fatigue variability behavior, especially in relation to the method of life prediction. In Part I of the paper, the concept of separate responses to stress level of the mean fatigue behavior and the life-limiting behavior and its relationship to sequential failures initiating from different scales of heterogeneity in IN100 is presented. In Part II, a life prediction method based on this description of fatigue variability is developed and discussed with the focus on increasing the reliability in predicted lifetimes.

2.0 MATERIAL AND EXPERIMENTAL PROCEDURE

Material

A P/M processed and subsolvus-treated nickel-based superalloy, IN100, was examined in this study. The microstructure of the alloy, shown in Fig. 1, consisted of the γ grains and primary, secondary, and tertiary γ' precipitates. The γ - primary γ' structure is shown in Fig. 1(a). The secondary γ' morphology is revealed in Fig. 1(b). The tertiary γ', which are much finer, were not resolved at this magnification. The γ grain size distribution is shown in Fig. 1(c). As shown, the mode was at about 3 - 4 μm. In addition to these phases, the microstructure also contained non-metallic constituent particles and pores typical of powder processed superalloy materials [11, 12]. The size distribution and number-density of pore and the constituent particles

were estimated based on an examination of about 100 mm^2 area of the material. The area number density of pore was estimated to be about 19/mm^2. The non-metallic particles (NMP) were relatively rare and their number-density was about 0.17/mm^2. The approximate volume densities could be derived following the formulations of Fullman [26] as adopted by Spowart, et. al. [27], and Yi and coworkers [21], and those were about 2445/mm^3 and about 10/mm^3 respectively for the pore and the NMP. The size distributions of the pore and the NMP are shown in Fig. 2 (a) and (b), respectively. The lognormal probability density function provided a good description of the size distributions, as shown. On an average the NMP were slightly larger than the pore. However, due to the very low number-density of the NMP, only a limited number of constituent particle measurements could be made in the area examined, which will produce some uncertainty with respect to the true NMP size distribution.

The 0.2% yield strength and the ultimate tensile strength of the material at the test temperature of 650°C were about 1100 and 1379 MPa, respectively. The elongation% at the same temperature was about 20%. The elastic modulus was about 186 GPa.

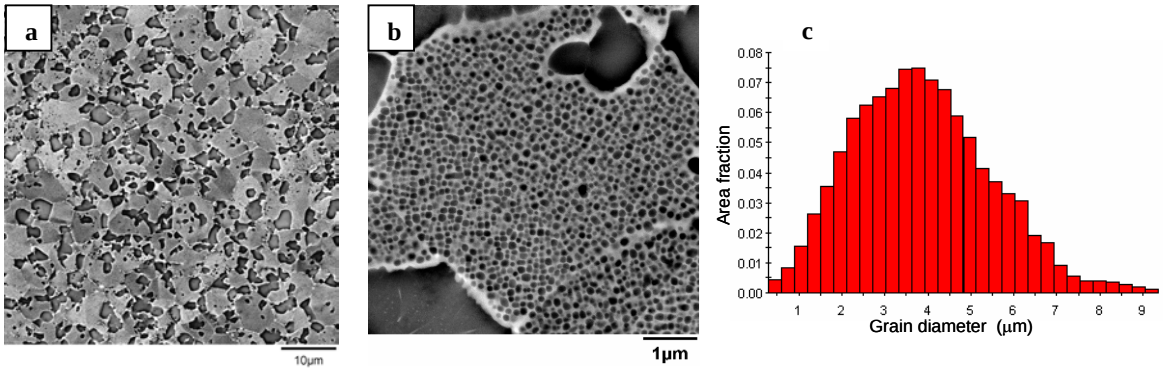

Figure 1. Microstructure of the IN100 material; (a) the γ and the primary γ' structure, (b) the secondary γ' morphology, and (c) the γ grain size distribution.

Experimental Procedure

The microstructure was characterized using a LEICA field-emission scanning electron microscope (SEM). The images were acquired at 15 KV accelerating voltage, with the beam current of 100 pA and a working distance of 15 mm. The γ-grain size distribution was determined by orientation imaging microscopy (OIM) scanning of a nominal area of the material. A TSL™ (a trademark of the EDAX Company) OIM camera and associated software were employed for that purpose. In order to determine the non-metallic particle and the pore size distributions, long duration, high-resolution scans of several large areas were acquired in the SEM. The size distributions were measured using the ImagePro™ image analysis program.

The specimens tested in this study were extracted in the circumferential orientation from a pancake forging of the material. A cylindrical, button-head test specimen was used, as described in [28] with the gage length of 15.2 mm and the diameter of 5 mm. The specimens had a low- stress-ground (LSG) finish.

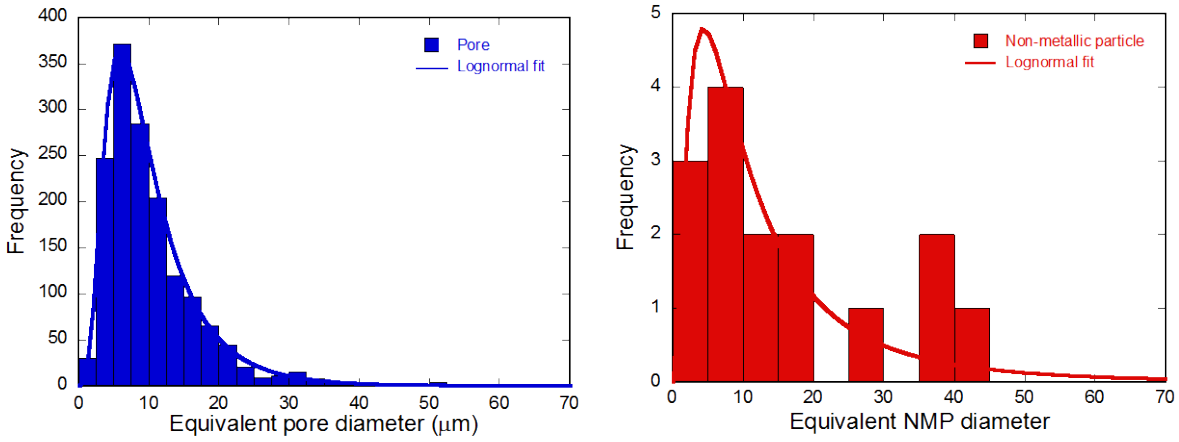

(a) (b)

Figure 2. The size distribution of microstructural features in the IN100 alloy; (a) pore, and (b) non-metallic particle.

The fatigue tests were conducted using an MTS servo-hydraulic test system with a 646 controller. An electric resistance furnace was mounted on the test frame. A high-temperature button-head gripping assembly was used in conjunction with a standard collet-grip system to transfer load to the sample. The hydraulic grip units were water-cooled. Temperature-control thermocouples were welded outside of the specimen gage section to maintain the test temperature at the specimen. The tests were performed in load control at the frequency of 0.33 Hz, the stress ratio (R) of 0.05, and the temperature of 650ºC.

A high temperature extensometer was used to record the stress-strain behavior throughout the test. A typical stress-strain profile in the first 10 cycles and beyond at the stress level of 1150 MPa is presented in Fig. 3. As shown, there was tendency to strain-harden within the first few cycles. This hardening behavior was also observed at other stress levels. The ratcheting behavior can also be seen in Fig. 3.

The small-crack growth behavior was recorded using an acetate replication technique. The small-crack specimens were electropolished to remove surface damage and residual stress from machining. The replication tapes were examined in an Olympus™ optical microscope for crack length measurements. The specimens were examined in a LEICA field emission Scanning Electron Microscope (SEM) upon fracture to document the crack initiation and growth characteristics. The crack initiation size was outlined in each sample and quantified using the ImagePro™ image analysis program.

3.0 RESULTS AND DISCUSSION

3.1 Fatigue Variability Behavior

The fatigue variability behavior of IN100 at 650°C is shown in Fig. 4 (a). As shown, while the mean-lifetime (illustrated by the dashed-line) and the life-limiting behavior tend to overlap at the highest stress level (1200 MPa), a separation between the two is seen at lower stress levels (σ_{max} = 1150 and 1100 MPa), such that the mean-lifetime is dominated by the more frequent and the longer-lifetime mechanism. This divergence of the mean behavior from the limiting response (as illustrated in Fig. 4(b)) resulted in an increase in the total variability with decreasing stress level. The fatigue variability behavior of IN100 can therefore be described as separation of a mean-dominating mechanism (or mechanisms) and a life-limiting mechanism as the stress level is decreased.

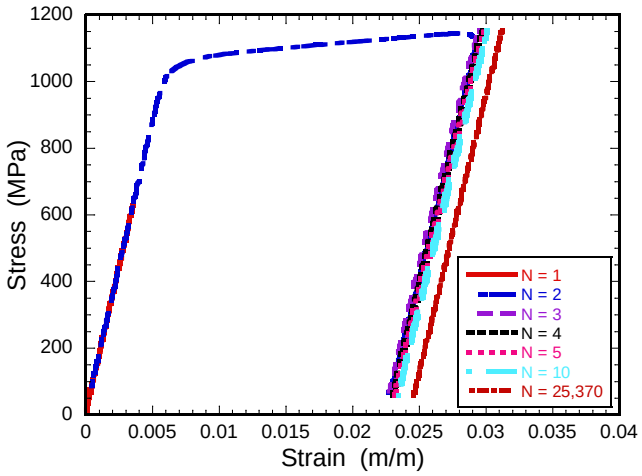

Figure 3. Typical stress-strain loop exhibited by IN100 under constant amplitude loading at σ_{max} = 1150 MPa.

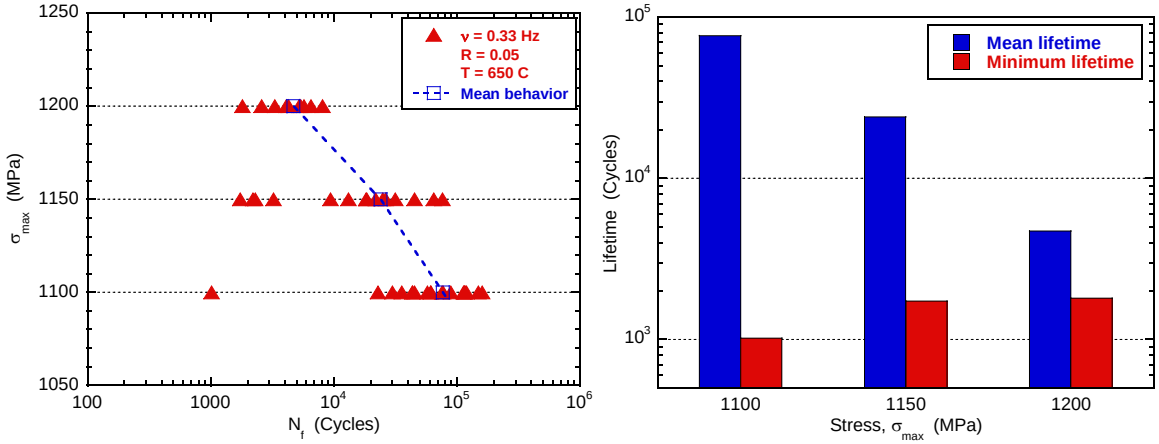

(a) (b)

Figure 4. The fatigue variability behavior of IN100; (a) Variability in lifetime, and (b) The mean vs. the minimum lifetime with respect to stress level.

The conventional understanding driving material design for fatigue resistance [29] and useful-lifetime prediction [30] appears to be guided by the mean-fatigue behavior. For instance, in the conventional approach, the effect of change in microstructure and external variables on the uncertainty in high cycle fatigue (HCF) lifetime is understood in terms of variability with respect to the expected mean-behavior [7, 9, 10, 30]. The underlying assumption is that, since the mean-lifetime is a strong function of microstructure and loading variables, the distribution in lifetime also follows the mean and can be calculated from deviations of these input variables from their mean values. This is clearly a valid description where the goal might be to affect only the average fatigue properties but this approach may not facilitate the understanding of the relationship of the input variables to the tails of the response. The conventional description may therefore be inadequate, as it appears to not account for the probability of a response that may not subscribe to the mean-fatigue dominating mechanism. In the present IN100 material, for example, the mean-lifetime and the life-limiting behavior (which is crucial in reliable life-prediction) respond differently to the stress level, causing separation between the trends for mean vs. minimum-life fatigue behavior (Fig. 4(a)). Therefore, although the mean-lifetime follows the expected response to stress level, it may not be accurate to extrapolate the variability about the mean to determine the lower-tail behavior, for e.g., the B0.1 lifetime [25].

With respect to the above discussion, it is also useful to plot the experimental points in the cumulative distribution function (CDF) space as shown in Fig. 5 (based on the lognormal probability density function (PDF)). While the CDF agreed well with the data at σ_{max} = 1200 MPa, the agreement was very poor at 1150 and 1100 MPa. A step-like shape of experimental points, illustrated by dashed lines, can be seen at σ_{max} = 1150 MPa. This indicates superposition of at least two mechanisms at that stress level producing the total variability [25]. Due to single instance of the worst-case failure at 1100 MPa, the step-like behavior although physically plausible is not yet revealed. The increase in uncertainty with decreasing stress level may therefore be related to this superposition of variability in the worst-case and the mean-dominating mechanism with diverging lifetimes.

Figure 5 also shows that the extrapolation of deviation with respect to the mean-behavior does not produce a consistent trend in the B0.1 lifetimes as a function of stress level. For example, a higher B0.1 lifetime is predicted at 1200 MPa, due to the decrease in the total variability, than at 1150 MPa. On the other hand, although a higher B0.1 lifetime is predicted at 1100 MPa, it is anticonservative with respect to the observed minimum lifetime due to the CDF being heavily biased towards the mean behavior in this case. As we show in [22], such anomalous predictions of the probabilistic lifetime-limit can be resolved in the framework of separate responses of the lower-tail and the mean-dominating behavior to microstructure and loading variables.

3.2 Competition between Mechanisms

Surface vs. Subsurface failures

The failures are characterized in terms of surface vs. subsurface crack initiation in Fig. 6(a). At the σ_{max} of 1200 MPa, the surface mechanism was observed exclusively. At the lower stress levels, however, a mix of surface and subsurface failures occurred such that the probability of subsurface failures abruptly increased below σ_{max} = 1200 MPa. Clearly, the life-limiting distribution consisted of only the surface initiated failures. It should be noted that by surface failure we refer to crack initiation from a microstructural feature either intersecting the surface or

just inside the surface (up to about one grain diameter). In the latter case, the ligament between the surface and the feature is thought to fail rapidly such that the problem can essentially be treated as surface failure [31].

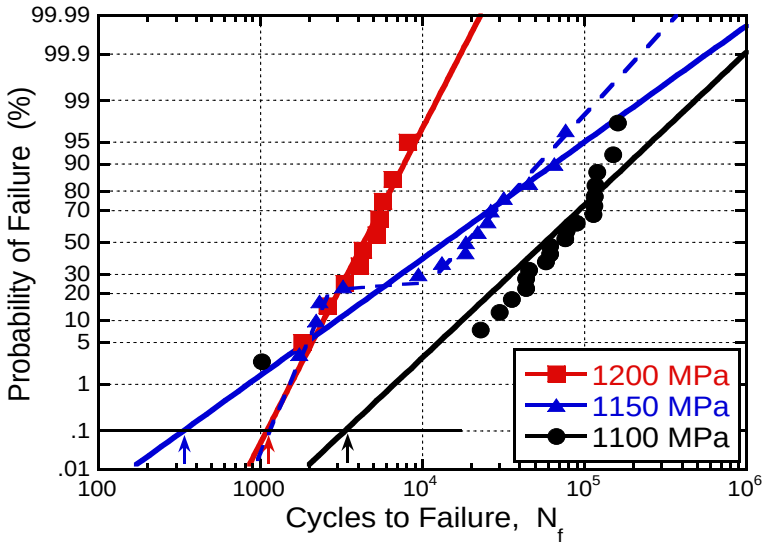

Figure 5. The experimental points plotted in the CDF space.

Crack initiation modes

In Fig. 6(b), the experimental points are identified in terms of the NMP vs. the pore-initiated failure. Comparing this with Fig. 6(a), samples can be classified into three failure mechanisms, i.e., failures from (i) surface NMP, (ii) subsurface NMP, and (iii) surface pore. Examples of each of these mechanisms are presented in Fig. 7 (a), (b), and (c) respectively. The samples in Fig. 7 were tested at the same σ_{max} level of 1150 MPa. As shown in Fig. 6 (a) and (b), the life-limiting distribution was produced by failure from surface NMP. On the other hand, the mean-lifetime dominating distribution was composed of surface-pore and subsurface-NMP failures. It is also clear from Fig. 6 that all subsurface failures were initiated at NMP and all pore-initiated failures were in the surface. This can be related to the number densities of these features. A relatively large number density of pores may make the probability of a critical surface-pore related site close to unity. On the other hand, a very small number density of non-metallic particle may result in only a small probability of finding a critical non-metallic particle related site in the surface.

Since the free surface and the region close to it see higher microplasticity level [32] than the bulk especially at low nominal stress level [32], the crack initiation is thought to be biased towards the surface. The distance of crack origin from the surface is shown with respect to lifetime in Fig. 8. For clarity, all surface failures have been plotted at d = 0 μm. As shown, the subsurface failures initiated anywhere from about 100 μm to about 2000 μm from the surface. Besides the fact that the surface NMP initiated failures had smaller lifetimes, there was no apparent correlation between the crack initiation distance and the lifetime of subsurface-initiated failures.

The relationship between the crack initiation size (in terms of crack initiation area measured on a fracture surface) and lifetime is shown in Fig. 9. Firstly, it is clear that the crack initiating pores had smaller sizes than the non-metallic particle. This may partly explain the

similar lifetimes of the surface-pore and the subsurface-particle failures in spite of the latter occurring in a pseudo vacuum condition. The range of crack initiation sizes for the worst-case failures, for example at 1150 MPa, was the same as that for the subsurface NMP failure. Therefore, for the particle-initiated failures the separation into the worst-case, and the mean-dominating distribution was not related to the size but the location, i.e., surface or subsurface. It is also interesting to note the tendency towards larger failure-initiating non-metallic particles at the lower stress level (1100 MPa).

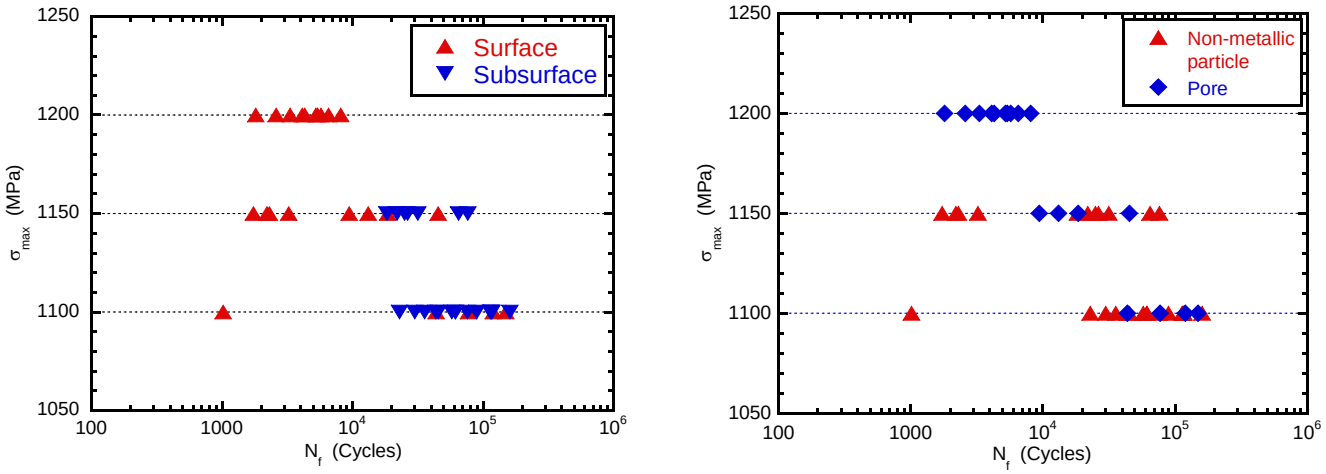

(a) (b)

Figure 6. Characterization of fatigue failures in IN100; (a) subsurface vs. subsurface initiated failures, and (b) non-metallic particle vs. pore related failures.

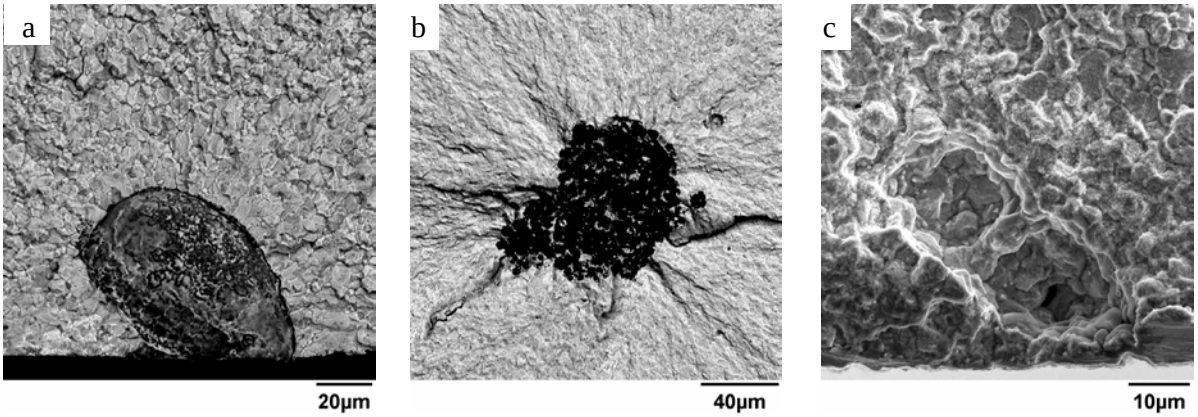

Figure 7. Examples of fatigue fractures at 1150 MPa; (a) failure from surface non-metallic particle, N_f = 2210 cycles, (b) failure from subsurface non-metallic particle, N_f = 25,081 cycles, and (c) failure from surface pore, N_f = 13,188 cycles. (a) and (b) are back scattered electron images and (c) is a secondary electron image.

A comparison of the crack initiation size distribution for the NMP and the void-initiated failures to the nominal size distributions is made in Fig 10 (a) and (b), respectively, in order to study the relative size ranges critical for a given failure mechanism. For clarity, the y-axis has been normalized in this figure due to the difference in the number of features measured in a nominal sample and the number of crack initiation size measurements. As expected, the crack initiation sizes were from the upper-tail of the nominal particle and pore size distributions,

although there was no clear correlation between lifetime and crack initiation size. This is similar to earlier results by Tryon and coworkers [33] in another Ni-based material and could be due to the effect of the crack initiation neighborhoods in addition to the size [33] and the small crack growth variability. It is also evident that the critical NMP sizes tend to be much larger than the crack-initiating pore sizes.

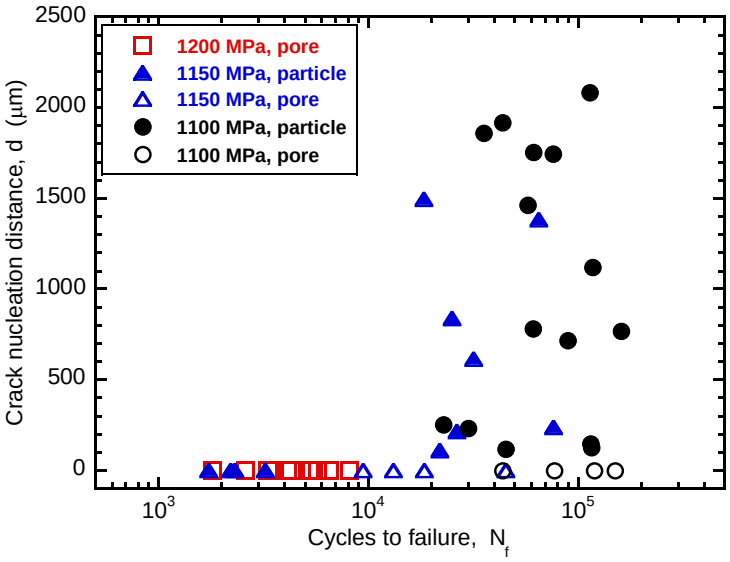

Figure 8. The crack initiation distance with respect to lifetime in IN100.

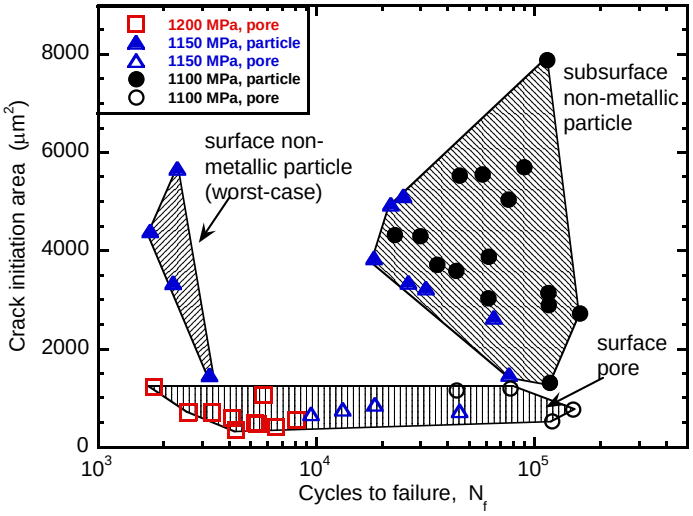

Figure 9. Crack initiation size – lifetime relationship in IN100 showing competition between mechanisms.

3.3 Ranking of Mechanisms

As discussed previously, the relative size distribution and the number density of microstructural features may produce different heterogeneity scales, affecting the probabilities and the order of selection of the mechanisms. This is suggested to produce the mean vs. the life-limiting effects on fatigue variability. It is important to recognize and understand these effects for not only reducing the uncertainty with life-prediction but also for increased reliability in the predicted useful lifetime. Here, by the "scale of heterogeneity" we imply the intensity of accumulated plastic deformation at the microscopic level. Analogies to some other physical systems can be drawn here, for instance, second-order phase transition as a function of temperature in ferromagnetism [34] causing development of ordered domains or earthquake dynamics [35] which are believed to follow a power-law scaling in terms of intensity of shocks in any given geographic region [35] and progress at several size scales. The statistical-physics based concepts applied to these other fields may also provide clues towards understanding the fatigue variability behavior. A detailed discussion will be the subject of another paper.

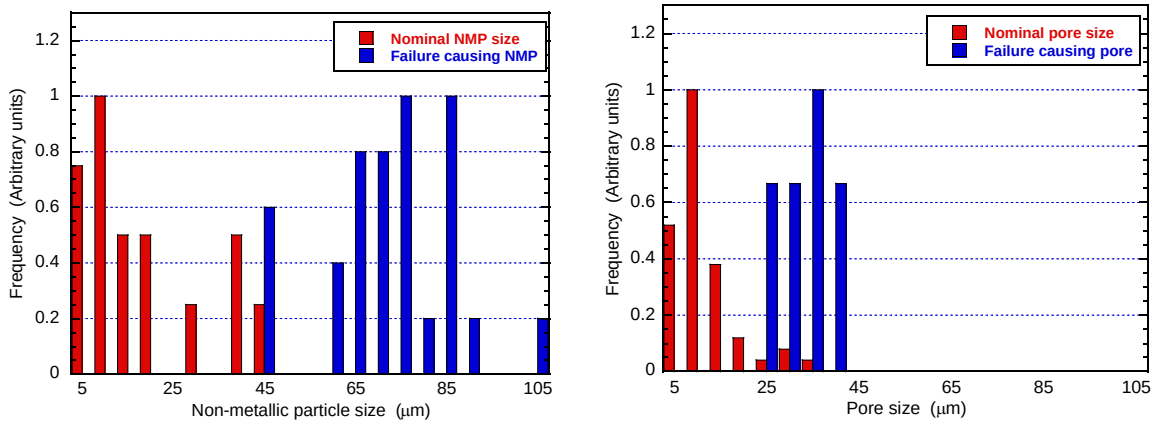

(a) (b)

Figure 10. A comparison of the critical microstructure sizes to the nominal distributions; (a) Critical NMP sizes, and (b) critical pore sizes.

Here, the ranking of mechanisms can be based on physical reasoning and experimental observation, as well as past experience with similar materials. As shown above, stress level plays an important role in determining the separation / overlap of the mean-dominating and the life-limiting behavior. Other studies [22, 24] describe the influence of microstructure and temperature on this separation / overlap of mechanisms. The role of these variables can be understood in terms of their influence on the homogeneity (or heterogeneity) of deformation [36].

At higher stress levels, under relatively homogenized deformation the mean and the life-limiting behavior can be thought to collapse and therefore indistinguishable from one another. As the stress level is decreased, different heterogeneity scales may develop [37] and evolve in time [38], even in materials with no constituent particles or voids [38]. With reference to IN100, one scale of heterogeneity that may develop with decreasing stress level is the deformation around NMPs. It is known that, under some circumstances, a NMP is preferred over a pore of equivalent size as the failure initiation site [14, 39]. This is due to the stress field generated around a NMP as a result of elastic incompatibility with the matrix, and also the thermal expansion mismatch [14, 39, 40]. Clearly, this may not be the case in all materials depending on whether the NMP has higher or lower stiffness and the coefficient of thermal expansion with

respect to the matrix [40]. It is also known, that a NMP or pore in the surface has higher driving force for crack initiation and propagation than a feature of the same size in the subsurface [19, 23]. From these two statements it can be derived, that a condition can exist where a subsurface NMP of relatively larger size may cause failure in preference to a surface pore. The very low-number density of NMP makes it highly non-uniformly distributed in a sample when compared to the pores; hence a very low probability of occurrence of the surface NMP initiated mechanism.

It can be suggested that under relatively uniform deformation, a decrease in the driving force differential between failure from a NMP and that from a pore may be related to the decreased effect of elastic incompatibility and particle related residual stress field at higher applied stresses. Hyzak and Bernstein [6] suggested that this is due to the decrease in the crack initiation life differential between pore and NMP at higher stress levels. In that case, the sites of NMPs may not be distinguishable as a higher heterogeneity scale to cause the subsurface-particle (or surface-particle) mechanism in favor of the surface pore-initiated failure. This might be another explanation for the results by Hyzak and Bernstein [5, 6] and Gabb, et. al. in the NASA studies [11, 12]. Hyzak and Bernstein's work [5, 6] also indicated a critical strain level below which the failure mechanism shifted from surface pore to subsurface NMP which is consistent with the above discussion. However, we did not see a sharp transition between pore vs. NMP-initiated failures (Fig. 5) meaning that there is some probability (at least in the theoretical sense) of each mechanism under all conditions. With a small number of tests, it is likely that only the mean-behavior is sampled at each stress level. Possibly, "sufficient" number of trials would have revealed the more complete fatigue variability behavior, including contributions from surface NMP and surface-void related failures, even at lower stress levels [5, 6]. We recognize that the "sufficient" number will be specific to a problem, depending on the size-distribution and number-density of the microstructural features, and may only be a theoretical possibility in some cases. In the least, it is crucial to develop a description of fatigue variability that provides a framework to assign probabilities to these effects. It is recognized that more work is required to resolve the stress-level effect on crack-initiation from NMP. The NASA study [11] has also recommended further experiments to understand the influence of temperature on failure initiation from a NMP.

Based on the above discussion, it is suggested that the ranking of crack initiating mechanisms should be in the order of decreasing scale of the heterogeneity involved in a mechanism, but it may be difficult to develop such a ranking that is consistent across all stress levels. For example, in the present case and other studies [5, 6, 11], the failure from NMP may not be the most dominant mechanism at all stress levels. One relatively consistent approach can be to consider the uniformity of distribution of a microstructural feature, which is related to the number-density of the features. Therefore, in the present case the mechanisms can be ranked in the following order: (I) failure from surface NMP, (II) failure from subsurface NMP, and (III) failure from surface pore. As indicated previously, with increasing stress level the damage accumulation at a NMP may not be distinct enough from that at a pore to be critical for crack initiation. Therefore, the condition for occurrence of the NMP initiated failure may be absent in almost all samples at 1200 MPa (Fig. 5), leading to the last mechanism in the sequence, i.e., failure from surface pore. The observations at 1150 and 1100 MPa are also consistent with this sequence of mechanisms. Given the very small number density of NMPs and a significantly more uniform distribution of pores, the likely criteria for failure can be listed as:

- If a "critical" NMP is present in the surface, the sample fails from mechanism I, irrespective of whether or not the condition for mechanisms II and III are present.

- If the criterion (i) is not met and a "critical" NMP is present in the subsurface, the sample fails from mechanism II, irrespective of whether or not the condition for mechanism III is present.
- If both criterion (i) and (ii) are not met then the sample fails from mechanism III – failure from a surface pore.
- Here by "critical" we imply the size necessary to cause the sufficient scale of heterogeneity for failure initiation for given microstructure and stress level. It is to be noted that, for the purpose of discussion, we have ignored the effect of the neighboring matrix at the pore and the NMP sites in determining the intensity of damage accumulation. However, the neighborhood effects are considered to play a very important role, as reported elsewhere [41].
- If p_I, p_{II}, and p_{III} represent the probabilities for the occurrence of condition for mechanisms I, II, and III, respectively, then the cumulative probability of failure can be expressed as the sum of the probabilities of each mechanism [20, 21, 23]:

$$p_f = p_I + (1 - p_I)\,p_{II} + (1 - p_I)(1 - p_{II})\,p_{III} \quad (1)$$

If none of the three criteria is met, the sample is expected to fail by crystallographic crack initiation or not at all within reasonable number of cycles. However, through simulation of the particle and the pore space in a sample, given their size distribution and number densities [42], it can be shown that in the present IN100 material there is almost 100% probability of occurrence of a critical pore in the surface. This, and the fact that the γ grain size distribution is much smaller than the pore sizes, makes it unlikely that the condition for surface pore failure will not be met in the present material. Eqn. 1 appears similar in form to the expressions derived by Todinov in [20], and Yi and coworkers in [21], but the distinction here is that the probability of failure is based on the ranking of mechanisms as related to the underlying heterogeneity scales that exist at any given condition. Therefore, in spite of the almost 100% probability of crack initiation from a surface pore, mechanism III remains dormant (at lower stress levels) until the conditions for the higher ranking mechanisms are present in a sample. Also, mechanisms II and III produce similar lifetimes but the former occurs in preference to the latter if the condition for it is present. The above criteria based on the ranking of mechanisms seem to account for these effects on fatigue variability.

The Source of Mean vs. Life-Limiting Behavior

As discussed above, the fatigue variability behavior seen here (Fig. 4) can be attributed to the relative number-densities and size-distributions of the microstructural features and the probabilities of occurrence of different scales of heterogeneity at a given stress level. However, this type of behavior is not limited to materials with constituent particles and pores. Even in materials with lower, or almost zero number-density of particles and pores, similar fatigue variability behavior was observed [22, 24, 43-45]. For example, in a supersolvus nickel-based superalloy with relatively larger γ grains and significantly lower pore content, the separation of lifetimes into mechanisms was related to crystallographic failure [24, 43]. In two microstructures of an α+β titanium alloy, such separation of the mean and the life-limiting response with decreasing stress level was seen to occur, seemingly due to finite probability of instant crack initiation from a particularly oriented equiaxed-α grain in certain lamellar α/β neighborhoods, even though the mean lifetime was clearly dominated by crack initiation [22]. We suggest that this might be the key factor driving the separation of the mean-dominating mechanism and

limiting behavior with increasing material heterogeneity. This can be stated as being related to the probability of a level of damage accumulation under any given loading condition that may cause relatively early failure-initiation, although the mean-lifetime is governed by a smaller-heterogeneity scale and therefore a relatively more uniformly distributed mechanism. Of course we recognize that in many cases such a probability can only be expressed in a theoretical sense and might not be seen experimentally.

4.0 CONCLUSIONS

The following primary conclusions can be drawn from this study:

- The mean and the life-limiting behavior of IN100 separated with decreasing stress level producing an increase in the lifetime variability.
- While the life-limiting behavior was related to failure by surface crack initiation from a non-metallic particle the mean-dominating lifetime distribution consisted of a mix of failures from surface-void initiated and subsurface non-metallic particle initiated cracks.
- A hierarchy of heterogeneity levels is proposed to develop under any given microstructure and loading condition producing sequential mechanisms such that a probability of failure exists from a relatively higher-ranked but rare heterogeneity level defining the life-limiting behavior, while the mean-dominating behavior occur from either a lower-ranked and more frequent heterogeneity scale or subsurface crack initiation.

REFERENCES

1. L. Christodoulou and J.M. Larsen, *JOM*, p. 15, March, 2004.
2. B. Cowles, *Mater. Sci. Engng*. Vol. A103, p. 63, 1988.
3. H. Ogi, M. Hirao, and S. Aoki, *J. App. Physics*, Vol. 1, p. 438, 2001.
4. J.D. Achenback, *Int. J. Solids and Struct.*, Vol. 37, pp. 13-27, 2000.
5. J.M. Hyzak, and I.M. Bernstein, *Metall. Trans.*, Vol. 13A, p. 33, 1982.
6. J.M. Hyzak, and I.M. Bernstein, *Metall. Trans.*, Vol. 13A, p. 45, 1982.
7. A. de Bussac, and J.C. Lautridou, *Fatigue Fract. Engng. Mater. Struct*., Vol. 16, p. 861, 1993.
8. A. Bruckner-Foit, H. Jackels, and U. Quadfasel, *Fatigue Fract. Engng. Mater. Struct.* Vol. 16, p. 891, 1993.
9. J. Luo, and P. Bowen, *Acta Materialia*, Vol. 51, p. 3521, 2003.
10. J. Luo, and P. Bowen, *Acta Materialia*, Vol. 51, p. 3537, 2003.
11. T.P. Gabb, J. Telesman, P.T. Kantzos, P.J. Bonacuse, and R.L. Barrie, *NASA/TM-2002 211571*, 2002.
12. T.P. Gabb, P.J. Bonacuse, L.J. Ghosn, J.W. Sweeny, A. Chatterjee, and K.A. Green, *NASA/TM-2000-209418*, 2000.
13. D. Eylon and J.M. Hyzak, *Metall. Trans*., Vol. 9A, p. 127, 1978.

14. D.A. Jablonski, *Materials Sci. Engng.*, Vol. 48, p. 189, 1981.

15. E.S. Huron and P.G. Roth, In: *Superalloys 1996,* 1996.

16. P.J. Laz and B.M. Hillberry, *Int. J. Fatigue*, Vol. 20, p. 263, 1998.

17. E.A. DeBartolo and B.M. Hillberry, *Int. J. Fatigue*, Vol. 23, p. S79, 2001.

18. S. Tanaka, M. Ichikawa, and S. Akita, *Engng. Fract. Mechanics*, Vol. 20, p. 501, 1984.

19. A. de Bussac, *Fatigue Fract. Engng. Mater. Struct*., Vol. 17, p. 1319, 1994.

20. M.T. Todinov, *Computers and Structures*, Vol. 79, p. 313, 2001.

21. J.Z. Yi, Y.X. Gao, P.D. Lee, H.M. Flower, and T.C. Lindley, *Metall. Mater. Trans*., Vol. 34 A, p. 1879, 2003.

22. S.K. Jha, M.J. Caton, and J.M. Larsen, *Mater. Sci. Engng. A*, Vol. 468-470, pp. 23-32, 2007.

23. K.S. Ravi Chandran and S.K. Jha, *Acta Materialia*, Vol. 53, p. 1867, 2005.

24. S.K. Jha, J.M. Larsen, and A.H. Rosenberger, *Acta Materialia*, Vol. 53, p. 1293, 2005.

25. S.K. Jha, J.M. Larsen, A.H. Rosenberger, and G.A. Hartman, *Scripta Materialia*, Vol. 48, pp. 1637-1642, 2003**.**

26. R.L. Fullman, *Trans. AIME*, Vol. 197, p. 447, 1953.

27. J.E. Spowart, B. Maruyama, and D.B. Miracle, *Mater. Sci. Engng*., Vol. A307, p. 51, 2001.

28. S.K. Jha, M.J. Caton, J.M. Larsen, and A.H. Rosenberger, In: *Materials Damage Prognosis*, J.M. Larsen, et. al. Eds, TMS Publ., pp. 343-350, 2004.

29. K.S. Chan and M.P. Enright, *Met and Mater. Trans. A*, Vol. 36A, p. 2621, 2005.

30. R. Tryon and A. Dey, *J. Aerospace Engng.*, Oct 2001, pp. 120, 2001.

31. A. Borbely, H. Mughrabi, G. Eisenmeier, and W.H. Hoppel, *Int. J. Fracture*, Vol. 115, p. 227, 2002.

32. M. Sauzay, and P. Gilormini, *Fatigue Fract. Engng. Mater. Struct.*, Vol. 23, p. 573, 2000.

33. R.G. Tryon, A. Dey, G. Krishnan, K.S.R. Chandran, and M. Oja, in Materials Damage Prognosis, J.M. Larsen, L. Christodoulou, J.R. Calcaterra, et. al. Eds., TMS Publ.,
p. 105, 2004.

34. K.H. Hoffman and M. Schreiber, Eds., Computational Statistical Physics, Springer Publ., pp.211-226, 2002.

35. J.B. Rundle, D.L. Turcotte, R. Shcherbakov, W. Klein, and C. Sammis, *Review of Geophysics*, Vol. 41, pp. 1019, 2003.

36. V.P. Bennet and D.L. McDowell, *Int. J. Fatigue*, Vol. 25, pp. 27-39, 2005.

37. O.B. Pedersen, *Acta Metall. Materialia*, Vol. 38, pp. 1221-1239, 1990.

38. X. Feaugas and M. Clavel, *Acta Materialia*, Vol. 45, pp. 2685, 1997.

39. M.M. Shenoy, R.S. Kumar, and D.L. McDowell, *Int. J. Fatigue*, Vol. 27, p. 113, 2005.

40. R. Bullough and L.C. Davis, *Acta Materialia*, Vol. 43, p. 2737, 1995.

41. M. Liao, *Symposium on Materials Damage Prognosis and Life Cycle Engng.*, Snowmass, CO, July, 2006.

42. S.K. Jha, M.J. Caton, J.M. Larsen, and A.H. Rosenberger, to be submitted.

43. S.K. Jha, J.M. Larsen, and A.H. Rosenberger, *JOM*, p. 50, Sep 2005.

44. S.K. Jha, J.M. Larsen, and A.H. Rosenberger In: Fatigue 2006, International Fatigue Congress, Atlanta, GA, 2006.

45. M.J. Caton, S.K. Jha, J.M. Larsen, and A.H. Rosenberger, In: Superalloys 2004.

Chapter V

THE MEAN VS. LIFE-LIMITING FATIGUE RESPONSE OF a Ni-BASE SUPERALLOY, PART II: LIFE-PREDICTION METHODOLOGY

S.K. Jha[1], M.J. Caton, and J.M. Larsen
US Air Force Research Laboratory, Wright-Patterson AFB, Dayton, OH 45431, USA
[1]Universal Technology Corporation, Dayton, OH 45432, USA

To be published in: *Metallurgical and Materials Transactions A*, 2008

ABSTRACT

In Part I [1], we showed that the mean fatigue behavior of IN100 separates from the life-limiting response with a decrease in the stress level. This separation of lifetimes was suggested to be related to the development of heterogeneity levels that produce sequential occurrence of "short-lifetime" and the "mean-lifetime" dominating mechanisms. Here, we show that the distribution in the life-limiting mechanism is controlled by small crack growth from the relevant microstructural scale in the surface, which may explain the significantly slower response of the lower-tail to the stress level, relative to the mean-lifetime response. We, therefore, describe the lifetime distribution in terms of superposition of the crack-growth-lifetime probability density and a mean-dominating density. Strategies for obtaining these probability density functions are discussed. A probabilistic life-prediction method is derived from this description and shown to provide significantly better representation of the lower-tail behavior over the traditional approach, and more reliable predictions of the probabilistic lifetime limit as a function of the stress level.

Keywords: Probabilistic fatigue life prediction, small-crack growth, dual response, separation of mechanisms, Ni-Base superalloy, IN100

1.0 INTRODUCTION

As discussed in Part I [1], an underlying assumption in the life prediction of fracture critical components has been that the lower-tail behavior is an extrapolation of random deviations from the mean-lifetime [2]. As such, many probabilistic life-prediction modeling approaches tend to be guided by the relationship of the mean-fatigue response to microstructure and loading variables [2-4]. In a recent study [5] we showed that these variables affect the lower-tail (or the life-limiting) behavior and the mean-lifetime to different degrees producing separation (or convergence) of the two responses. In other materials, we have shown [5] that the life-limiting behavior can be probabilistically described by the crack-growth regime, which explains its much slower response to stress level and other variables. This was suggested [6] to be due to the development of a hierarchy of heterogeneity levels under any given average microstructure and loading condition that produces a probability of the predominantly crack-growth-controlled mechanism. These heterogeneity levels can be related to the local microstructure. For instance in the $\alpha+\beta$ titanium alloy, Ti-6Al-2Sn-4Zr-6Mo (Ti-6-2-4-6), four microstructural configurations were identified which were suggested to produce the ranking of heterogeneous deformation scales and sequential invocation of failure from these at any given stress level [6].

The above description of fatigue variability may represent a new framework in which to assess the role of microstructure and loading variables in the probability of failure. In Ti-6-2-4-6, we have shown that changes in microstructure and test temperature has strong effects on the

mean-lifetime but the lower-tail behavior remains almost unaffected [5] due to its dependence on the crack growth lifetime. The strong role of the crack growth regime in the life-limiting behavior indicates that, for any given microstructure, certain local microstructural configurations may emerge with some probability, producing a purely crack-growth-controlled mechanism. The probability of such a mechanism will decrease with an increase in the scale of the underlying microstructural configuration and, in many cases, may not be realized in a limited number of experiments. However, a reliable probabilistic life-prediction approach, that is relatively independent of the number of tests, could be based on the crack growth description of the lower-tail behavior [5, 7]. This part of the paper, therefore, addresses these life-prediction issues with respect to the IN100 nickel-based superalloy. We determine the role of crack growth in the separation of the mean-behavior from the life-limiting response and the total lifetime variability. We present a description of fatigue variability in terms of the superposition of the crack growth probability density upon the mean-dominating density. We apply this description in a life-prediction methodology and demonstrate, with examples, the significance of the approach for reliably predicting the probabilistic lifetime limit.

2.0 ROLE OF SMALL-CRACK GROWTH IN THE LIFE-LIMITING MECHANISM

The details on the material and the experimental procedures have been provided in Part I [1] of the paper. The small and long-crack growth behaviors of IN100 are presented in Fig. 1. The effect of crack initiation from a non-metallic particle (NMP) vs. a pore is illustrated in Fig. 1(a) and the effect of stress level for a given crack initiation mode is shown in Fig. 1(b). The variability in the long crack growth regime is shown with the help of a threshold experiment and several constant K_{max} (where K is the stress intensity factor) type experiments. As shown, the variability in the long crack growth was not significant when compared to the total lifetime-variability observed in the stress-lifetime (S-N) space. The small crack growth rates were obtained from 3-point sliding polynomial fit to the crack length vs. lifetime data. All small-crack curves shown in the plots were from naturally-initiated cracks. A small-crack effect [8] is clearly present at this size scale (Fig. 1), such that the cracks grow below the ΔK threshold (ΔK_{th}) for long cracks and also have faster growth rates at the same ΔK level. Secondly, there is a significantly larger degree of variability in the small-crack growth regime when compared to the long-crack regime (Fig. 1).

A comparison of the behaviors of the NMP vs. pore initiated cracks indicates faster growth rates in the former case (Fig. 1(a)). This may be attributable to the tensile residual stress field around a NMP due to the thermal expansion mismatch [9], as well as the elastic incompatibility [10] with the surrounding matrix material. A reasonable degree of stress level effect on the small crack growth rates is also evident from Fig. 1(b). These small crack growth effects play a very important role in the proposed life prediction modeling and need to be accurately accounted for.

The measured crack initiation size distribution [1] and the variability in the small-crack growth regime can be used to evaluate the role of crack growth in the life-limiting mechanism. Towards this end, deterministic calculations were first performed to estimate the upper and lower bounds on crack-growth lifetimes. The bounds corresponded to the slowest and the fastest small-crack growth rates, in conjunction with the smallest and the largest crack initiation size, respectively. Due to relatively insignificant variability in the long-crack regime, an average long-

crack curve was used beyond the ΔK value where the degree of variability in the small-crack behavior was reduced to the similar level as in the long-crack regime.

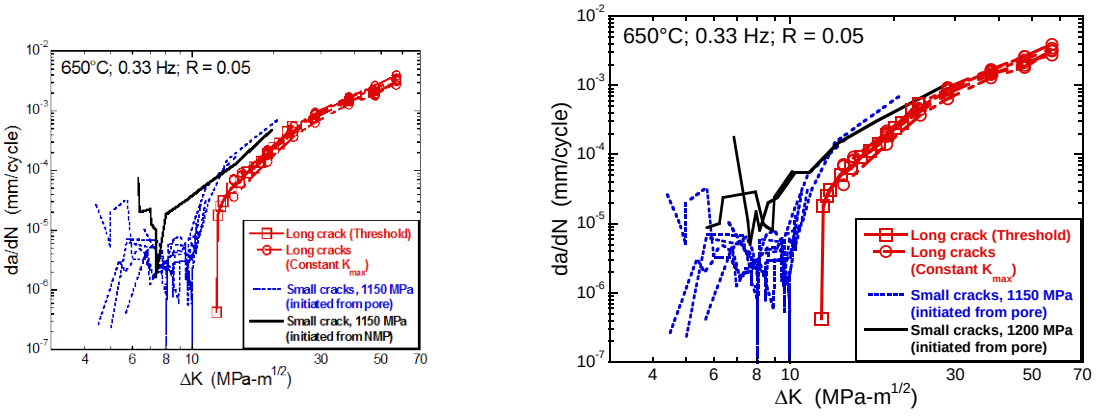

(a) (b)

Figure 1. Variability in (a) the long crack growth, and (b) the small crack growth regime of the IN100 material.

Forman and Shivakumar [11] proposed a K-solution for the problem of an elliptical surface crack in a solid cylinder, assuming crack extension according to the shape that produced the highest level of K. According to them [11] for tension loading the stress intensity factor, K_I has the form:

$$K_I = \sigma F(\lambda)\sqrt{\pi a} \tag{1}$$

where, σ is the applied stress level, ***a*** is the maximum crack depth from the surface, and the factor F(λ) is similar to a shape factor and described in [11]. It is a function of λ, which is the normalized crack depth *a*/D where D is the sample diameter.

The fastest and the slowest small crack curves were expressed in terms of multiple power-law segments fitted to the respective log(da/dN) vs. log(ΔK) data as illustrated in Fig. 2. This approach has been adopted in other studies as well [12, 13]. The crack growth lifetime can then be calculated as the total time spent in the small and the long crack regime:

$$N_{FCG} = \int_{a_i}^{a_0} \frac{da}{f(\Delta K)}\bigg|_{small-crack} + \int_{a_0}^{a_f} \frac{da}{f(\Delta K)}\bigg|_{long-crack} \tag{2}$$

where, a_i is related to the crack initiation size measured on the fracture surface, a_0 is the crack depth corresponding to the transition to the long-crack behavior (Fig. 2), and a_f is the final crack depth at the time of fracture. There were cases where the small crack regime could be best represented by two power-law segments (Fig. 2). Then, the small crack growth lifetime term in Eqn. 2 was composed of two parts. The function *f(ΔK)* describes the da/dN - ΔK relationship and is a function of crack depth, *a*. In the Paris-law [14] form it is expressed as:

$$f(\Delta K) = C\Delta K^m \tag{3}$$

where, C and m are the Paris constants and ΔK is given by Eqn. (1).

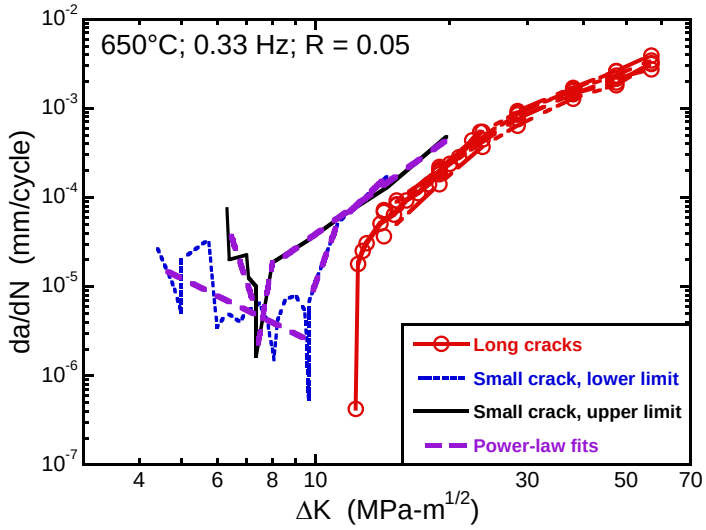

Figure 2. Bounding small-crack growth curves and corresponding power-law fits used in the calculations.

Since the life-limiting behavior corresponded to crack initiation from a NMP, the NMP-initiated small crack growth behavior ought to be used in the calculation. However, due to the small frequency of occurrence of this mechanism, only one NMP-initiated small crack growth curve was available (Fig. 1(a)). As an approximation, the upper and lower bounds on the small crack growth behavior were taken to be the measured NMP-initiated curve and the upper-bound of the pore-initiated small crack growth curves respectively, as illustrated in Fig. 2. Similarly, due to the limited small crack growth data at 1200 MPa, the small crack behavior was assumed to range between the measured upper bound curve at 1200 MPa (Fig. 1(b)) and the upper-limit of the small crack behavior at 1150 MPa. These approximations were considered reasonable in representing the shift towards higher growth rates, both under a NMP-related crack initiation and with stress level.

In the calculations, the limits on the initial crack initiation size (a_i) were based on the NMP-related sizes measured in the fractured surfaces. Assuming that the crack attains a near-semi-circular shape within the first few cycles of initiation [15], two different schemes for determining the initial crack size were employed. In these, the a_i was taken as (i) the radius of the semicircle of equivalent area [16], and (ii) the radius of the semicircle circumscribing the crack initiating feature [17].

The results presented in Fig. 3 show the calculated bounds on the crack growth lifetime. The solid lines show the first scheme (radius of equivalent semicircle) and the dotted lines indicate the lifetimes assuming the second scheme (i.e., in terms of the major-axis), considering the surface NMP-initiation at all stress levels. Due to the suggested overlap of the mean and the life-limiting behavior at 1200 MPa [1], the estimated crack growth limits tend to describe the entire range of lifetimes. On the other hand, at the lower stress levels, the predicted bounds on the crack growth lifetimes reasonably describe the life-limiting failure distribution, as well as the minimum lifetime. Although the crack growth bounds contain the life-limiting failures, its range appears wider than seen in experiments. This is attributed to the very limited number of life-limiting observations in a statistical sense. The mean lifetime, however, separates from the surface crack-growth-controlled mechanism (Fig. 3) as the stress level is decreased. We see this

type of response in other nickel and titanium-based materials [5, 18-20], even in the absence of NMP or pore-related crack initiation, where the life-limiting behavior is controlled by crack growth, producing a separation of the mean-lifetime. These calculations suggest that the variability in the life-limiting mechanism is driven by crack growth from the relevant microstructure scale.

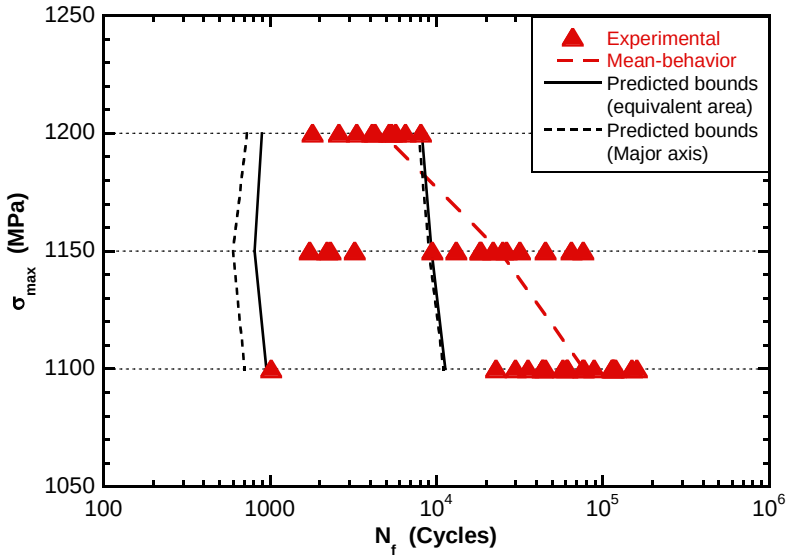

Figure 3. The predicted bounds on the crack growth lifetimes for the surface-NMP-initiated failures.

3.0 THE LIFE PREDICTION METHODOLOGY

It is important to emphasize that the key to developing the alternate life prediction methodology is the recognition that the mean and the lower-tail behavior respond differently to the stress level and microstructural modifications [5] producing a separation / overlap between the two with respect to these variables. The increased lifetime variability with decreasing stress level can therefore, be related to the crack-growth control of the life-limiting behavior resulting in its slower reaction to stress level, and the consequent increased separation of the mean-behavior from the crack-growth-controlled response. The separation of the two responses and the dependence of the life-limiting mechanism on crack growth, even in the absence of particle or pore-initiated failures [18, 21, 22], point towards a more fundamental nature of fatigue variability behavior. It can be hypothesized that under any given microstructure and loading condition, the lower-tail of the fatigue lifetime distribution is controlled by a crack growth dominated mechanism, while the mean-behavior responds at a different (and faster) rate to these variables. Clearly, the number of trials before this dual behavior is revealed will vary in each case but it is reasonable to suggest that the theoretical possibility of its existence cannot be ignored and needs to be described probabilistically. This may be especially relevant from a reliable life prediction perspective.

3.1 Calculation of the lifetime probability density

The above hypothesis, which is clearly applicable in case of the present IN100 material, allows a breakdown of the total uncertainty in lifetime into the variability in the crack growth lifetime (life-limiting) and the mean-lifetime controlling mechanisms. The total lifetime

probability density function (PDF) can, therefore, be described by a superposition of the crack growth density and the mean-dominating density as:

$$f_t(x) = p_l f_l(x) + p_m f_m(x) \quad (4)$$

Where, $f_t(x)$, $f_l(x)$, and $f_m(x)$ are the total PDF, the crack growth PDF (corresponding to the life-limiting mechanism), and the PDF describing the mean-lifetime dominating mechanism, respectively. The individual PDFs, $f_l(x)$ and $f_m(x)$, were taken as the lognormal density. These are weighted by the probability of occurrences, p_l and p_m of the respective responses [19, 23] such that $p_l + p_m = 1$.

3.2 Procedure for calculating $f_l(x)$ and $f_m(x)$

Life-limiting density, $f_l(x)$

In order to derive the total lifetime density, $f_t(x)$, the constituent densities, $f_l(x)$ and $f_m(x)$, were separately calculated and then weighted by suitable probability of occurrences. The crack growth density, $f_l(x)$, can be simulated using the small crack growth data (Fig. 1(b)) and the distribution in the crack initiation size (measured in the fracture surfaces) reported in Part I [1]. For this purpose, the crack initiation size, shown in Fig. 4(a), was modeled by the lognormal probability density. The small crack growth rate was correlated to ΔK by power-law segments as illustrated in Fig. 2. This approach averages the fluctuations in growth rate of a given crack but maintains the variation in the rates between different cracks that is attributed to the local microstructural environment. Other approaches that account for the variability in the small crack growth rates in life prediction have been suggested [24, 25] and can be implemented for the present purpose.

The random variables and their parameters used in the simulation of fl(x) have been listed in Table I. These were the crack initiation size, ai and the crack growth variables, C′ and m. The variable C′ is related to the Paris coefficient, C, as $C = e^{C'}$. The maximum likelihood estimate (MLE) was used to obtain the statistical parameters of C′ and m (Table I) from the power-law fits to the experimental small crack growth curves. As given in Table I, a_i was modeled by the lognormal density function, and C′ and m were modeled by the normal density. The crack growth parameters are strongly correlated as reported in other studies [12, 26]. The correlation coefficient in the present problem was determined to be -0.98. The Monte Carlo simulation therefore, involved sampling from the joint probability density of C′ and m, presented in Fig. 4(b). The crack growth lifetime in each simulation step was calculated according to Eqn. 2. The number of Monte Carlo samples was 10,000, which were used to construct the crack growth density, $f_l(x)$. Note in Table I that the small crack growth behavior at 1100 MPa was assumed to be the same as at 1150 MPa. Additional small crack data at these stress levels and under the specific condition of NMP-initiated crack will further increase the accuracy of the life-prediction model described here.

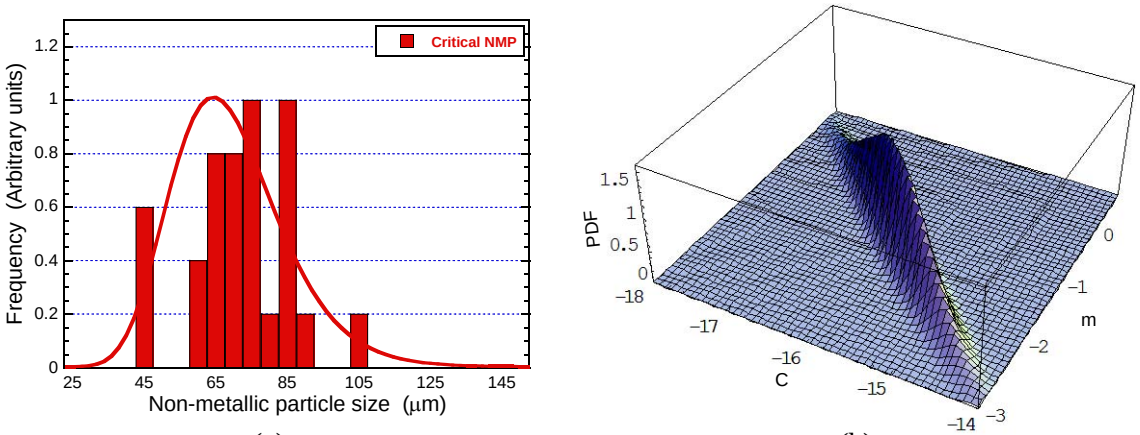

Figure 4. Example of inputs to the simulation of the crack growth density, $f_l(x)$; (a) Crack initiation size distribution and (b) joint probability density of C and m.

The CDFs corresponding to the simulated crack growth densities are compared to the experiment in Fig. 5. At 1200 MPa (Fig. 5(a)), the calculated CDF agreed well with the experiment. At 1150 and 1100 MPa, the crack growth density reasonably described the life-limiting response. At 1150 MPa (Fig. 5(b)), this is illustrated by plotting the experimental life-limiting points as a separate distribution. Notably, the solitary life-limiting point at 1100 MPa (Fig. 5(c)) is accounted for by this approach. This may otherwise necessitate a large number of experiments to reveal, depending on the probability of occurrence.

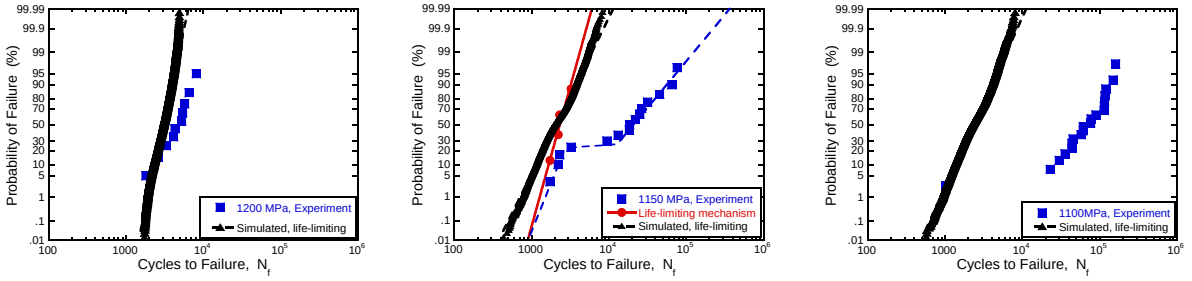

Figure 5. Simulated life-limiting probability densities ($f_l(x)$) in IN100; (a) σ_{max} = 1200 MPa, (b) σ_{max} = 1150 MPa, and (c) σ_{max} = 1100 MPa.

Mean-dominating density, $f_m(x)$

The mean-dominating density, $f_m(x)$, was calculated from 4 randomly selected total lifetime experiments at each stress level. This is illustrated in Fig. 6. The MLE was then used to determine the parameters of $f_m(x)$, given in Table I. It is to be noted that the mean fatigue response is the often characterized behavior and used for the purpose of material design, as well as for life prediction. Such data, if available, can also be used with suitable statistical analysis to derive $f_m(x)$.

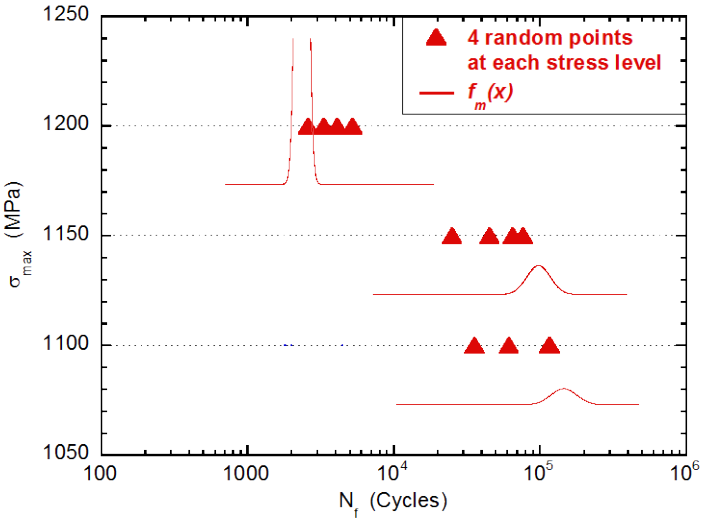

Figure 6. Illustration of the calculation of the mean-dominating density, $f_m(x)$.

3.3 Predicted lifetime densities and probabilistic limits

The calculated lifetime probability densities are shown in Fig. 7 and the corresponding CDFs are presented in Fig. 8. Here, the weighting factors, p_l and p_m, were obtained from the S-N experiments and are listed in Table I. However, it can be shown that the lower tail of the lifetime density and the probabilistic limit (for e.g., the B0.1 lifetime) is very weakly affected by p_l or p_m within a reasonable range of values [7]. Furthermore, in the limiting case (i.e., when $p_l \rightarrow 1$), the B0.1 lifetime obtained from the crack growth density, $f_l(x)$, forms the lower-bound of the B0.1 lifetime predicted by the bimodal density [7]. Therefore, although the factors, p_l and p_m, are important in accurately describing the total lifetime density and the effect of material and extrinsic variables on the lifetime variability, these do not significantly affect the calculation of the probabilistic lifetime limit.

In Fig. 7, the traditional description of fatigue variability, where the lower tail of the distribution is assumed to result from random deviations from the mean behavior, has also been plotted for comparison. The B0.1 lifetimes have been indicated by vertical lines and the experimental points are represented by open symbols. Figures 7 and 8 clearly indicate that the suggested lifing model provides a significantly better representation of the fatigue variability behavior. This is particularly evident from Fig. 8, where the experimental points show reasonable agreement with the calculated CDFs for the p_l values listed in Table I. The calculated lifetime densities appear to effectively capture the effect of stress level on the lifetime variability, indicated by both Figs. 7 and 8. At 1200 MPa, the densities, $f_l(x)$ and $f_m(x)$ overlap and can be considered to be indistinguishable from one another. With decreasing stress level, the separation between the two PDFs increases (Fig. 7) promoting the increased lifetime variability.

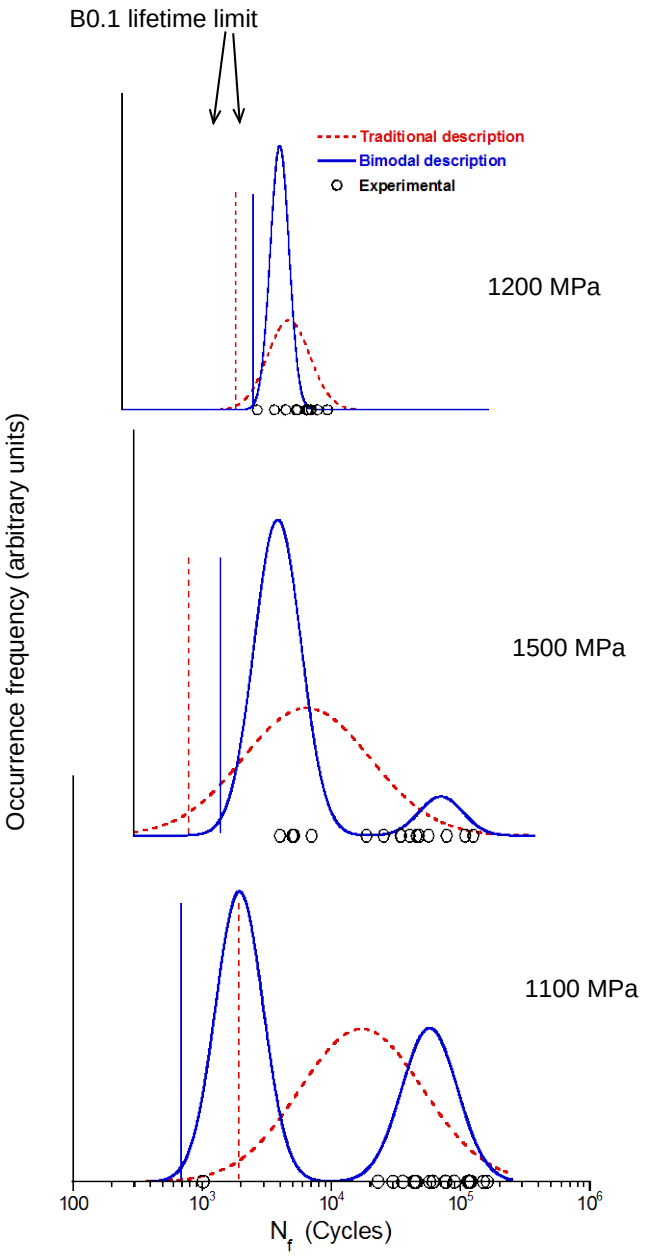

Figure 8. The calculated lifetime densities and the B0.1 lifetimes with respect to stress level in IN100.

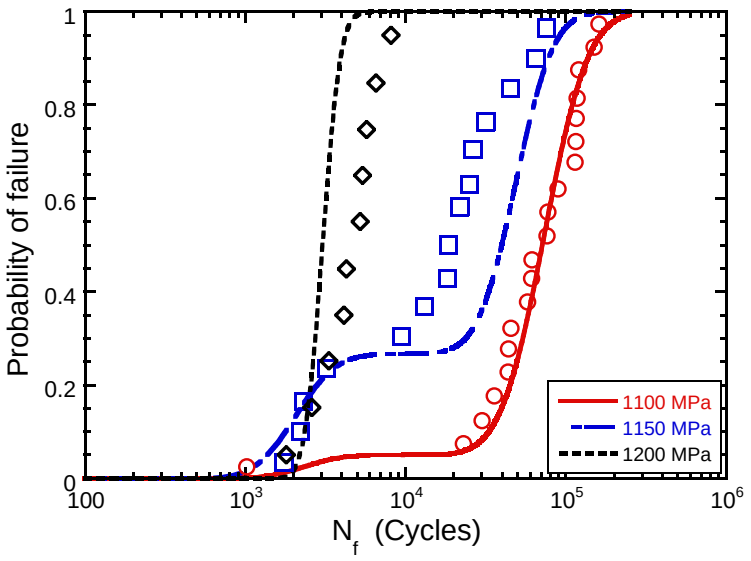

Figure 9. The predicted CDFs with respect to stress level in IN100.

An even more relevant outcome of this approach can be the consistency in prediction of the probabilistic lifetime limit or the B0.1 lifetime. In the conventional description (Fig. 7), the B0.1 lifetimes show a physically counterintuitive trend with respect to stress level [1], besides being heavily dependent on the number of experiments. For example (in the traditional approach) the B0.1 lifetime appears to vary from an over-conservative value at 1150 MPa, which is lower than the B0.1 lifetime predicted at 1200 MPa, to a non-conservative value at 1100 MPa. On the other hand, Fig. 7 illustrates that the proposed model produces, perhaps, a physically consistent trend in the B0.1 lifetime as a function of the stress level, and its prediction is almost independent of the total number of fatigue experiments thereby, significantly decreasing the uncertainty in the probabilistic limit. As stated earlier, Fig. 7 also shows that the bimodal lifetime density accounts for the single life-limiting failure at 1100 MPa, detection of which may require a large number of experiments due to its low frequency of occurrence. Note, however, that the experiments alone are not sufficient in accurately predicting the B0.1 lifetime without the key understanding of the role of the separation of the mean behavior from the crack-growth-controlled response in the lifetime variability.

The above method also suggests that, from the perspective of predicting the probabilistic lifetime limit, the crack growth density, $f_l(x)$ is sufficient. This is because, the B0.1 lifetime from the proposed lifetime density is lower-bounded by the probabilistic limit derived from $f_l(x)$. This is illustrated in Fig. 9 with the help of the data at 1150 MPa. The crack growth density is compared to the calculated total lifetime density, $f_t(x)$, and also to the traditional description. The PDFs and the corresponding CDFs are shown in the bottom and the top plot respectively. The B0.1 lifetimes have been indicated. Expectedly, the B0.1 lifetimes predicted by the crack growth density and the bimodal lifetime density are similar. With respect to the traditional description of fatigue variability, the crack growth density produces a more accurate but also a more reliable B0.1 lifetime, irrespective of the number of total-lifetime experiments. This creates the potential for a significant reduction in uncertainty in probabilistic lifetime-limit prediction, as indicated in Fig. 9.

This paper is concerned with demonstrating the concept of separation of the mean vs. the crack-growth-controlled life-limiting behavior, in describing the effect of stress level on the lifetime distribution and the probabilistic lifetime limit in IN100. The same framework can be applied to predict the effect of a host of other variables, such as the microstructure and the dwell time, on the probabilistic limit. This, coupled with the ability to obtain multiple small crack growth curves from a single experiment by artificial crack initiation from Focussed Ion Beam (FIB) machined notches [27] may further enable a very efficient and reliable prediction of the effect of both the intrinsic and the extrinsic variables on the probabilistic lifetime-limit.

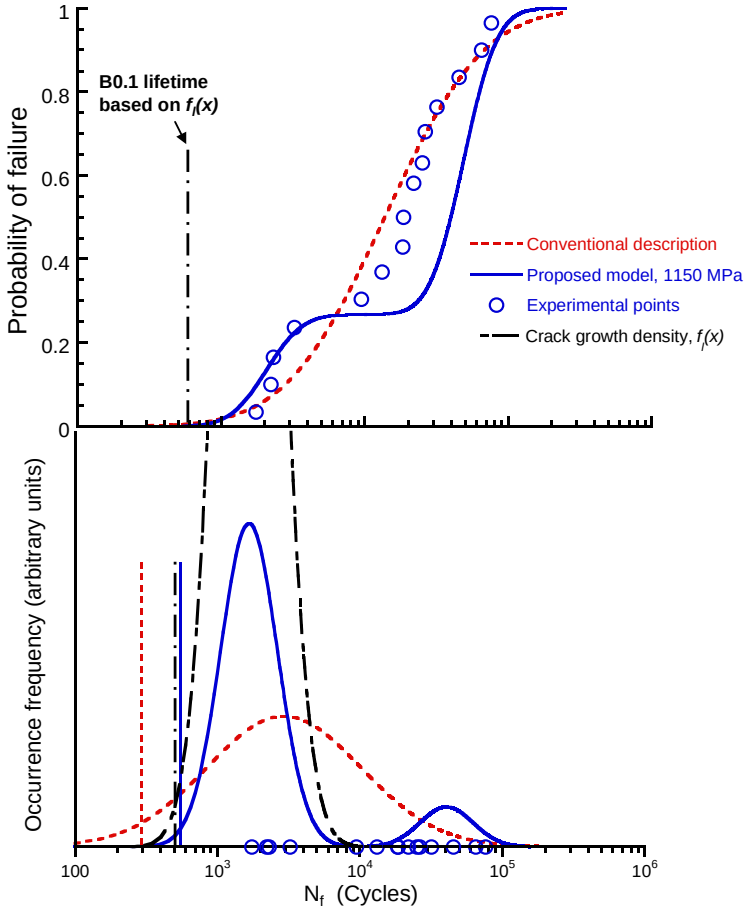

Figure 10. Illustration of the proposed life prediction approach based on the crack growth density compared to the total lifetime density (σ_{max} = 1150 MPa).

4.0 CONCLUSIONS

The following main conclusions can be drawn from this study:

- It may not be accurate to deduce the lower-tail of the fatigue lifetime variability from an extrapolation of the deviations about the mean behavior.

- The lower-tail of the lifetime distribution of the IN100 material can be described by a crack growth probability density, which is superimposed upon the mean-lifetime dominating density to produce the total fatigue variability description.
- The increase in lifetime variability with decreasing stress level is suggested to be due to the weak response of the crack-growth controlled density to stress level but a stronger response of the mean-dominating density producing increased separation between the two.
- The crack growth PDF is simulated using the small-crack growth data and the distribution in the crack initiation size and applied in a life-prediction method, which produces a more reliable probabilistic lifetime-limit almost independent of the number of total lifetime experiments, besides resolving the physically anomalous trends in the lifetime-limit with respect to stress level.

ACKNOWLEDGEMENTS

This work was performed at the Air Force Research Laboratory, Materials and Manufacturing Directorate, Wright-Patterson Air Force Base, OH. The partial financial support of the Defense Advanced Research Project Agency (DARPA) under DARPA orders M978, Q588, P699, and S271 with Dr. Leo Christodoulou as the program manager is gratefully acknowledged. Essential support was also provided by the Air Force Office of Scientific Research (AFOSR) with Dr. Victor Giurgiutiu as the program manager. We acknowledge Mr. Phil Buskohl and Ms. Lindsey Selegue for their assistance with the replication-based small-crack growth experiments.

REFERENCES

1. S.K. Jha, M.J. Caton, and J.M. Larsen, Part I of this paper.
2. J.N. Yang and W.J. Trapp, *AIAA Journal*, Vol. 12, pp. 1623-1630, 1974.
3. R. Tryon and A. Dey, *J. Aerospace Engng.*, p.120, 2001.
4. K.S. Chan and M.P. Enright, *Journal of Engineering for Gas Turbines and Power*, Vol. 124, pp. 889-885, 2006.
5. S.K. Jha, M.J. Caton, and J.M. Larsen, *Materials Science and Engineering A*, Vol. A468-470, pp. 23-32, 2007.
6. S.K. Jha and J.M. Larsen, in *Very High Cycle Fatigue, VHCF-4*, 2007.
7. S.K. Jha, J.M. Larsen, and A.H. Rosenberger, in review, *Engineering Fracture Mechanics*.
8. J. Lankford, T.S. Cook, and G.P. Sheldon, *Int. J. Fracture*, Vol. 17, pp. 143-155, 1981.M.
9. M. Shenoy, R.S. Kumar, and D.L. McDowell, *Int. J. Fatigue*, Vol. 27, p. 113, 2005.
10. R. Bullough and L.C. Davis, *Acta Materialia*, Vol. 43, p. 2737, 1995.
11. R.G. Forman, and V. Shivakumar, in *Fracture Mechanics: 17th Volume*, ASTM STP 905, J.H. Underwood, R. Chait, C.W. Smith, D.P. Wilhem, W.A. Andrews, and J.C. Newman, Eds., ASTM, Philadelphia, pp. 59-74, 1986.

12. J. Luo, and P. Bowen, *Acta Materialia*, Vol. 51, p. 3521, 2003.

13. J. Luo, and P. Bowen, *Acta Materialia*, Vol. 51, p. 3537, 2003.

14. P.C. Paris and F. Erdogan, *J. Basic Engineering, Trans. ASME*, Series D, Vol. 85, pp. 528-534, 1963.

15. K. Gall, M.F. Horstemeyer, B.W. Denger, D.L. McDowell, and J. Fan, *Int. J. Fracture*, Vol. 108, pp. 207-233, 2001.

16. J.C. Newman, Jr., E.P. Phillips, and H.M. Swain, *Int. J. Fatigue*, Vol. 21, pp. 109-119, 1999.

17. E.A. DeBartolo and B.M. Hillberry, *Int. J. Fatigue*, Vol. 23, p. S79, 2001.

18. S.K. Jha, J.M. Larsen, and A.H. Rosenberger, *Acta Materialia*, Vol. 53, p. 1293, 2005.

19. S.K. Jha, J.M. Larsen, A.H. Rosenberger, and G.A. Hartman, *Scripta Materialia*, Vol. 48, pp. 1637-1642, 2003.

20. S.K. Jha, J.M. Larsen, and A.H. Rosenberger In: *Fatigue 2006*, International Fatigue Congress, Atlanta, GA, 2006.

21. S.K. Jha, J.M. Larsen, and A.H. Rosenberger, *JOM*, p. 50, Sep 2005.

22. M.J. Caton, S.K. Jha, J.M. Larsen, and A.H. Rosenberger, In: *Superalloys 2004*.

23. A.H. Fischer, A. Abel, M. Lepper, A.E. Zitzelsberger, and A. von Glasgow, *Microelectronics Reliability*, Vol. 47, pp. 445, 2001.

24. M.D. Halliday, C. Cooper, P. Poole, and P. Bowen, *Int. J. Fatigue*, Vol. 25, pp. 709-718, 2003.

25. M.E. Robinson and M.J. Crowder, *IEEE Transactions on Reliability*, Vol. 51, pp. 216 – 222, 2002.

26. C.G. Annis, Jr., in *Probabilistic Aspects of Life Prediction*, ASTM-STP 1450, W.J. Johnson and B.M. Hillberry, Eds., ASTM International, West Conshohocken, PA, 2003.

27. S.K. Jha, M.J. Caton, J.M. Larsen, and A.H. Rosenberger, in *Materials Damage Prognosis*, TMS Publications, 2005.

Chapter VI

PREDICTING THE EFFECT OF DWELL TIME ON THE PROBABILISTIC LIFETIME LIMIT IN A NICKEL-BASED SUPERALLOY

S.K. Jha[1], M.J. Caton, and J.M. Larsen
US Air Force Research Laboratory, AFRL/RXLMN, Wright-Patterson Air Force Base, OH 45433
[1]Universal Technology Corporation, 1270 N. Fairfield Rd., Dayton, OH 45432

To be published: *Superalloys-2008*, 2008.

ABSTRACT

The mean and the life-limiting behavior under fatigue of the nickel-based superalloy, IN100, separated (or converged) as a function of stress level and dwell loading. This behavior was related to the control of the life-limiting behavior by the small-crack growth regime, producing its much slower response to stress level and dwell-time, relative to the mean-lifetime behavior. The lifetime probability density is therefore, modeled as a superposition of the crack growth lifetime density and a mean-lifetime density. The crack growth density is calculated with the help of small-crack growth data and the distribution in the crack initiation size. The mean-lifetime density is estimated from a relatively small number of total lifetime fatigue tests. In IN100, we apply this approach to predict the effects of stress level and dwell time on the lifetime distribution and the B0.1 (1 in 1000 probability of failure) lifetime limit.

Keywords: Probabilistic life prediction, mean vs. life-limiting fatigue, IN100, small crack growth, crack initiation size, dwell fatigue

1.0 INTRODUCTION

Accurate life prediction of fracture critical components is essential for safe and reliable operation, as well as for cost effective life cycle management [1]. A probabilistic lifing method allows for the incorporation of material and microstructural uncertainties, and service-related variability in loading, environment, inspection, etc. into the life-prediction model. Often, in the past, the approach has been to empirically determine the uncertainty factors that would represent the variability in otherwise deterministically calculated lifetime [2, 3]. Recently, the emphasis has increasingly been on physics-based probabilistic life prediction methods, where the lifetime is explicitly modeled in terms of the uncertainty in the intrinsic material factors and the extrinsic variables [4, 5]. However, the focus has been on the mean-fatigue relationship to these variables and the probabilistic treatment is accomplished by randomizing the parameters in such relationships [5, 6]. In other words, the lifetime variability is considered as due to random deviations from the mean behavior and hence, the lower-tail is derived by extrapolating the deviations about the mean. The “mean-based” approach to fatigue variability may, in some cases, produce inconsistent probabilistic lifetime-limits with respect to material and extrinsic variables necessitating a large number of experiments for verification, as illustrated in [7, 8].

Another approach to probabilistic life-prediction could be to consider, that in any material the microstructure can randomly arrange into local configurations [9, 10]. These configurations can vary in terms of their size scale and/or the degree of heterogeneous deformation upon fatigue loading, and will occur with differing probabilities. Then, the total lifetime variability can be described as a probabilistic realization of sequential failure mechanisms occurring in the order of

decreasing heterogeneity level [9]. Theoretically, under any nominal microstructure and fatigue loading, it is possible to assign a probability to the occurrence of a microstructural configuration where crack initiates almost instantaneously. The lower-tail behavior in this approach is therefore, limited by the (small + long) crack growth regime. This hypothesis also implies that, for a given crack initiation location (surface or subsurface), the mean-lifetime-dominating mechanisms are associated with relatively lower heterogeneity levels and bear a larger role of the crack initiation regime. The mean-behavior, therefore, is considered to respond differently than the lower-tail behavior, to the microstructure and loading variables. For example in Ti-6Al-2Sn-44Zr-6Mo (Ti-6-2-4-6), an $\alpha+\beta$ titanium alloy, the crack initiation regime is significantly more sensitive to stress level and temperature when compared to the crack growth rates. This was shown to produce an increased separation between the mean-lifetime and the life-limiting behavior with a decrease in either the stress level or the temperature [7].

In this paper, the above approach is applied to describing the fatigue variability behavior of the nickel-based superalloy, IN100. The effects of stress level and dwell time on the mean vs. the life-limiting behavior are evaluated. The lifetime probability density and the B0.1 lifetime limit are predicted as a function of stress level and dwell time, with the help of small-crack growth data and a relatively small number of total lifetime experiments.

Material and Experimental Procedure

Material

The material in this study was a fine-grained, subsolvus powder-processed nickel-based superalloy, IN100. The median γ-grain size was about 4 μm. The microstructure of the alloy is presented in Fig. 1 showing the γ-primary-γ' structure (Fig. 1(a)) and the secondary γ' precipitates (Fig. 1(b)).

Experimental Procedure

The specimens for the stress-lifetime (S-N) fatigue and the small crack growth tests were extracted by electro-discharge machining in the circumferential orientation from a pancake forging of the material. The specimens had cylindrical gage with button-head ends. The gage length was 15.2 mm and the diameter was 5 mm. The gripping assembly was designed to extend into the furnace and was held at temperature during the elevated temperature tests. The S-N fatigue specimens were run in the low stress ground surface condition.

The fatigue experiments were conducted in load control using an MTS servo-hydraulic test system with a 458 controller. The test temperature was 650°C. An ATS dual-zone resistance-heated furnace was used for this purpose. Thermocouple leads were welded to the ends of the specimen gage to control and monitor the temperature during the test. The frequency of 0.33 Hz and the stress ratio of 0.05 were employed. The dwell fatigue tests were run with 6 seconds dwell at the peak load while maintaining the other experimental conditions the same.

The small crack growth experiments were run in the same test system under no-dwell and 6 seconds dwell conditions. An electropolished surface condition was used for these experiments. The acetate replication technique was employed to record crack lengths at predetermined intervals. At each replication step, the test was interrupted, and the specimen was unloaded and cooled down to room temperature. The replication was done under a hold load of 60% of the peak load in the fatigue cycle.

The microstructure and the fatigue fracture surfaces were characterized using a Leica field emission scanning electron microscope (SEM). The crack initiation size was measured on the fracture surfaces using the ImagePro™ image analysis program. The crack length measurement on the replicas was done in an Olympus optical microscope.

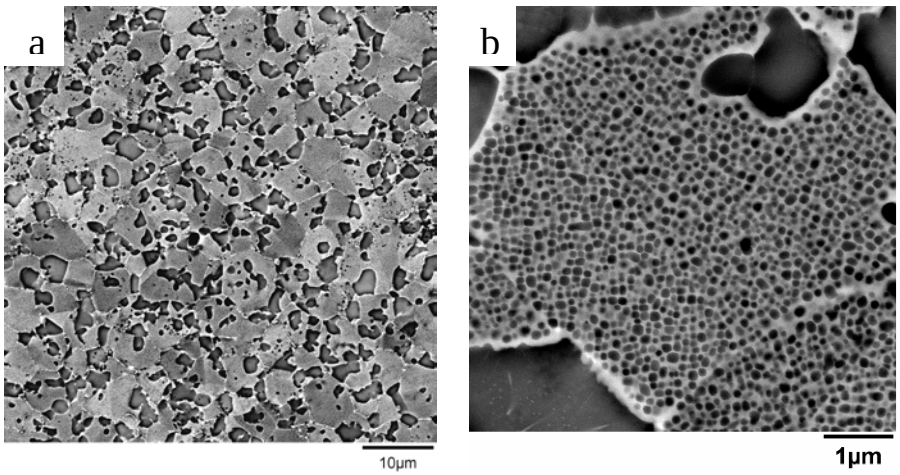

Figure 1. Microstructure of IN100; (a) the γ-primary-γ´ morphology and (b) the secondary γ´ structure.

Results and Discussion

Description of fatigue variability and the role of small crack growth

The fatigue variability behavior of IN100 under constant amplitude loading at 650°C is shown in Fig. 2. The mean vs. life-limiting behavior is illustrated in Fig. 2(a) and the cumulative distribution functions (CDF) are plotted in Fig. 2(b). Figure 2(a) indicates that a separation of lifetimes occurred with a decrease in the stress level causing the mean-lifetime, represented by the dashed line, to diverge from the life-limiting response. Such a separation could occur when, relative to the mean-dominating behavior, the life-limiting behavior has a much slower response to stress level. Besides the stress level, the mean and the life-limiting behavior can be affected to different degrees as a function microstructure and temperature producing separation / overlap between the two as shown in [7].

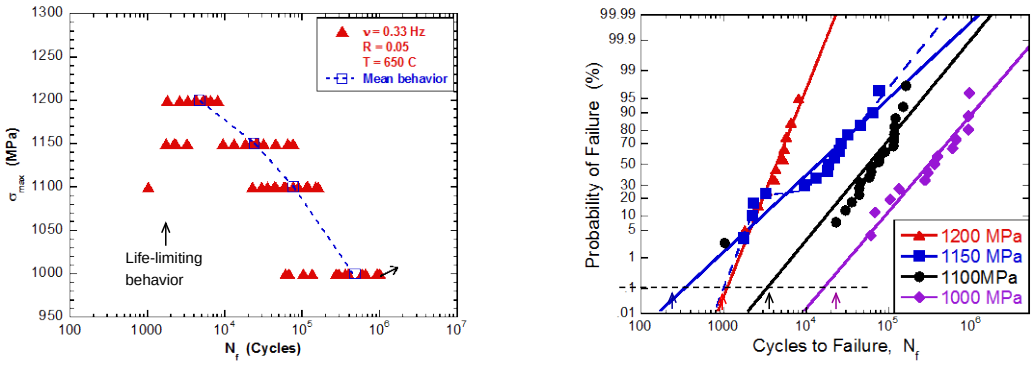

(a) (b)

Figure 2. The fatigue variability behavior of IN100; (a) The mean vs. life-limiting behavior and (b) Cumulative distribution functions showing the B0.1 lifetimes.

Figure 2(b) shows that the B0.1 lifetimes (indicated by arrows) based on the extrapolation of total variability to the lower tail do not exhibit a consistent trend with respect to stress level. For example, a significantly higher B0.1 lifetime is predicted at 1200 MPa than at 1150 MPa. On the other hand, although the predicted B0.1 lifetime at 1100 MPa is larger than at 1150 MPa, it is non-conservative with respect to the observed minimum lifetime at that stress level. Such anomalous trends may be attributable to the assumption that the increase in uncertainty with respect to stress level (or any other variable) can be described as an increase in the deviation from the mean behavior. Further, it is noted that, while in some cases, the separation of lifetimes may not be discernible; in others it may require an impractical number of experiments to observe the same. In the following sections we discuss, perhaps, a more accurate representation of the lower tail and the total lifetime probability density, which provides physically consistent probabilistic lower lifetime-limits, independent of the number of total-lifetime experiments.

An examination of the crack initiation modes revealed that the life-limiting distribution, at lower stress levels, consisted of surface non-metallic particle initiated failures while the mean-dominating distribution consisted of a mixture of subsurface NMP-initiated and surface pore-initiated failures. This is summarized in Fig. 3 in terms of the crack initiation size vs. lifetime relationship. Figure 3 shows that there is a slight tendency towards larger NMP-related crack initiation sizes at 1100 MPa than at 1150 MPa. However, the separation of lifetimes is governed by the mode and the location of crack initiation rather than the size.

The Role of the small crack growth regime. As stated previously, the separation of mean-lifetime behavior from the life-limiting response with decreasing stress level can be attributed to the relatively stronger sensitivity of the mean-behavior to stress level. In other materials, including Ti-6-2-4-6 [7, 9, 10] and a γ-TiAl based alloy [8], we have shown that this slower response of the life-limiting behavior to stress level is due to its dominance by the crack growth regime. Physically, this was reasoned as due to the development of a hierarchy of heterogeneity levels at any given loading condition producing a sequential selection of failure mechanisms in the order of decreasing heterogeneity level [9]. A probability can, therefore, be assigned to the occurrence of a purely crack growth lifetime controlled mechanism, irrespective of the nominal microstructure and loading condition [9]. The variability in the crack growth behavior, therefore, is a critical input in describing the lower tail of the lifetime probability density.

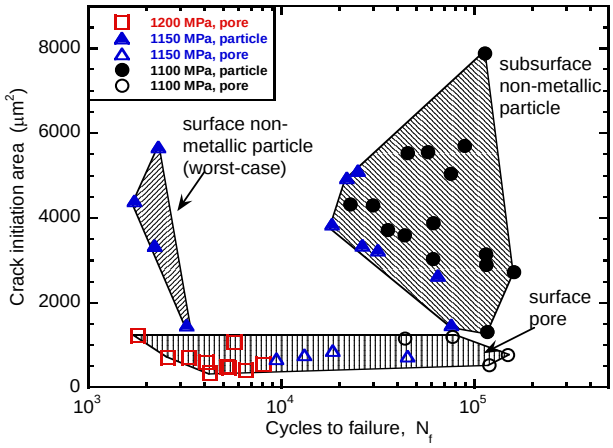

Figure 3. The separation of lifetimes with respect to crack initiation mechanisms in IN100.

The variability in the small crack growth rates in IN100 at 650°C is compared to the long crack growth regime in Fig. 4. The crack growth rates were calculated by using the three-point sliding polynomial fit to the crack depth (*a*) vs. cycle (N) data. The stress intensity factor was calculated using the Foreman and Shivakumar K-solution for an elliptical surface crack in a round bar [11]. In addition to the round-bar geometry, some of the small crack growth data shown in Fig. 4 were obtained from square cross-section samples but with similar cross-sectional area and gage length as the cylindrical specimens. The K-solution for elliptical surface crack by Newman and Raju [12] were used for crack growth analysis in this geometry.

Figure 4(a) compares the growth rates of the NMP and the void initiated cracks and Fig. 4(b) shows the effect of stress level on the small crack growth behavior. These figures indicate that the long crack growth behavior showed a significantly less degree of variability than the small crack regime. Furthermore, the variability in the small crack growth behavior (for void-initiated cracks at 1150 MPa) reduced to a similar level as in the long crack beyond the crack length of about 100 μm. Clearly, the NMP-initiated small cracks showed higher growth rates than the pore-initiated cracks (Fig. 4(a)). Besides the relatively larger crack initiation sizes associated with the NMP (Fig. 3), this could also be due to the tensile residual stress field around a NMP due to the elastic incompatibility as well as, the thermal expansion mismatch with the matrix material [13, 14]. The effect of stress level on the small crack growth behavior also appears to be significant (Fig. 4(b)) in this material. These small crack growth effects need to be accounted for, and will play an important role in the proposed probabilistic life-prediction model.

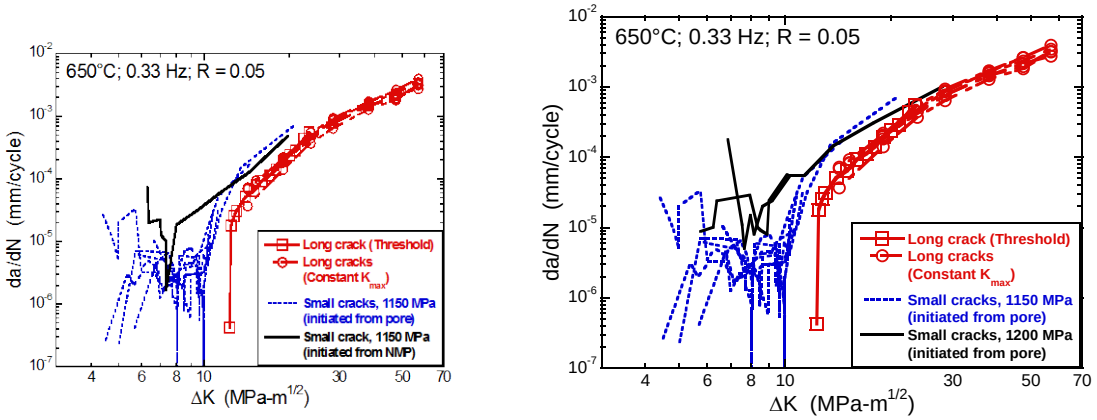

(a) (b)

Figure 4. Small crack growth behavior of IN100; (a) Effect of crack initiation from NMP vs. pore and (b) Effect of stress level on the growth rates.

The role of small crack growth in the separation of mean and the life-limiting behavior is illustrated by Fig. 5. The crack growth bounds indicated in the figure were calculated by considering the upper and the lower bound on the small crack growth behavior in conjunction with the maximum and the minimum crack initiation size respectively. The life-limiting behavior corresponded to crack initiation from a NMP. However, due to the small frequency of occurrence of the NMP-initiated mechanism, only one small crack growth curve was available in that crack initiation mode (Fig. 4(a)), which was taken as the upper bound of the small crack growth behavior for the calculation purposes. The lower limit of the NMP-initiated small crack growth behavior was assumed to correspond to the upper-bound crack growth curve of the pore-initiated mechanism (Fig. 4(a)). Similarly, due to the small number of small crack growth

experiments at 1200 MPa, the upper-bound small crack growth curve from the pore-initiated mechanism at 1150 MPa was also taken as the lower-limit curve at 1200 MPa. These approximations were considered suitable in capturing the shift to higher small crack growth rates with stress level, and for crack initiation from a NMP. Additional small crack growth data under these specific conditions will certainly improve the accuracy of the predictions. The limiting small crack growth curves were fitted with power-law segments to obtain the crack growth rate (da/dN) – ΔK relationship for the lifetime calculations. For crack initiation size calculation, two schemes were used as indicated in Fig. 5. In these, the crack depth, *a*, was taken as (i) the radius of the equivalent semicircle with the same area as the crack initiating feature, and (ii) the radius of the semicircle circumscribing the crack initiation feature. The range in the NMP-related crack initiation sizes, which were measured in the fracture surfaces, was used in the calculations at all stress levels.

Figure 5 shows, that the calculated crack growth bounds reasonably represent the range in the life-limiting behavior. The mean-lifetime response, on the other hand, separates from the crack-growth-controlled behavior with decreasing stress level. The lifetime probability density can therefore, be modeled as a superposition of the crack growth behavior upon the mean-lifetime behavior. The effect of microstructure and loading variables on the lifetime variability can then be evaluated by separating their effects on the crack growth lifetime and the mean lifetime, as illustrated in a forthcoming section.

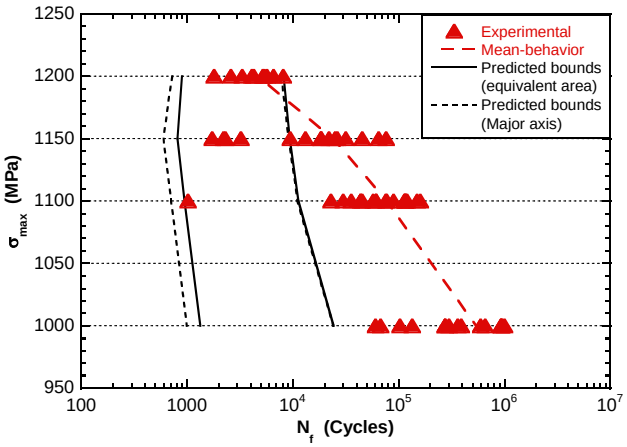

Figure 5. Role of small crack growth in the separation of mean-behavior from the life-limiting response.

Effect of dwell loading on the mean vs. life-limiting behavior

From the above discussion, the effect of dwell loading on the lifetime variability can be described in terms of separate effects on the crack growth lifetime and the mean-dominating behavior. The small crack growth data, obtained at 1150 and 1100 MPa, with 6 second dwell at the peak load is shown in Fig. 6. The figure indicates that, while the long-crack regime was not significantly influenced by the dwell loading, it had a significant effect on the small crack growth rates when compared at the same stress level. Also, there was a strong effect of stress level on the small crack growth regime under dwell loading. As indicated previously, in the proposed life-prediction approach, characterizing these effects is vital in determining the life-limiting behavior and the probabilistic lifetime limit.

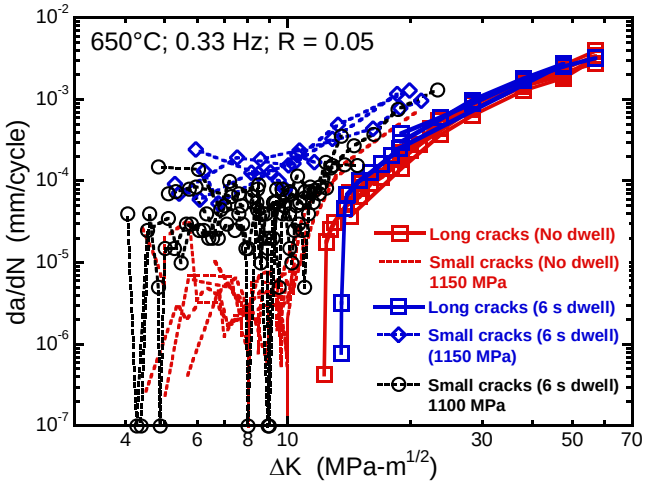

Figure 6. The effect of dwell time on the small crack growth regime in IN100.

The mean vs. life-limiting behavior under dwell loading is presented in Fig. 7. The figure shows that the 6 second peak dwell produced a significant reduction in the mean-lifetime (in terms of cycles) but a much weaker effect on the life-limiting behavior. The calculated crack growth bounds, based on the small crack growth variability at 1100 MPa (Fig. 6) and the range in the crack initiation sizes, are superimposed in the figure and, once again, illustrates that the life-limiting fatigue response is reasonably captured by the range in the crack growth lifetime. Comparing the two cases, i.e., with and without dwell, it appears that the separation of mean from the life-limiting behavior is related to this control of the life-limiting response by the crack growth regime, which promoted a smaller degree of change in the life-limiting behavior with respect to both the stress-level and the dwell-time. The mean-lifetime, on the other hand, showed a significantly stronger sensitivity to these variables.

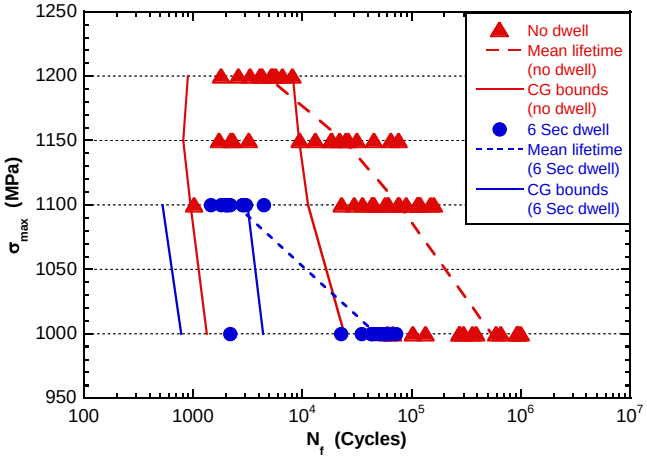

Figure 7. The role of small crack growth in the effect of dwell time on the mean vs. life-limiting fatigue response.

Calculation of the lifetime probability density

Calculation Procedure. The different rates of response of the crack-growth-controlled behavior and the mean-dominating behavior, as discussed above, may explain the increased

separation/overlap between the two as a function of stress level and dwell time, thereby affecting the total lifetime variability. The lifetime probability density can therefore, be represented as a superposition of the crack growth probability density function (PDF) and a mean-dominating PDF [10]:

$$f_t(x) = p_l f_l(x) + p_m f_m(x) \tag{1}$$

where, $f_t(x)$, $f_l(x)$, and $f_m(x)$ are the total lifetime, the life-limiting, and the mean-dominating probability densities respectively. The weighting parameters, p_l and p_m, are the probability of occurrences of the crack-growth-controlled and the mean-dominating mechanism respectively. It can be shown that the lower-tail of the above bimodal probability density, which is most pertinent in the calculation of the probabilistic lifetime-limit, is strongly governed by $f_l(x)$ and does not show substantial change within reasonable range of values of p_l and p_m [10]. Furthermore, the probabilistic limit, for e.g., the B0.1 lifetime, can be shown to be bounded by the B0.1 lifetime obtained from the crack growth density [10] (i.e., $p_m \rightarrow 0$). In the present case, the values of p_l and p_m were derived from the S-N experiments.

The life-limiting density, $f_l(x)$, was simulated by using the crack initiation size distribution [7] and the small crack growth data. The crack initiation size was measured on the fatigue fracture surfaces and was modeled by the lognormal probability density function. This is shown in Fig. 8(a). The small crack growth data were fitted by multiple power-law (Paris) segments [15] such that:

$$\frac{da}{dN} = e^C \Delta K^m \tag{2}$$

The Paris-type coefficient and exponent, C and m, were treated as random variables and were modeled by the normal density function [16]. The parameters of C and m were derived by the Maximum Likelihood Estimate (MLE) method using the available small crack growth data. It is also recognized that the variables, C and m are strongly negatively correlated [15, 16] and this correlation was invoked in the simulation of lifetimes. The joint PDF of C and m for the lower-ΔK small-crack growth segment in the no-dwell case is presented in Fig.

8 (b).

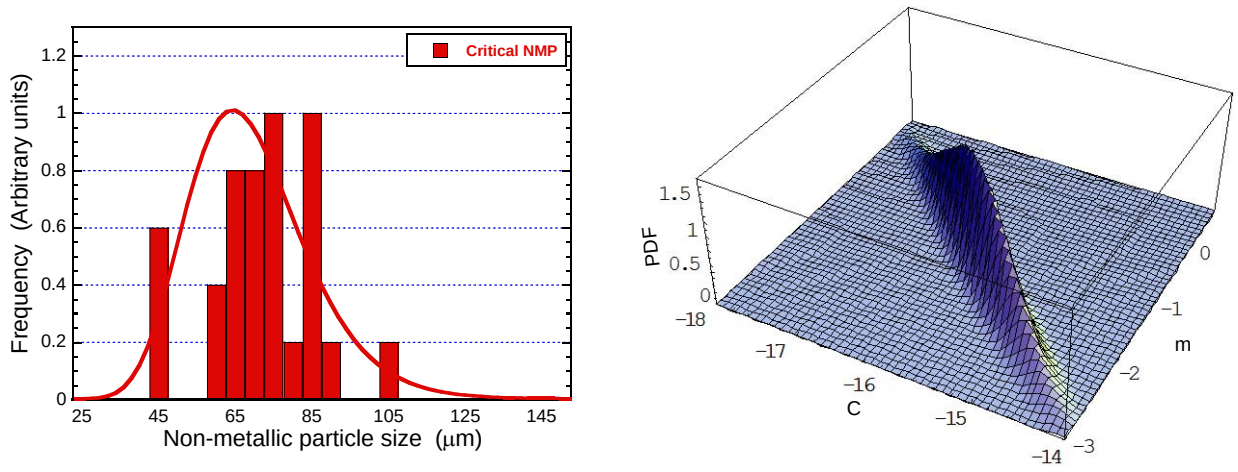

(a) (b)

Figure 8. Examples of input to the simulation of the life-limiting probability density, $f_l(x)$; (a) The crack initiation size distribution for the NMP initiated cracks in terms of the diameter of the equivalent circle, and (b) The joint PDF of the small crack growth variables, C and m for the case of 0 dwell time.

The CDFs associated with the simulated life-limiting densities, $f_l(x)$, are shown in Figs. 9 and 10 for the 0 second and the 6 second peak dwell cases, respectively. The crack-growth-controlled densities show reasonable correspondence with the observed distribution in lifetime at the higher stress levels, as in Figs. 9(a) and 10 (a) (due to convergence of the mean and the life-limiting behavior) but describe the life-limiting response at the lower stress levels, as illustrated in Figs. 9(b and c) and 10(b).

The mean-dominating density, $f_m(x)$, can be estimated by running a relatively small number of S-N experiments under the conditions of interest. This is illustrated in Fig. 11. Here, 4 tests were randomly selected at each stress level and for the no-dwell and the peak dwell condition. The parameters of $f_m(x)$ were then determined by the MLE method assuming the lognormal model.

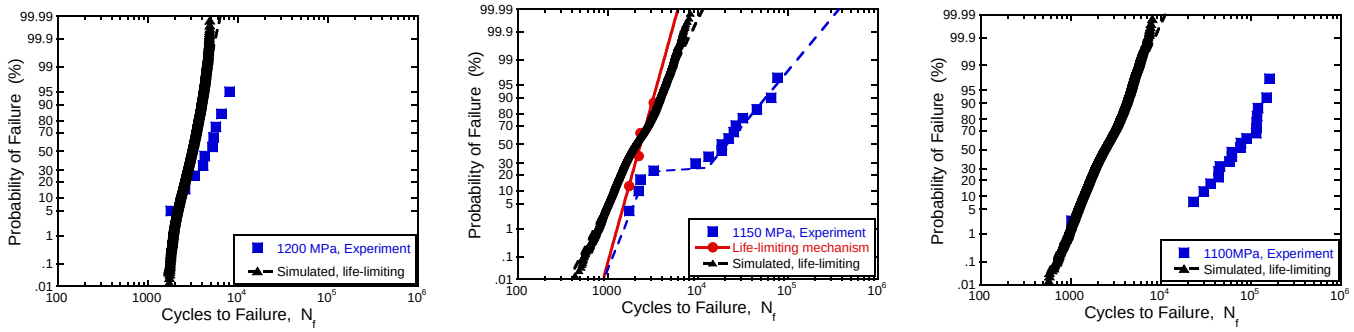

(a) (b) (c)

Figure 9. The CDFs of the calculated life-limiting probability densities for the case of no-dwell; (a) σ_{max} = 1200 MPa, (b) σ_{max} = 1150 MPa, and (c) σ_{max} = 1100 MPa.

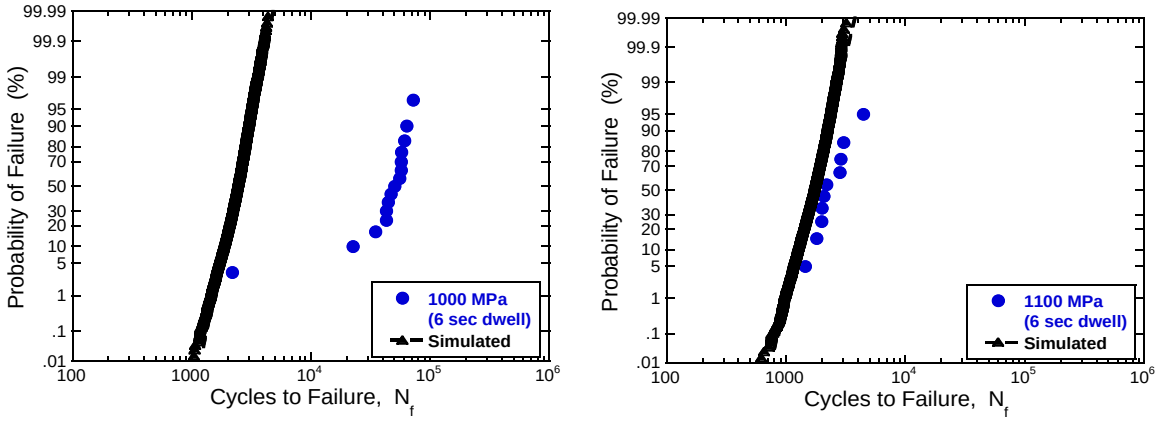

(a) (b)

Figure 10. The CDFs associated with the calculated life-limiting densities for the case of 6 second peak dwell; (a) σ_{max} = 1100 MPa and (b) σ_{max} = 1000 MPa.

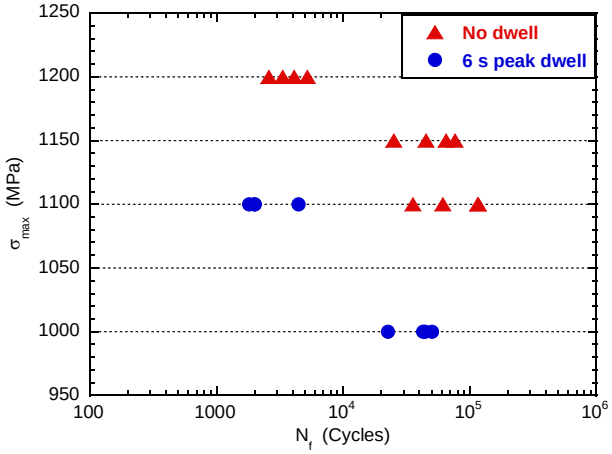

Figure 11. I nput data (4 random tests at each stress level) for obtaining the mean-lifetime-dominating density, $f_m(x)$.

Predicted Lifetime Densities. The predicted lifetime densities, calculated according to Eqn. (1), are shown in Figs. 12 (a) and (b) for the two loading conditions. The conventional description of fatigue variability, where the lower tail is considered as an extrapolation of deviations from the mean behavior, is also plotted in these figures. The B0.1 lifetimes obtained by the two approaches have been indicated by vertical lines and the experimental points are represented by open symbols. The results show that the suggested lifetime modeling provides a more accurate representation of the effect of stress level and dwell time on fatigue variability. Especially, the predictions of the lower tail and the B0.1 lifetimes are more consistent with respect to these variables and almost independent of the number of S-N tests therefore, significantly decreasing the uncertainty in the probabilistic lifetime limit. For example, although the total variability (and mean-lifetime) increased with decreasing stress level and dwell time, this is attributed to the separate degree of effects of these variables on the small crack growth regime and the mean-lifetime behavior. Consequently, the lower-tail and the B0.1 lifetime are not entirely dependent on the mean-behavior or the number of data points, producing, perhaps, a physically more accurate trend in the probabilistic lifetime limits (Fig. 12).

As indicated above, a distinct attribute of the suggested method is that, the predictions of the B0.1 lifetimes are not heavily dependent on the time consuming, and often expensive S-N fatigue experiments. Notably, the predicted CDFs account for the solitary life-limiting failure at 1100 MPa with no-dwell (Fig. 11(a)) and at 1000 MPa under dwell loading (Fig. 11(b)), which, due to the small probability of occurrence, otherwise requires a relatively large number of total lifetime experiments to capture. Nonetheless, the key to the method is the recognition that the lifetime variability is a result of separate responses of the crack-growth-controlled behavior and the mean-dominating behavior with respect to both the intrinsic and the extrinsic variables. Therefore, merely a large number of experiments may still not be sufficient in accurate prediction of the probabilistic lifetime limits without the paradigm shift in the description of fatigue variability.

Conclusions

Based on this study, the following concluding points can be made:

- The effect of stress level and dwell time on the fatigue variability and the probabilistic lifetime limit can be accurately predicted by considering separate responses of the crack-growth-controlled life-limiting behavior and the mean-lifetime behavior to these variables.
- The lifetime probability density can therefore, be modeled as a superposition of the crack growth lifetime density and the mean-dominating density.
- The B0.1 lifetimes predicted by this approach show a more consistent trend with respect to stress level and dwell time independently of the number of S-N fatigue experiments therefore, significantly decreasing the uncertainty in these probabilistic limits.

Acknowledgements

This work was performed at the Air Force Research Laboratory, Materials and Manufacturing Directorate, Wright-Patterson Air Force Base, OH. The partial financial support of the Defense Advanced Research Project Agency (DARPA) under DARPA orders M978, Q588, P699, and S271 with Dr. Leo Christodoulou as the program manager is gratefully acknowledged. Essential support was also provided by the Air Force Office of Scientific Research (AFOSR) with Dr. Victor Giurgiutiu as the program manager. We acknowledge Mr. Phil Buskohl and Ms. Lindsey Selegue for their assistance with the replication-based small-crack growth experiments.

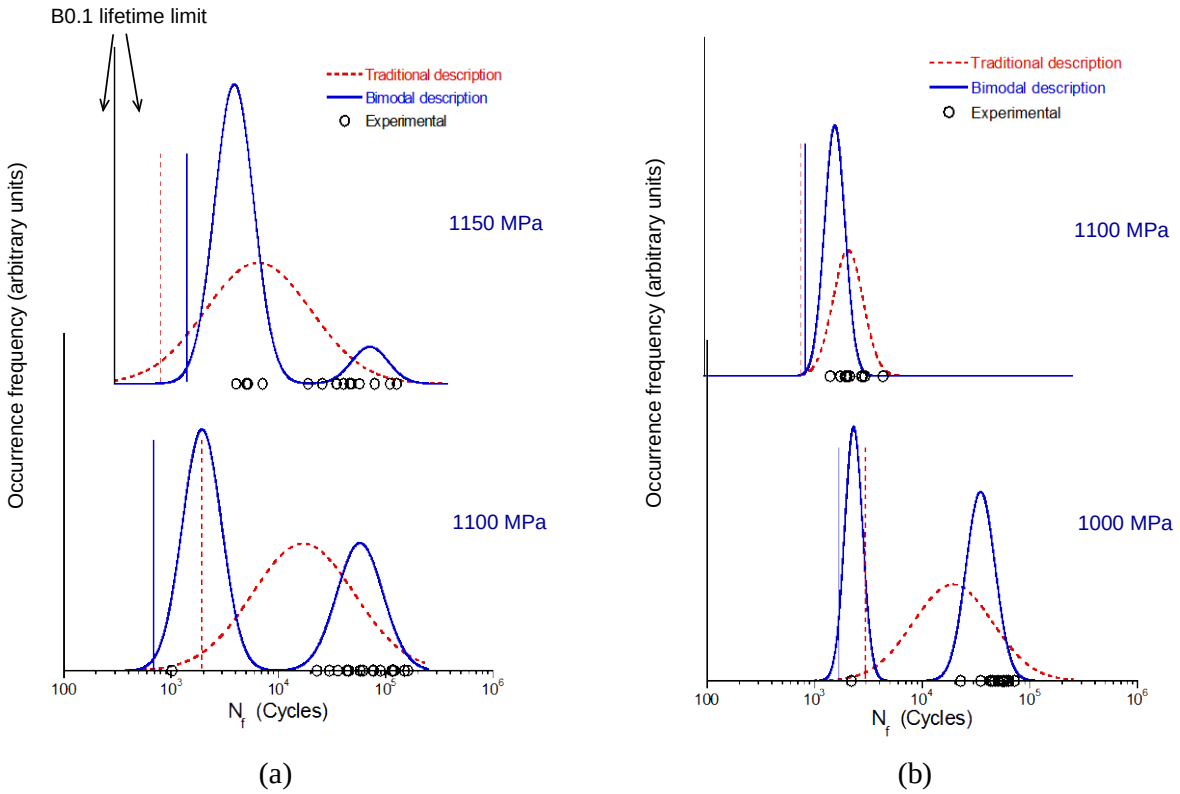

Figure 12. Predicted lifetime probability densities and the B0.1 lifetimes based on the proposed fatigue variability description; (a) no-dwell and (b) 6 second peak dwell.

References

1. L. Christodoulou and J.M. Larsen, *JOM*, p. 15, March, 2004.
2. J.W. Lincoln, *Journal of Aircraft*, Vol. 22, 1985.
3. J.N. Yang and W.J. Trapp, *AIAA Journal*, Vol. 12, pp. 1623-1630, 1974.
4. R. Tryon and A. Dey, *J. Aerospace Engng.*, p.120, 2001.
5. K.S. Chan and M.P. Enright, *Journal of Engineering for Gas Turbines and Power*, Vol. 124, pp. 889-885, 2006.
6. A. de Bussac, and J.C. Lautridou, *Fatigue Fract. Engng. Mater. Struct.*, Vol. 16, p. 861, 1993.
7. S.K. Jha, M.J. Caton, and J.M. Larsen, *Materials Science and Engineering A*, Vol. A468-470, pp. 23-32, 2007.
8. S.K. Jha, J.M. Larsen, and A.H. Rosenberger, *Acta Materialia*, Vol. 53, pp. 1293-1304, 2005.
9. S.K. Jha and J.M. Larsen, in *Very High Cycle Fatigue*, *VHCF-4*, 2007.
10. S.K. Jha, J.M. Larsen, and A.H. Rosenberger, in review, *Engineering Fracture Mechanics*.

11. R.G. Forman, and V. Shivakumar, in *Fracture Mechanics: 17th Volume,* ASTM STP 905, J.H. Underwood, R. Chait, C.W. Smith, D.P. Wilhem, W.A. Andrews, and
J.C. Newman, Eds., ASTM, Philadelphia, pp. 59-74, 1986.

12. J.C. Newman, Jr. and I.S. Raju, *Engineering Fracture Mechanics,* Vol. 15, pp. 185-192, 1981.

13. M.M. Shenoy, R.S. Kumar, and D.L. McDowell, *Int. J. Fatigue*, Vol. 27, p. 113, 2005.

14. R. Bullough and L.C. Davis, *Acta Materialia*, Vol. 43, p. 2737, 1995.

15. J. Luo, and P. Bowen, *Acta Materialia*, Vol. 51, pp. 3537-3550, 2003.

16. C.G. Annis, Jr., in *Probabilistic Aspects of Life Prediction,* ASTM-STP 1450, W.J. Johnson and B.M. Hillberry, Eds., ASTM International, West Conshohocken, PA, 2003.